Model Membranes to Study the Lipid-Reactivity of HIV-1 Antibodies and Vaccine Antigen

by

Gregory James Hardy

Department of Mechanical Engineering and Materials Science
Duke University

Date:_____

Approved:

_____
Stefan Zauscher, Supervisor

_____
S. Munir Alam

_____
Joseph Shapter

_____
Piotr Marszalek

_____
Thomas McIntosh

Dissertation submitted in partial fulfillment of
the requirements for the degree of Doctor
of Philosophy, in the Department of
Mechanical Engineering and Materials Science in the Graduate School
of Duke University

2014

ABSTRACT

Model Membranes to Study the Lipid-Reactivity of HIV-1 Antibodies and Vaccine Antigen

by

Gregory James Hardy

Department of Mechanical Engineering and Materials Science
Duke University

Date:_____

Approved:

_____
Stefan Zauscher, Supervisor

_____
S. Munir Alam

_____
Joseph Shapter

_____
Piotr Marszalek

_____
Thomas McIntosh

An abstract of a dissertation submitted in partial
fulfillment of the requirements for the degree
of Doctor of Philosophy in the Department of
Mechanical Engineering and Materials Science in the Graduate School of
Duke University

2014

Abstract

One promising HIV-1 vaccine target is the membrane-proximal external region (MPER) of viral gp41. MPER is poorly immunogenic, however, the two rare neutralizing antibodies (NAbs), 2F5 and 4E10, bind to MPER with great neutralizing ability. Although their neutralizing mechanism represents a promising framework for the design of new HIV-1 liposomal vaccine candidates, this mechanism remains poorly understood. It is known that 2F5 and 4E10 are required to first associate with HIV-1 lipids before binding to the target MPER antigen, however, little is known about how lipid membranes contribute to NAb-antigen binding. To this end we have developed model membrane systems to study NAb and antigen lipid interactions.

We first created a surface plasmon resonance (SPR) spectroscopy based assay that monitors antibody binding to thiol monolayers that mimic the surface-chemical properties of lipid membranes. Next, we focused on recreating the lipid phase organization (*i.e.*, domain formation) of native membranes by using supported lipid bilayers (SLBs). We used simple SLB compositions to model the liquid-disordered (L_d) and gel phases. To create the HIV-1 envelope, we used a complex SLB composition that contains an L_d and liquid-ordered (L_o) phase. To reliably create model HIV-1 SLBs, we developed an SLB formation technique that uses amphipathic, α-helical peptides as a catalyst to generate complex SLBs that have a high cholesterol content and contain

multiple lipid types. We used atomic force microscopy (AFM) to visualize membrane domains, antigen presentation, and antibody-membrane interactions on all SLB surfaces.

Results from experiments using thiol monolayers showed that binding of NAb to hydrophobic functional groups was significantly greater than that of control monoclonal antibodies. This supports the hypothesis that these NAbs embed into the hydrophobic membrane core. Our experiments on SLBs demonstrate that 2F5/4E10 do not interact with the highly ordered gel and L_o domains in the SLB but exclusively bind to the L_d phase. This suggests that 2F5/4E10 require low membrane order and weak lateral lipid-lipid interactions to insert into the hydrophobic membrane interior. Thus, vaccine liposomes that primarily contain an L_d phase are more likely to elicit the production of lipid reactive, 2F5- and 4E10-like antibodies, compared to liposomes that contain an L_o or gel phase. In the context of liposomal antigen presentation, our results show that the presence of the $MPER_{656}$ antigen can severely limit the L_d area available for antibody interactions. Subsequently, this reduces the amount of $MPER_{656}$ that is accessible for 2F5/4E10 binding, since $MPER_{656}$ preferentially localizes to the L_d area. If L_d forming lipid components are used in vaccine liposomes, it is important to ensure that the presence of antigen does not inhibit large-scale L_d formation.

Dedication

This dissertation is dedicated to my parents for providing the inspiration and support to pursue the great moments in life.

Contents

List of Tables

List of Figures

List of Abbreviations

POPC	1-palmitoyl-2-oleoyl-sn-glycero-3-phosphocholine
POPE	1-palmitoyl-2-oleoyl-sn-glycero-3-phosphoethanolamine
POPS	1-palmitoyl-2-oleoyl-sn-glycero-3-phospho-L-serine
ODT	1-octadecanethiol
MUD	11-mercapto-1-undecanol
AUT	11-amino-1-undecanethiol
MUA	11-mercaptoundecanoic acid
AFM	Atomic force microscopy
AH	Alpha-helical
BCD	Bubble collapse deposition
CDR	Complementary determining region
CH	Cholesterol
θ_c	Critical concentration of vesicle surface coverage
ΔD	Damping oscillation change
DPN	Dip-pen nanolithography
HIV	Human immunodeficiency virus
L_d	Liquid-disordered
L_o	Liquid-ordered
R_{max}	Maximum SPR binding capacity
MPER	Membrane-proximal external-region
mAb	Monoclonal antibody
NAb	Neutralizing antibody
NR	Neutron reflectivity
PBS	Phosphate buffered saline
QCM-D	Quartz crystal microbalance with dissipation monitoring
Δf	Resonance frequency change
nSLD	Scattering length density
SAM	Self-assembled monolayer
SM	Sphingomyelin (brain)
SLB	Supported lipid bilayer
SPR	Surface plasmon resonance
T_m	Transition temperature (melting)

Acknowledgements

I would like to acknowledge and thank my advisor, Professor Stefan Zauscher for being an exceptional mentor. He has provided invaluable insight, guidance, and patience at all the right moments. For their steady support and expertise, I am thankful for my committee members: Professors Munir Alam, Thomas McIntosh, Joe Shapter, and Piotr Marszalek. Thank you to Dr. Dr. Michael Hirtz for hosting my research in Karlsruhe and for sharing his nano-fabrication expertise. I am especially grateful to Professor Joe Shapter for hosting my apprenticeship in his lab. This experience was one of the highlights of my graduate career and provided me with the research skills that would prove to be the foundation of my dissertation.

There are many other people that have helped me arrive at the completion of my PhD and enriched the experience along the way. Thank you to Elizabeth Hanlon, Tim Hanlon, Trisha Boulware, Aditee Kurane, Rahul Nayak, Kara Anasti, Jaclyn Lautz, R.P. Czekay, Robert Gerszten, Carla Sturdivant, Kathy Parrish, Aven Garms, Mathew Lee, Robert Ferris, the entire Zauscher Lab, Chad Gibbs, Elise Corwin, Monty Reichert, Tyler Thornton, and my parents, Tom and Teresa Hardy.

Finally, I would like to acknowledge financial and training support from the Center for Biomolecular and Tissue Engineering (CBTE) and the Structural Biology and Biophysics (SBB) program (Duke University), grant funding from the National Institutes of Health (NIH) and the Duke University Center for AIDS Research (CFAR), and visiting

scholarship funding from the East Asia and Pacific Summer Institutes program, Australian Academy of Science, Burroughs Wellcome Fund, and the Karlsruhe House of Young Scientists (Karlsruhe Institute of Technology).

Chapter 1. Background Information

1.1 Introduction

This dissertation is focused on studying protein-membrane interactions in the context of HIV-1 vaccine designs. Model membrane systems that reflect the native HIV-1 lipid envelope will be used to study protein-membrane interactions using HIV-1 neutralizing antibodies (2F5 and 4E10) and recombinant HIV-1 vaccine antigen ($MPER_{656}$).

Chapter 1 presents background information on the mechanism of 2F5/4E10 HIV-1 neutralizing antibodies (including lipid membrane contributions), model lipid systems, and the major biophysical tools utilized in this research. Chapter 2 presents a surface plasmon resonance (SPR) spectroscopy based assay that monitors antibody binding to thiol monolayers, which mimic chemical properties of lipid membranes. While thiol monolayers have the advantage of easily modeling the chemistry of common lipid head groups, they fail to capture the dynamic lipid mobility and complex lipid organization found in native membranes. Thus, Chapter 3 introduces techniques to model this complex lipid environment using supported lipid bilayers (SLBs).

For simple, binary or tertiary lipid compositions, there are many established SLB formation methods. However, to form SLBs that contain a more complex, biomimetic lipid composition (*i.e.*, many lipid types with high cholesterol content) there are obstacles for SLB formation for which there are few reliable solutions. Chapter 4 addresses this problem by presenting a novel technique to easily and reliably overcome

obstacles for creating complex SLBs that more accurately mimic the native HIV-1 lipid envelope. Chapter 5 describes how this SLB research platform is used to visualize membrane domains, antigen presentation, and antibody-membrane interactions. Taken together, the results provide progress towards the development of model membrane research platforms and important information for HIV-1 vaccine design, specifically for the design of liposomes that attempt to optimize antigen presentation and elicit membrane dependent neutralizing antibodies. Chapter 6 summarizes major conclusions and outlines future work that builds off these results to help further shape next-generation vaccine designs. Finally, Appendix A presents progress towards a membrane screening platform fabricated by dip-pen nanolithography and Appendix B contains detailed protocols essential to this research.

1.2 Human Immunodeficiency Virus Vaccine Design

Induction of broadly neutralizing antibodies against HIV-1 remains an unprecedented challenge.[1, 2] One promising vaccine target is the membrane-proximal external region (MPER) of viral gp41, which is a highly conserved region across diverse HIV-1 strains. When bound by an antibody, its transient epitopes effectively prevent viral fusion with the host cell membrane.[3] Nevertheless, MPER is poorly immunogenic due to its transient structure and poor sterics, limiting accessibility for immune recognition. In part, these limitations help explain why membrane-proximal neutralizing

antibodies (NAbs) have only rarely been isolated during natural HIV-1 infection.[4] Two such NAbs that bind to MPER with great strain breadth and neutralizing ability are 2F5 and 4E10. Their neutralizing mechanism represents a promising framework for the design of new HIV-1 liposomal vaccine candidates, yet this mechanism is only poorly understood.

Although antigens embedded in liposomes facilitate high affinity interactions that are selective for NAbs, it was shown that it is not sufficient to simply induce antibodies that bind MPER antigens to achieve neutralization.[5-7] In order to mimic 2F5/4E10's neutralizing ability, immunogens must elicit antibodies that also react with the HIV-1 lipid envelope. However, these gp41 MPER polyreactive antibodies are likely subjected to immunological tolerance[8, 9] and are thus rarely induced by either infection or immunization. Nevertheless, some level of polyreactivity can be tolerated and can even confer an advantage in binding of certain pathogens.[10-12] In fact, high affinity gp140 antibodies from HIV-1 are more frequently polyreactive[13, 14] and such a trait is observed in the case of both neutralizing and non-neutralizing gp41 antibodies.[15] Thus, a certain level of polyreactivity may be permissible for several HIV-1 NAbs and developing a SLB research platform for studying the nature of these interactions is critical for understanding the human antibody responses against HIV-1.

1.3 NAb Neutralizing Mechanism

In vitro studies have shown that 2F5 and 4E10 successfully inhibit the fusion process of HIV-1 by binding the MPER of gp41 during a two-stage mechanism: the NAbs first interact nonspecifically with the viral lipid membrane and then with the target MPER antigen.[16, 17] One explanation for this two-stage interaction is that NAb-membrane interactions likely direct high NAb concentrations toward the viral surface, where the NAb's ability to diffuse within the viral membrane could better position it to encounter and extract its sparse MPER epitope from within the lipid bilayer.[18] Figure 1.1 shows the location of 2F5 and 4E10's MPER epitope relative to the viral envelope and other broadly neutralizing antibodies. Besides binding kinetics, there is very little experimental evidence detailing this lipid reactivity in HIV-1 neutralization. The recent literature on 2F5/4E10-membrane reactivity simply states that reactivity exists, and that neutralization is dependent on membrane reactive CDR H3 loops.[19] Mechanistic details of how membrane properties influence NAb-lipid and NAb-antigen interactions remain unknown.

This unexpected interaction between lipids and 2F5/4E10 is potentially mediated by their long complementary determining region (CDR) H3 loop.[20] CDR H3 contains unusually large numbers of hydrophobic and membrane-reactive residues that can embed in the viral membrane.[18, 21] CDR H3 regions mediate a reversible attachment to the viral membrane; which is a required first step for neutralization.[19] This

phenomenon may explain why simple peptide immunogens that mimic neutralizing epitopes on gp41 do not elicit NAbs *in vivo*,[5-7] and it is clear that gp41 MPER is not the sole determinant of neutralizing ability.[19] In order to mimic 2F5 and 4E10's *in vitro* neutralizing ability, *in vivo* immunogens must elicit antibodies that also react with the HIV-1 lipid envelope. How to design immunogens to do this remains largely unknown.[7]

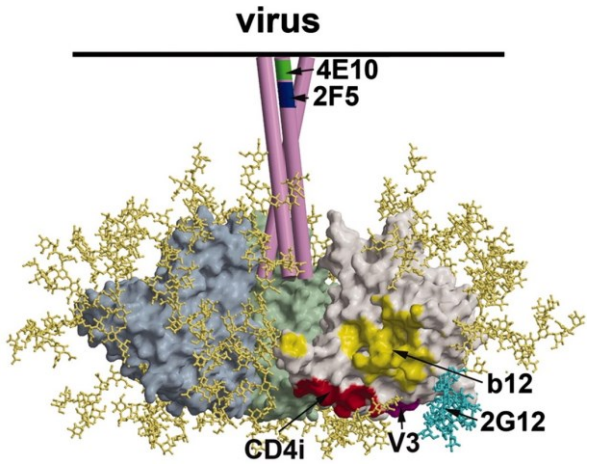

Figure 1.1: Schematic of the envelope spike of HIV-1 showing the location of neutralizing antibody epitopes. gp120 is shown in grey, pale green, and pale blue. gp41 is shown in pink. Carbohydrate chains are shown in yellow. The approximate epitope locations for broadly neutralizing antibodies are indicated. Adapted with permission from reference [22]. Copyright (2005) National Academy of Sciences.

1.4 Polyreactivity and Immune Tolerance

There is much evidence indicating that B cells that express self-reactive receptors are subjected to negative selection[23], which results in significant purging of

polyreactivity in the mature B cell population.[24] However, a predominant population (~70%) of memory B cells against HIV-1 gp120 and gp41 are polyreactive.[12, 13, 17, 25, 26] This suggests that polyreactivity is conserved despite negative selection mechanisms. Furthermore, the detection of such polyreactive responses in both elite controllers and clade A non-controllers suggested that this is a general phenomenon associated with human antibody responses to HIV-1 envelope[13] and that not all polyreactive B cells are subjected to tolerance. The enhancement of binding avidity due to heteroligation is one plausible explanation for the positive selection of such polyreactive B cells.[12] Several, more recently described antibodies have acquired ability to interact with glycans, a self-antigen, in addition to HIV-1 epitopes on gp120, V1V2.[10, 11, 27] Together these results suggest that the evolution of the above polyreactive antibodies involved a fine-tuning of self-reactivity below a threshold level that is permissible. Thus, small subsets of mature naïve B-cells (between 5-20%) are capable of escaping immune tolerance while maintaining poly or self-reactivity[28, 29] and B cells can also re-acquire poly or self-reactivity during the germinal center reaction.[30]

In the case of gp41 MPER monoclonal antibodies, results from 2F5 knock-in mice suggested that HIV-1 MPER antigen reactivity was under more stringent tolerance control than lipid reactivity *per se*.[9, 24] Furthermore, the unmutated ancestor (putative germline) of 2F5 binds more strongly to lipids than the mature 2F5 mAb,[31] and thus suggests that lipid reactivity might be fine-tuned and antigen affinity enhanced during

antibody maturation. A corollary to the above is that lipid binding *per se* is not totally prohibitive and in the mature antibody both self and antigen reactivity may be conserved. The polyreactive trait is also not limited to NAb and non-neutralizing gp41 antibodies that show substantial binding to lipids and protein autoantigens.[15] In fact, humans do naturally produce antibodies that can bind to many lipid types, including phospholipids[32, 33], cholesterol[34, 35] and squalene.[36] Furthermore, during phase 1 clinical trials, passive administration of 2F5/4E10 to HIV-1 patients resulted in no deleterious autoimmune response, indicating that pathogenicity is not a concern for induction of such antibodies.[37-39] However, how to design immunogens and adjuvants that allow targeting of B cells that can make antibodies that bind to both gp41 MPER and lipids is not sufficiently understood.

1.5 Membrane Properties Influencing Antibody-Lipid Interactions

Understanding membrane properties that influence antibody-lipid interactions are essential to the design of next-generation HIV-1 vaccines. For example, lipid compositions conducive to eliciting NAbs can be selected for the assembly of vaccine liposomes. Liposomes are currently a common vehicle for delivering vaccine packages, consisting of antigens, immunogenic lipids, and adjuvants. When designing liposomal vaccines, immunologists are largely focused on antigen sequence, the presented conformation of the membrane integrated antigen, and the adjuvant used to initiate the

body's immune response. Given the importance of 2F5/4E10's lipid reactivity, we argue that the lipid composition of the liposome must not be overlooked and is an essential component of the vaccine package that can influence B cell receptor recognition (and thus dictate antibody production). It is clear that lipid composition affects the liposomal membrane properties, and membrane properties directly influence antibody interactions. Thus, by studying how membrane properties contribute to lipid-antibody interactions, we will identify lipid compositions that will elicit favorable antibody-lipid interactions.

To determine the driving factors dictating adsorption of antibodies to the HIV-1 envelope, it is necessary to understand common forces governing protein adsorption. The adsorption of soluble proteins onto the surface of lipid membranes is often driven by hydrophobic interactions. Proteins interacting with a solid hydrophobic surface in solution (*i.e.*, gold) are known to adsorb to the surface by re-folding to position their hydrophobic core to contact the hydrophobic surface. This adsorption is driven by an effort to minimize entropic energy. Protein adsorption onto lipid bilayers can also be driven by the same hydrophobic effect. Hydrophobic regions of a protein may insert into the hydrophobic core of the lipid bilayer to achieve a more favorable entropic organization in its solvent. Thus, it is hypothesized that 2F5/4E10's CDR H3 hydrophobic loop may insert into the hydrophobic core of the bilayer.

1.6 Membrane Organization and Lipid Domains

Currently it is believed that membranes, including the HIV-1 envelope, organize into distinct lipid regions or domains (Fig. 1.2), and that these lipid regions might act as binding sites for neutralizing antibody interactions and control antigen presentation in vaccine liposomes. The HIV-1 envelope contains a lipid composition that differs from that of host cell membranes[40] as HIV-1 acquires its membrane envelope by budding from isolated islands of membrane lipids enriched in cholesterol and sphingomyelin. Thus, major differences include elevated levels of cholesterol and sphingomyelin in addition to anionic lipids,[41] all of which have been shown to contribute to heterogeneous lipid domain formation.[42-45] Cholesterol's preference for saturated lipid tails drives this phase separation. These membrane domains are characterized by distinct lipid/lipid interactions and packaging from the surrounding medium. As a result, these membrane domains also have different physico-chemical properties, such as fluidity, thickness, and head-group chemistry, which could be exploited by an immune response in order to generate lipid-reactive, broadly neutralizing antibodies to HIV-1. It is likely that lipid domains drive protein-membrane interactions and control conformations of transmembrane and membrane associated peptides.[46] Yet, the size, physical properties, and dynamics of such lipid domains are poorly characterized for the

HIV-1 lipid envelope, and it is still unknown how lipid domains contribute to NAb-membrane interactions and antigen presentation.

Due to packing characteristics of phospholipids, two main domain types form: (i) liquid-disordered (L_d), and (ii) gel domains (Fig. 1.2A). The transition temperature (T_m) (*i.e.*, melting temperature) of the lipid will determine at what temperature the lipid will melt from the gel to the L_d domain. Furthermore, cholesterol and sphingolipids have a tendency to self-associate within the L_d domain and to phase separate into highly ordered, tightly packed islands, known as liquid ordered (L_o) domains or lipid rafts (Fig. 1.2B).[47, 48] Cholesterol's strong interaction with sphingomyelin is believed to result from cholesterol's ability to interact along the entire length of sphingomyelin's saturated acyl chains.[49]

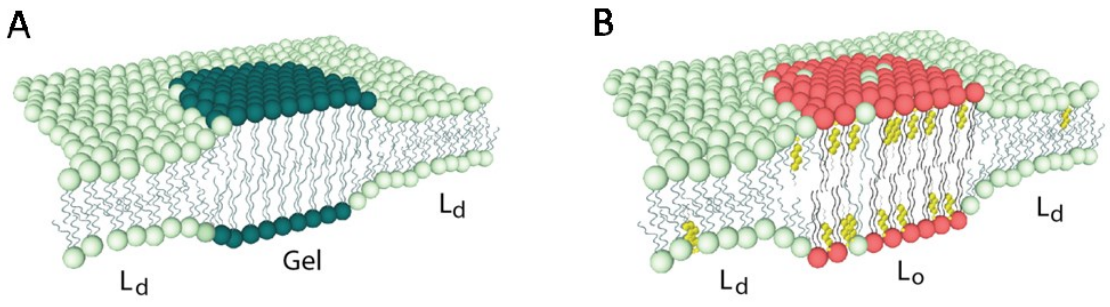

Figure 1.2: Schematic representations of lipid organization. (A) Gel domain (dark green) surrounded by L_d phase (light green). (B) L_o domains consisting of sphingomyelin (red) and cholesterol (yellow) in an L_d phase (light green).

The lipid diffusivity between the L_o and L_d phase differs by a factor of 2-10, depending on experimental details/systems.[50-52] Such diffusivity differences are important because the ability of NAbs to insert into the lipid bilayer may be related to lipid diffusivity in the domains. It is hypothesized that areas of high lipid diffusivity are easier to penetrate then areas of low lipid diffusivity, which will have stronger lateral lipid-lipid interactions and thus, be more difficult for antibodies to overcome the activation energy required to penetrate into the hydrophobic core. How these areas of different diffusivities dictate antibody-membrane interactions remains to be explored.

Given the presence of high concentrations of cholesterol and sphingomyelin in the HIV-1 membrane, it is likely that lipid domains/rafts populate the membrane surface. We modeled the native HIV-1 lipid envelope with a lipid composition of POPC:POPE:POPS:sphingomyelin:cholesterol (9.35 : 19.25 : 8.25 : 18.15 : 45.00) and observed phase separated bilayers at 37 °C (Chapter 4), that contained L_o domains within an L_d phase. The observed domain formation in the model HIV-1 membrane agrees with the phase diagram of POPC, PSM, and cholesterol at 37 °C (Fig. 1.3).[53] The expected location of the model HIV-1 SLB within the phase diagram is indicated by the red triangle.

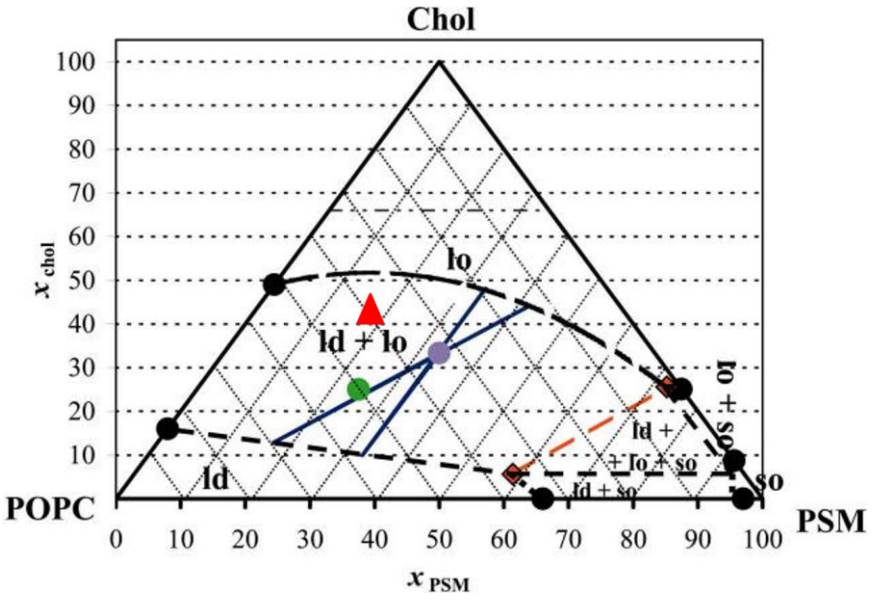

Figure 1.3: POPC:PSM:CH phase diagram at 37 °C. Circles are experimental points, the red triangle indicates the expected location of the model HIV SLB composition. Adapted with permission from reference [53]. Copyright (2003) Biophysical Journal.

1.7 Model Membrane Systems

We first use simple, self-assembled thiol monolayers (SAMs), whose head groups mimic the chemistry of viral and host membrane lipids, to characterize and better understand antibody-lipid interactions. Antibody screening was performed by anchoring the self-assembled thiol monolayers on custom surface plasmon resonance (SPR) sensor chips (Fig. 1.4). Our thiol monolayers exhibited a range of chemical functionalities (*i.e.*, variations in hydrophobicity and surface charge) that also occur in the phospholipid head-groups of both the native host CD4+ cells and the HIV-1 virion. The details and results from this screening platform are presented in Chapter 2.

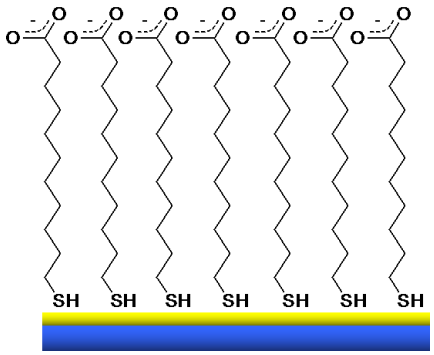

Figure 1.4: Schematic of a 11-mercaptoundecanoic acid (MUA) thiol SAM on a gold coated SPR sensor chip.

While thiol SAMs on gold allow the use of SPR to characterize NAb-SAM interactions, they fail to capture the fluidity and complex lipid organization found in native membranes. Thus, we have expanded our model membrane platform to include supported lipid bilayers (SLBs). Briefly, SLBs contain a single lipid bilayer supported on a substrate, with a thin (1-2 nm) hydration layer between the bilayer and the substrate surface (Fig. 1.5). Although the SLB is stable and confined in two dimensions to the substrate surface, it can recapitulate the lateral lipid diffusivity and lipid organization of native cell membranes. Furthermore, the planar orientation of SLBs allows the use of many quantitative surface characterization techniques that are able to provide unique insights into membrane functions and protein-membrane interactions. Details of SLB formation techniques are discussed in Chapter 3, while Chapter 4 presents a novel SLB

formation technique to reliably create SLBs that more accurately mimic native membrane compositions.

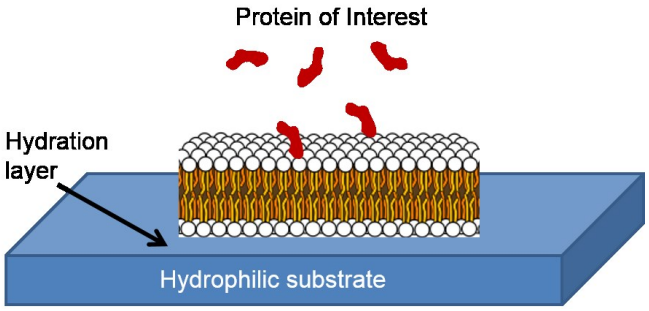

Figure 1.5: Schematic of a supported lipid bilayer (SLB) interacting with protein. SLB is submerged in liquid (not shown).

1.8 Biophysical Tools Applied to SLB Research Platform

While SLBs lend themselves to study by a number of biophysical tools, in the research discussed here we will largely utilize the following: (i) quartz crystal microbalance with dissipation monitoring (QCM-D), (ii) surface plasmon resonance (SPR), (iii) atomic force microscopy (AFM), and (iv) neutron reflectivity (NR).

1.8.1 Quartz Crystal Microbalance with Dissipation Monitoring

Quartz Crystal Microbalance with Dissipation Monitoring (QCM-D) measures, in real-time, mass adsorbed and desorbed from a substrate by monitoring the resonance frequency change (Δf) of an oscillating quartz crystal. In the limit of thin, elastic layers,

the relationship between a quartz crystal's resonance frequency change and the mass of the adlayer is linear, and described by the Sauerbrey equation.[54] Viscoelasticity of the adlayer can also be detected by monitoring the damping of the crystal's oscillation (ΔD), which can give insight into the conformational changes occurring during vesicle fusion and peptide-lipid interactions. Figure 1.6 shows frequency and dissipation plotted as a function of time during SLB formation via vesicle fusion from zwitterionic phosphatidylcholine vesicles. First, vesicles are sparsely adsorbed onto the silica surface, resulting in a large frequency drop due to the increase in associated mass from the buffer trapped within and between the intact vesicles. Concurrently, the adsorbed vesicles contribute to an increase in dissipation due to their viscoelastic properties. Once the vesicle surface coverage reaches a critical concentration (θ_c, indicated by the * in Fig. 1.6), the vesicles spontaneously rupture and fuse to form a continuous SLB.[55-58] The frequency increase is due to SLB displacement of adsorbed vesicles and the buffer released from within the vesicle interior. Thus, for vesicles composed of 1-palmitoyl-2-oleoyl-sn-glycero-3-phosphocholine (POPC), a complete bilayer is characterized by a dip in Δf and peak ΔD with time, resulting in a final Δf of ~ –26 Hz and a ΔD of ~ 0.2 x 10^{-6} (Fig. 1.6).[59]

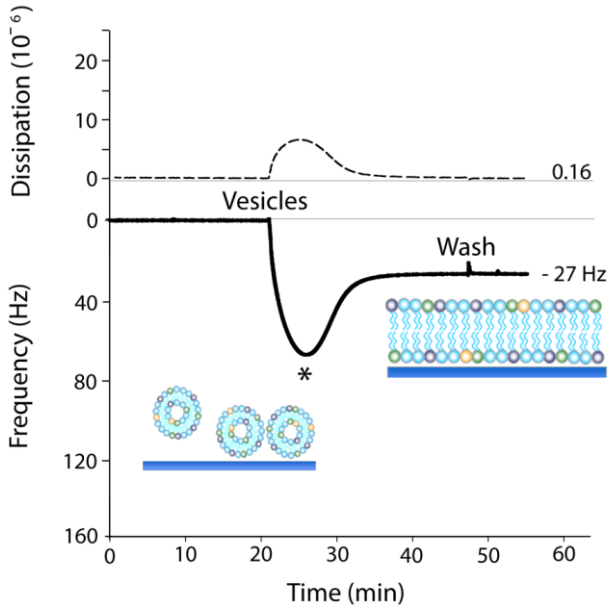

Figure 1.6: QCM-D frequency (solid line) and dissipation (dashed line) response plotted as a function of time for SLB formation from pure POPC vesicles via vesicle fusion. (*) indicates the critical concentration of vesicle surface coverage (θ_c).

While QCM-D serves as a reliable method to confirm bilayer formation on the meso- and macroscales, it is limited in the detection of minor bilayer defects and in characterizing details in the physical properties of SLBs. Past QCM-D studies have found that for different vesicle compositions, final Δf and ΔD values can differ substantially, *e.g.*, up to 30% for Δf.[60, 61] The interpretation of such differences is difficult, given that Δf represents an averaged, surface-associated mass, and does not differentiate between mass contributions from the lipids, the associated buffer, or the hydration layer. Furthermore, ΔD provides qualitative insights into the structure of surface-associated mass and cannot quantitatively identify structural properties such as

bilayer thickness, defects, or lipid packing density. Thus, QCM-D should be used in combination with other techniques, such as neutron reflectivity, ellipsometry, surface plasmon resonance, fluorescence recovery after photo-bleaching, and atomic force microscopy to confirm details of SLB formation and to quantify SLB properties.

1.8.2 Surface Plasmon Resonance

Surface plasmon resonance (SPR) is a technique that is used to monitor the change in dielectric properties and the corresponding change in refractive index above a plasmon-producing, metal-liquid interface.[62] When incident light is shone through a prism onto the backside of a metallic layer, an evanescent electromagnetic field can be produced at the liquid-solid interface. The angle of reflection is dependent on the refractive index of the thin layer adjacent to the metallic surface. Adsorption of molecules (*e.g.*, antibodies) to the metallic surface will result in a shift in the intensity minimum. This shift indicates a change in refractive index, and correspondingly, a change in adsorbed mass. For immunological-based experiments, SPR is often used to interrogate antibody-ligand interactions by determining association/dissociation rates and the binding constant (K_D). A review of how SPR is used to advance HIV-1 vaccine efforts and other viral vaccines can be found in reference [63].

1.8.3 Atomic Force Microscopy

Atomic force microscopy (AFM) is a type of high-resolution scanning probe microscopy technique, with resolution on the order of fractions of a nanometer; *i.e.*, significantly higher than the optical diffraction limit used in traditional light microscopy.[64] An AFM obtains high-resolution images by scanning the surface with a cantilever that contains a sharp tip at its end. Forces between the tip and the sample lead to a deflection of the cantilever. The deflection is measured using a laser spot reflected from the top surface of the cantilever onto a photosensitive detector (Fig. 1.7). For the research presented here, intermittent contact mode (Tapping Mode) will be the primary mode of operation for the AFM. In tapping mode, the cantilever is oscillated close to its resonance frequency. The oscillation amplitude, phase, and resonance frequency are modified by tip-sample interaction forces. These changes in oscillation provide information about the sample's surface characteristics. Tapping mode is gentle enough to preserve the integrity of supported lipid bilayers and membrane associated proteins.[55, 65]

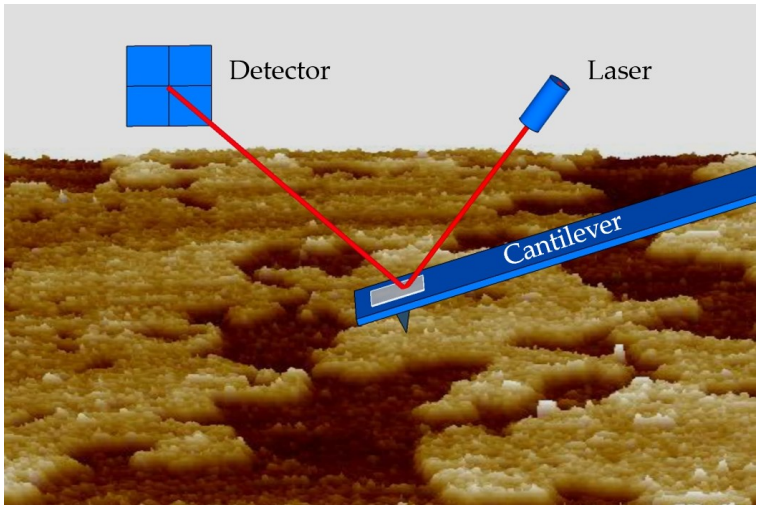

Figure 1.7: Schematic of AFM cantilever scanning SLB surface. For clarity, the fluid cell is omitted. SLB is a 3D rendering of POPC:POPE (1:1) resulting in taller, gel domains in a lower, L_d phase.

The AFM is an essential tool for imaging, measuring, and manipulating matter at the nanoscale and provides sufficiently high, lateral imaging resolution to identify membrane nano-domains and single antibody-antigen complexes.[47] Using AFM we can obtain topography images to visualize antibody-membrane binding at antibody concentrations a factor of 10 less than those typically used in SPR measurements. SPR-based analyses have been a large driving force behind advances in immunogen design. However, there is still a large gap in understanding the lipid reactivity of 2F5/4E10. AFM can complement SPR measurements by resolving how antibodies spatially interact with the viral membrane. AFM is used to reveal complex membrane topography of lipid domains and associated proteins with Ångstrom vertical resolution and approximately 5-10 nm lateral resolution. Here, we have optimized our SLB systems to resolve both

antibody and antigen interactions with domain separated SLBs. Figure 1.8 shows an example AFM height image of a POPC:POPE SLB that contains the gel and L_d phase. The domain height difference is approximately 6 Å.

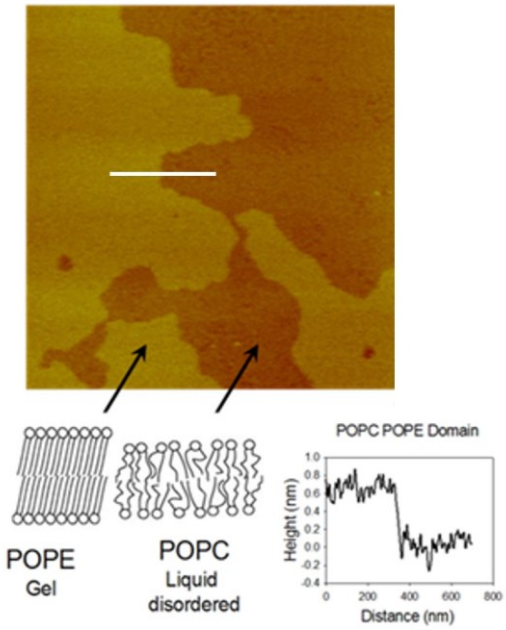

Figure 1.8: AFM height image of SLB domains consisting of POPC:POPE (1:1). The taller (brighter) domain consists mainly of POPE in the gel phase. The lower (darker) domain consists mainly of POPC in the liquid-disordered phase. A 700 nm cross-section at the interface of the two domains (white line on image) reveals a height different of about 6 Å.

1.8.4 Neutron Reflectivity

While AFM can provide high lateral resolution (in-plane) of our SLB platform, it cannot provide information on buried interfaces in the Z, or out-of-plane direction. Thus

we complement AFM imaging with neutron reflectivity (NR) measurements, to provide information on the out-of-plane composition and organization of SLBs and SLB/protein assemblies, with atomic resolution. NR is a surface-sensitive technique that provides molecular-scale information about the structure of interfacial layers perpendicular to an interface.[66] The technique involves shining a highly collimated beam of neutrons onto SLBs and measuring the intensity of reflected radiation as a function of angle or neutron wavelength. The exact shape of the reflectivity profile provides detailed information about the structure, vertical position, and orientation of chemical constituents of the SLB and associated antigens and antibodies.

Applied to SLBs, NR measurements provide additional information compared with traditional reflectivity measurements employing X-rays, for example. Since neutron reflectivity probes nuclear contr3ast, rather than electron density, it is more sensitive than X-ray diffraction for measuring lighter elements found abundantly in biological samples (such as hydrogen, carbon, nitrogen, and oxygen).[67] Isotope sensitivity also allows contrast to be selectively controlled and greatly enhanced to detect antigens and antibodies that contain isotopic labeling.[68] Neutrons are also highly penetrating yet non-perturbing to delicate biological samples such as lipid bilayers and membrane-associated proteins. To gain Ångstrom resolution of biological structures immunologist have typically used X-ray crystallography.[69] Yet membrane proteins have been proven to be extremely difficult to crystallize in their native context of lipid membranes. Thus, a

significant advantage of neutron reflectivity over X-ray crystallography is its ability to gain Ångstrom vertical resolution and conformational details of membrane bound proteins, including weak membrane-associated proteins.

Neutron reflectivity data from SLBs are predominantly analyzed by fitting models of simulated reflectivity profiles to experimental data. The reflectivity simulation relies on modeling the contributions from different parts of the experimental scattering length density profile in a way that describes their distribution along the surface normal direction.[70] The most common and simplest models include layered box models and the optical matrix method,[71] or the Parratt recursion algorithm.[72]

Chapter 2. Screening the Interactions between HIV-1 Neutralizing Antibodies and Model Lipid Surfaces

This research was performed in collaboration with Dr. Yee Lam (Mechanical Engineering and Materials Science) who assisted with experimental design. Shelley Stewart and Kara Anasti (Duke Human Vaccine Institute) performed the SPR experiments.

2.1 Introduction

Despite the significance of 2F5/4E10 lipid reactivity there is little experimental evidence detailing these NAb-membrane interactions. Simple and efficient screening assays are needed to further define these and understand NAb neutralization and autoreactivity, specifically in the context of how exposed chemical groups from lipid membranes help drive antibody interactions. To this end we have developed a surface plasmon resonance (SPR) spectroscopy based assay that monitors antibody binding to thiol monolayers, which mimic salient surface chemical properties of lipid membranes. Specifically, we probed the relative importance of charge and hydrophobicity on antibody-surface interactions. We found that NAb binding to hydrophobic thiol surfaces was significantly greater than that of control monoclonal antibodies (mAbs). Furthermore, we confirmed the importance of charge mediated antibody surface interactions, originally suggested by results from mAb interactions with conventional lipid vesicle/bilayer surfaces. Our approach thus provides an efficient and useful tool to screen interactions of mAbs and lipid-reactive NAbs with a broad range of biologically relevant surface chemistries. The research within Chapter 2 is published in the *Journal of Immunological Methods*.[73]

2.2 Background

In this work, we present a simple screening platform to characterize antibody interactions with chemical mimics of viral and host membrane lipids to better understand antibody-lipid interactions. We employ thiol self-assembled monolayers (SAMs) that exhibit a range of chemical functionalities (namely variations in hydrophobicity and surface charge) presented on common membrane phospholipids of both the native host CD4+ cells and the HIV-1 virion (Fig. 2.1). These thiol SAMs (Fig. 2.1B) present polar (11-mercapto-1-undecanol (MUD)), nonpolar (1-octadecanethiol (ODT)), positively charged (11-amino-1-undecanethiol (AUT)), and negatively charged (11-mercaptoundecanoic acid (MUA)) end-functionality, serving as simple chemical mimics for corresponding lipid head-groups (Fig. 2.1A). Antibody screening was performed by anchoring the thiol SAMs on custom surface plasmon resonance (SPR) sensor chips (depicted in Fig. 2.1C).

It is an important and difficult challenge to develop membrane reactive NAbs that selectively target viral lipids and avoid native host cells. Used with SPR and other biophysical diagnostic tools, our thiol surfaces may provide insight on required chemical structures that could be mimicked on non-human immunogens. Immunogens comprised with non-human components, such as plant lipids, can potentially present chemical groups that will elicit antibodies with similar 2F5/4E10-membrance reactivity,

but yet be different enough in structure to avoid autoreactivity with host cell membranes.

There are many biosensors that effectively probe antibody-membrane interactions. These sensors make use of calorimetry, acoustic (*e.g.*, quartz crystal microbalance), and near-field optical (*e.g.*, SPR) assays.[74] SPR is one of the most powerful sensing assays in that it can provide information on the specificity, kinetics, and affinity of antibody interactions in a label-free environment. This avoids expensive reagents such as fluorescently labelled compounds and secondary antibodies used in standard ELISAs. Recently, significant progress has been made in developing lipid bilayer systems to be used in biosensor assays, including SPR. These model systems include supported lipid monolayers, tethered lipid bilayers,[75] pore-spanning bilayers,[76] and polymer supported lipid bilayers, which have all been engineered to screen protein interactions. However, preparation of these planar lipid systems is not always straightforward. For example, the morphology of model membranes formed on surfaces such as the commonly used SPR Biacore L1 chip, can vary between intact vesicles, a planar lipid bilayer, and even the exposed underlying polymer surface.[74] This variety arises from the complex interplay of the variables that determine whether vesicles rupture to form the desired planar lipid bilayer. Important variables include the temperature, pH, ionic strength and buffer composition, size of the lipid vesicles, lipid transition temperatures, degree of acyl chain saturation, and the presence of cholesterol.

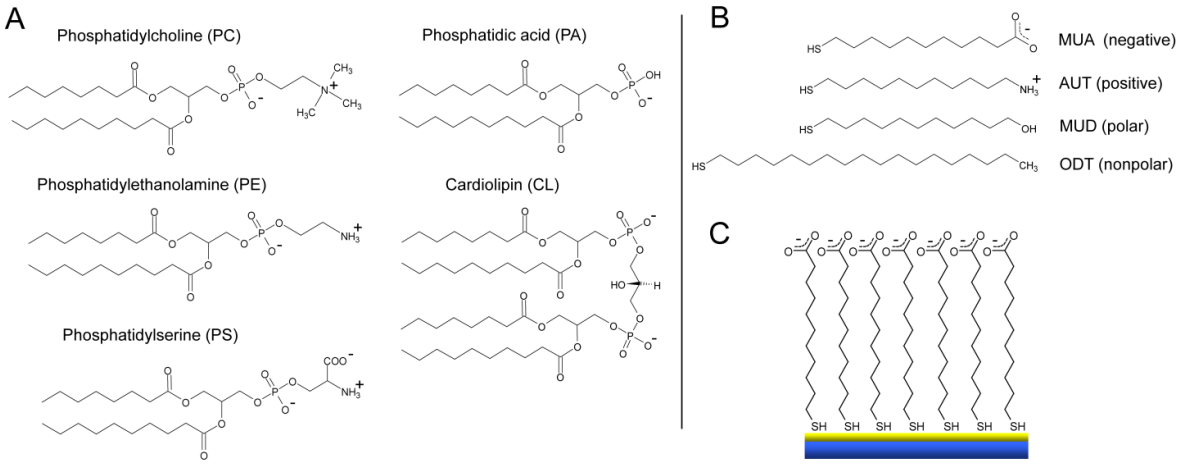

Figure 2.1: Model thiol SPR system. (A) Typical membrane phospholipids, except for cardiolipin. Cardiolipin is most often found in the mitochondria of cells, however, NAbs have been shown to bind cardiolipin. For simplicity, the acyl chain for all lipids is shown saturated with an abbreviated chain length. (B) ω-substituted alkane thiols used to mimic membrane phospholipids. At pH 7.4 thiol monolayers were negatively charged MUA, positively charged AUT, polar MUD, and nonpolar ODT. (C) Schematic of MUA surface on a gold coated SPR sensor chip.

The thiol monolayers prepared here offer a simple alternative to planar lipid bilayers for screening antibody interactions. Thiol surfaces remain stable for months when stored in thiol solution and are economical to produce with high reliability in a large range of screening conditions. Furthermore, the chemical versatility and the well-characterized nature of thiol monolayers also allow distinct chemical groups to be isolated during antibody screening. Our screening platform thus provides an efficient and useful tool not only to study a required step in the mechanism of HIV-1

neutralization, but also to study antibody autoreactivity, especially for newly generated antibodies.

2.3 Results and Discussion

Using SPR spectroscopy, we investigated the binding behavior of a panel of neutralizing (4E10, 2F5), lipid reactive (4E10, 2F5, IS4, IS1, P1), and non-lipid reactive nor neutralizing (A32, 13H11) antibodies (Table 2-1). Antibodies were tested on four model surfaces: negatively charged MUA (contact angle of 33 ± 3°), polar MUD (contact angle of 21 ± 3°), positively charged AUT (contact angle of 60 ± 4°), and nonpolar ODT (contact angle of 104 ± 3°) (Fig. 2.2).

Table 2.1: Panel of screened antibodies and their properties.

Antibody	Description	Lipid Reactivity	Neutralizing Ability
4E10	Human anti-cardiolipin IgG, binds gp41 in MPER	CL, PS, PE, PC, SM [26]	Broad, potent
A32	Human IgG binds gp120	None	None
2F5	Human anti-cardiolipin IgG, binds gp41 in MPER	CL [26]	Broad, potent
13H11	Murine mAb binds gp41 in overlapping region of MPER with 2F5. Blocks 2F5.	None	None, control
IS4	Human anti-phospholipid syndrome IgG,	CL [77]	None
IS1	Human anti-phospholipid antibody	CL, POPS [78]	Unpublished
P1	Human anti-cardiolipin IgG	CL (personal communication, S. Alam)	Unpublished

2.3.1 Antibody Screening on Thiol Surfaces

Representative SPR curves, in which response units (RU) are plotted as a function of time, are shown in Figures 2.2A-C. The low levels of 13H11 binding on all surfaces, seen in representative SPR curves (Fig. 2.2C), was attributed to nonspecific interactions. Although 13H11 shares an epitope on viral envelope protein gp41 with 2F5, it is not known to be lipid reactive. Thus, the binding response of 13H11 was subtracted as background from all experiments. The average amount of all antibodies which remained bound following one injection cycle is shown for each of the four model surfaces (Fig. 2.3). These data demonstrate that our simple and versatile model surfaces are able to differentiate between NAb binding and binding of other mAbs.

Both 2F5 and 4E10 bound at highest levels to hydrophobic ODT surfaces and had significantly higher binding compared to all other antibodies tested (Figs. 2.2A-B, and Fig. 2.3). These results are supported by structural information which shows that the CDR3 region on NAbs 4E10 (EGTTGWGWLGKPIGAFAH)[79] and 2F5 (RRGPTTLFGVPIARGPVNAMDV)[80] contain unusually large numbers of hydrophobic and membrane reactive residues (underlined). 4E10's CDR3 contains zwitterionic tryptophan residues that not only interact with polar head groups but can also embed into the hydrophobic bilayer.[81] 2F5 bound significantly less on hydrophobic ODT than 4E10, but binding was still significantly elevated relative to all other antibodies. This result was expected as 2F5's lipid reactivity is less, relative to that

of 4E10.[26] The relative binding levels of 2F5 versus 4E10 on ODT were also similar to binding levels on cardiolipin seen in previous ELISA studies (roughly 1:2).[26]

The SPR screening of NAb 4E10 showed strongest binding on hydrophobic ODT surfaces (Fig. 2.3A) followed by positive AUT (Fig. 2.3D), then negative MUA (Fig. 2.3B). This suggests that if 4E10 is able to penetrate into the membrane bilayer, hydrophobic interactions may dominate its membrane interactions. Furthermore, these results indicate that charge interactions likely contribute to lipid binding as well. 4E10's high affinity to anionic cardiolipin demonstrates this potential charge effect.[26]

Human mAb A32 binds a site far from the lipid membrane on viral envelope protein gp120, and is not known to be lipid reactive. A32 had weak binding to all thiol surfaces, with no particular preference for any one model surface. The lipid reactive CDR3 in IS4 contains positively charged arginine residues,[77] and during IS4 screening, the highest binding response occurred on negatively charged MUA thiols (Fig. 2.3B). Furthermore, mAb IS1 is known to interact with cardiolipin and (1-palmitoyl-2-oleoyl-sn-glycero-3-phospho-L-serine) POPS, which are both negatively charged. This apparent preference for negatively charged lipids is recapitulated by IS1 binding most strongly to negative MUA thiols. mAb P1 interacts with negatively charged cardiolipin, which is also recapitulated by comparable levels of binding to negatively charged thiols. These antibody-binding observations are consistent with a charge based interaction mechanism.

These results demonstrate that simple, well-characterized self-assembled thiol monolayers on gold present a surface capable of distinguishing between broadly neutralizing and control antibodies as well as discern the salient aspects of antibody-lipid interactions.

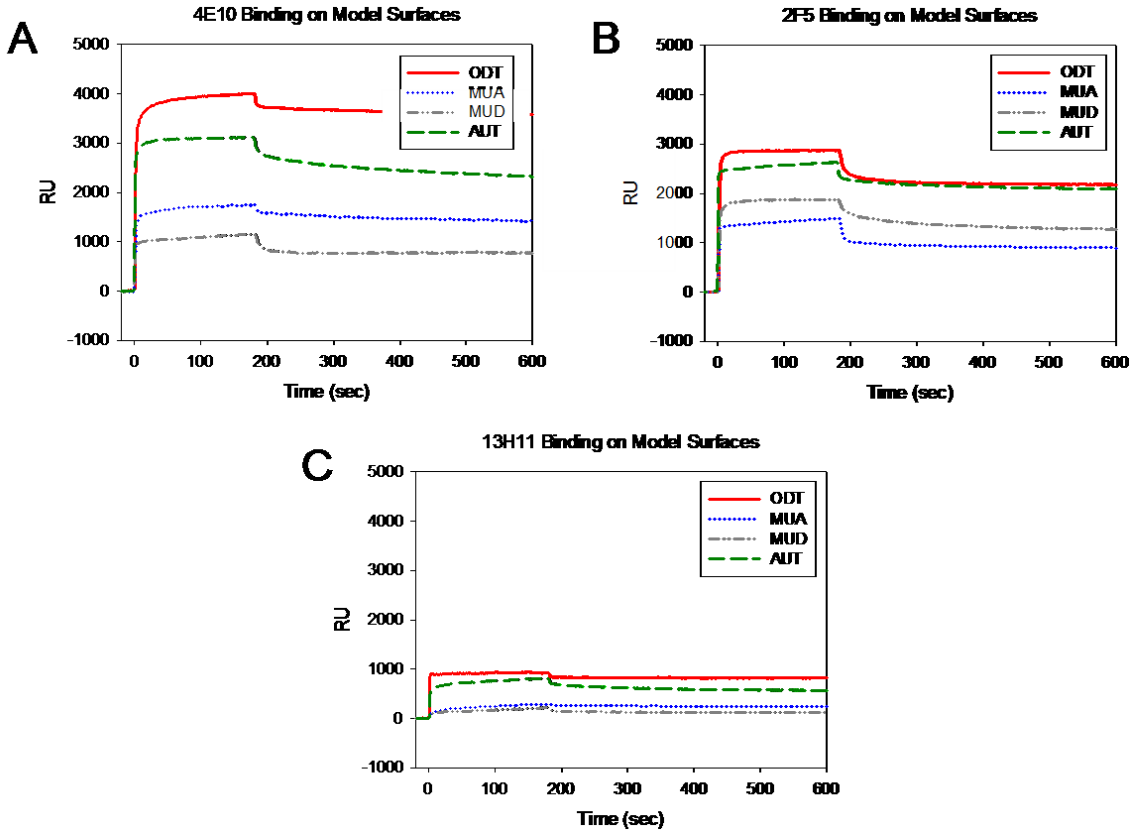

Figure 2.2: Antibody-thiol SPR binding curves. (A-C) Representative SPR response curves for 4E10, 2F5, and 13H11 to model surfaces.

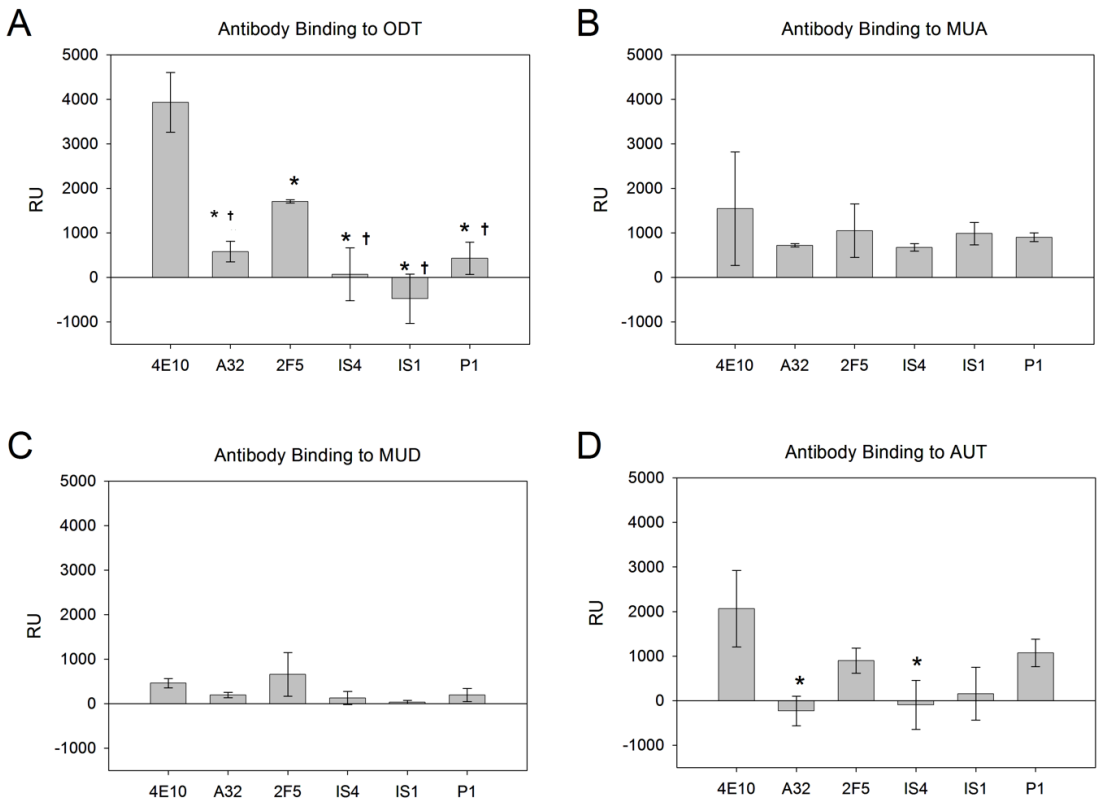

Figure 2.3: Mean RU value from each antibody grouped for each of the four thiols used (n=3). * Signifies statistically significant ($p<0.05$) when compared to 4E10. † Signifies statistically significant ($p<0.05$) when compared to 2F5. The negative amount of bound antibody is due to RU levels below 13H11 background, which was attributed to nonspecific interactions and subtracted from all RU values.

2.3.2 Antibody Binding on Lipid versus Thiol Model Surfaces

To further investigate the binding behavior of our antibodies, we prepared lipid surfaces using POPS liposomes on a commercially available L1 chip (Biacore, Sweden). Notably the topography of these lipid surfaces is not clearly defined, possibly presenting a vesicular surface and/or planar lipid bilayer.[74] We monitored binding of 4E10, 2F5, IS4, and IS1 to this more physiologically relevant POPS lipid surface (Fig. 2.4A) to

compare with the binding behavior on the model MUA thiol surface (Fig. 2.4B). All kinetic data (Fig. 2.4C) was fitted using a bivalent analyte model to incorporate the bivalent nature of antibody binding. 2F5 binding to POPS was below baseline behavior (similar to A32 and 13H11 binding) preventing the accurate calculation of kinetic data.

The MUA surface packing density is approximately three times greater than that of POPS surfaces due to the tightly packed thiol groups.[82, 83] We thus expect that densely packed thiol surfaces also exhibit a higher surface charge density compared to that of the lipid surfaces. Specifically, a charge-based interaction is likely for mAbs IS1 and IS4, which have a positively charged membrane-reactive region, and could thus explain why MUA surfaces had overall slightly higher antibody binding compared with the lipid surfaces. Importantly, however, the binding order of IS1, IS4, and 2F5 was consistent between the thiol and lipid surfaces, with IS1 binding the highest followed by IS4 and 2F5, respectively. Furthermore, the half-life of IS1 and IS4 correlated well between the POPS and MUA surface. These results are consistent with known antibody properties. For example, IS1 and IS4 bind strongly to negatively charged cardiolipin. Additionally, 2F5 is known to interact only weakly with POPS,[26] and bound at lowest levels on both POPS and MUA surfaces. On MUA, 4E10 bound at relatively higher levels than IS1. While 4E10 and IS1 reached an equivalent average steady state association on POPS, 4E10 exhibited much larger variability on the MUA surface (Fig. 2.3B). Taken

together, these observations suggest that the interaction characteristics of mAbs with both the thiol and lipid surfaces are largely conserved.

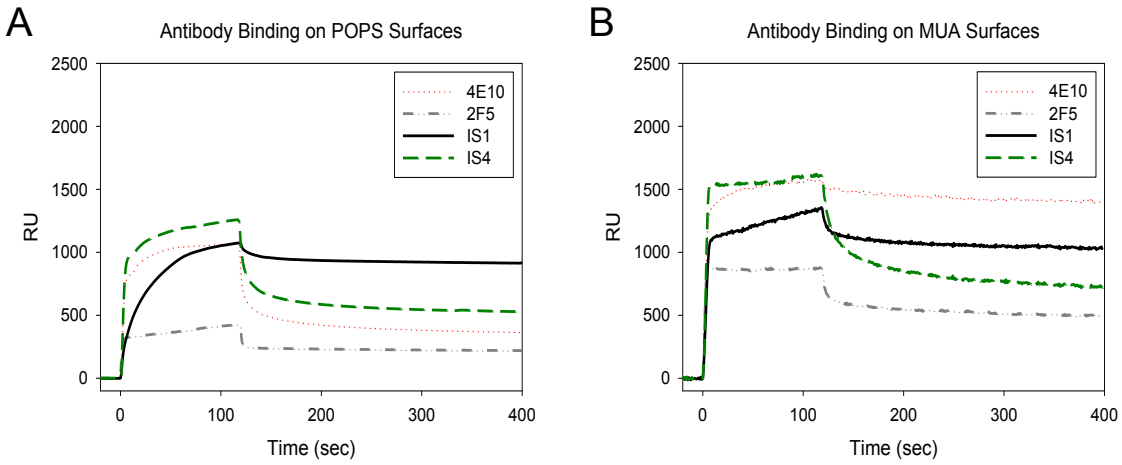

C

	POPS			MUA		
Antibody	**Rmax (RU)**	**Kd (M)**	**half life (min)**	**Rmax (RU)**	**Kd (M)**	**half life (min)**
4E10	940	6.00E-06	1.1	2730	5.07E-07	5.3
IS4	1180	1.30E-06	1.6	1550	4.11E-08	2.7
IS1	1500	9.60E-07	23	1430	3.30E-08	25.4

Figure 2.4: 4E10, 2F5, IS1, and IS4 binding on standard lipid surfaces versus thiol model surfaces. (A) Representative SPR response curves for antibodies on negative POPS. (B) Representative SPR response curves for antibodies on negative MUA. (C) Kinetic properties of antibodies binding on lipid (POPS) and thiol (MUA) model surfaces. Analysis for 2F5 was not performed due to below background binding.

2.4 Conclusions

The model surfaces used here admittedly lack many characteristics of the complex lipid bilayer including, membrane proteins, lipid heterogeneity, and membrane mobility. Nevertheless, by simply mimicking lipid chemistry these thiol substrates

allowed us to isolate and distinguish chemical groups that could potentially contribute to specific antibody-lipid interactions. Our results showed that only 2F5 and 4E10 bound strongly to hydrophobic thiols. This observation correlates with findings that suggest that 2F5 and 4E10 embed into the hydrophobic membrane core. This NAb-lipid interaction could then facilitate NAb's ability to diffuse within the viral membrane, positioning the NAb to more likely encounter its sparse MPER antigen. We note, however, that the NAb's high affinity for hydrophobic ODT could be attributed to structural conformations (denaturation) of the NAb, which may not occur at the membrane interface. Regardless, this information translates to vaccine design by suggesting that immunogens designed to elicit 2F5/4E10-like antibodies may require an accessible hydrophobic component available for B-cell receptor recognition.

The hydrophobic ODT surface clearly distinguished between neutralizing and non-neutralizing antibodies, both lipid reactive and non-lipid reactive, and thus, is promising as a proficient screening platform for broadly neutralizing mAbs that are designed to replicate 2F5 and 4E10's neutralizing breadth and efficacy. If these antibodies have similar binding interaction to ODT thiol surfaces as 2F5/4E10, then they may also possess the same broadly neutralizing ability as 4E10/2F5. In order to determine if specific chemical groups have cooperative effects, the complexity of the model system can be increased by creating mixed monolayer systems or by introducing

different end-functionalized thiols. Peptides specific for 4E10 or 2F5 could also be incorporated into the model surface system via covalent attachment.

In conclusion, the surface chemical diversity that can be achieved with thiol SAMs provides a useful and simple platform for screening a wide variety of monoclonal antibodies for 2F5/4E10-like lipid reactivity. These model surfaces also provide a method to infer the importance of different chemical functionalities on NAb-lipid interactions. Such information may contribute to a more complete mechanistic understanding of HIV-1 neutralization as provided by 2F5 and 4E10, and ultimately help guide vaccine design efforts.

2.5 Materials and Methods

2.5.1 Antibodies

Human mAb A32 against HIV-1 envelope gp120 was the generous gift of James Robinson, Tulane University, New Orleans, LA and was purified as previously described.[84] Anti-HIV-1 gp41 (anti-membrane proximal) NAbs 4E10 and 2F5 were purchased from Polymun, Inc., Vienna, Austria. Anti-cardiolipin mAbs IS4 and IS1 were provided by Pojen Chen, University of California, Los Angeles and were derived from an APS patient. Hybridomas were generated as previously described.[85] Mouse mAb 13H11 was produced from splenocytes from a mouse immunized with HIV-1 envelope oligomer CON-S[86], as described.[84] P1 was purified using Protein A / Protein G

immunoaffinity. All mAbs were purified by affinity chromatography on anti-immunoglobulin columns.[87]

2.5.2 Lipid Preparation

Palmitoyl oleoyl phosphatidyl serine (POPS) in chloroform (Avanti Polar Lipids) was brought to room temperature for one hour, dried under nitrogen for five minutes, and then dried under vacuum for three hours. The lipid film was reconstituted in 37 °C PBS without Ca^{2+} and Mg^{2+}, pH 7.4 (Gibco Invitrogen, Grand Island, NY), vortexed, sonicated, and extruded 11 times through first a 0.4 μm filter (Whatman, Florham Park, NJ), and then through a 0.1 μm filter (Whatman).[88] The concentrated lipid solution was then diluted to 0.1 mg/ml in PBS w/o Ca^{2+} and Mg^{2+} and vortexed immediately before use. Lipid solutions were used within eight hours after extrusion.

2.5.3 Model Surface Preparation

Glass cover slips (VWR) were first cleaned for 30 minutes using a "Piranha" solution (1:3 H_2SO_4: H_2O_2) and then rinsed copiously with deionized water and dried under nitrogen. Finally, 5 nm chromium and 45 nm gold were evaporated onto their surface. The coated glass cover slips were sonicated in ethanol before being incubated in 1 mM solutions of mercaptoundecanoic acid (Sigma), mercaptoundecane thiol (Sigma), aminoundecanethiol (Dojindo), or octadecanethiol (Sigma) for at least 12 hours, and up

to one month. Before each experiment, slides were sonicated in thiol solution, rinsed with ethanol, and dried with nitrogen. They were then immediately mounted into BIAcore cassettes (BIAcore Inc.), and placed in a BIAcore 3000 or 1000 instrument for SPR measurements.

2.5.4 Surface Plasmon Resonance

Surface plasmon resonance (SPR) measurements were performed on a BIAcore 3000 or 1000 (BIAcore Inc., Uppsala, Sweden) instrument. BIAevaluation 3.0 software (BIAcore Inc.) was used to evaluate the data assuming a bivalent analyte model. For model surfaces, binding of proteins was monitored in real-time at 25^{o}C with a continuous flow of PBS, pH 7.4 (Gibco Invitrogen, Grand Island, NY) at 5 μl/min. For lipid surfaces, POPS liposomes were incubated on a BIAcore SPR L1 chip. A blank in-line reference surface was used to determine non-specific or bulk responses. Bound protein was removed from the liposome sensor surfaces following each cycle of mAb binding by octyl β-D glucopyranoside, and 5 s injections each of 5 mM HCl then 5 mM NaOH.

Chapter 3. Techniques to Form Complex Biomimetic Supported Lipid Bilayers via Vesicle Fusion

3.1 Introduction

Vesicle fusion has long provided an easy and reliable method to form supported lipid bilayers (SLBs) from simple, zwitterionic vesicles on siliceous substrates. However, for complex compositions, such as vesicles with high cholesterol content and multiple lipid types, the energy barrier for the vesicle-to-bilayer transition is increased or the required vesicle-vesicle and vesicle-substrate interactions are diminished. Thus, for vesicle compositions that more accurately mimic native membranes, vesicle fusion often fails to form SLBs. In Chapter 3 we review two approaches to overcome these barriers to form complex, biomimetic SLBs via vesicle fusion: (i) optimization of experimental conditions (*e.g.*, temperature, buffer ionic strength, osmotic stress, cation valency, and buffer pH), and (ii) α-helical (AH) peptide-induced vesicle fusion. Collectively, this chapter introduces vesicle fusion techniques that can be generalized for many biomimetic vesicle compositions and many substrate types, and thus will aid efforts to reliably create complex SLB platforms on a range of substrates. The information within Chapter 3 is published in *Current Opinion in Colloid and Interface Science*.[89]

.

3.2 Background

Native plasma membranes contain a complex, heterogeneous distribution of lipids and membrane proteins which interact to create important biological functions. To investigate this complex membrane environment significant progress has been made to model native membranes. The most common systems include lipid monolayers, lipid vesicles, and supported lipid bilayers (SLBs). While each system has its advantages, SLBs are particularly valuable due to their ease of formation and their lipid arrangement. SLBs constitute a single lipid bilayer on a solid substrate, typically glass, silica, or mica. The hydrophilic head groups of one lipid leaflet face the substrate where they are separated by a thin hydration layer. Their hydrophobic acyl chains interact with the acyl chains of the second lipid leaflet, whose hydrophilic head groups face the bulk solution and are available to interact with analytes (proteins, cells, nanoparticles, etc.). The SLB is stable and confined in two dimensions to the substrate surface, yet it can recapitulate the lateral lipid diffusivity of native cell membranes. Furthermore, the planar orientation of SLBs allows the use of many quantitative surface characterization techniques that are able to provide unique insights into membrane functions.

There are many techniques to create SLBs, including Langmuir-Blodgett/Schäfer deposition,[90] spin coating,[91] microcontact printing,[92] solvent-exchange deposition,[93] lipid-surfactant micelles,[94] evaporation induced assembly,[95] bubble collapse deposition,[96] lipid dip-pen nanolithography,[97] and vesicle fusion.[98]

Langmuir-Blodgett/Schäfer (LB/LS) deposition and vesicle fusion are perhaps the most commonly used techniques to form SLBs. Briefly, LB/LS deposition is achieved by transferring a lipid monolayer contained at an air-liquid interface to a solid substrate. The substrate is passed through the lipid monolayer a second time to assemble the final SLB. SLB formation via vesicle fusion typically occurs by adsorption of lipid vesicles to a substrate, followed by vesicle rupture, fusion, and bilayer spreading. Of these techniques, vesicle fusion is the most simple, versatile, and widely accessible since it does not require sophisticated equipment to produce high quality SLBs. These advantages position vesicle fusion to play an important role in advancing SLB research platforms, particularly in regards to creating complex, multi-component SLBs that more accurately mimic native cell membranes. Thus, this chapter will focus on vesicle fusion techniques to form complex SLBs. Other SLB forming techniques and model lipid systems are discussed in recent review articles.[99, 100]

SLBs that contain one or two zwitterionic lipid types, and are supported on siliceous substrates (*e.g.*, glass, silicon oxide, or mica), have long provided the foundation of model SLB systems.[101] These simple SLBs have been exceptionally successful at mimicking the basic structure and dynamics of the plasma membrane; however, they fail to capture the highly complex lipid environment that often determines native biological functions. For example, there are about 100 lipid species in the simple red blood cell alone, and more than 600 lipid species in most plasma

membranes.[102] Considering this extensive membrane diversity, SLBs with one or two lipid types can be inadequate when attempting to accurately model native cell membranes.

Successful SLB formation via vesicle fusion largely depends on the lipid components of the vesicles being used. In attempts to increase SLB complexity, such as by incorporating cholesterol, charged lipids, or phase separating lipid compositions, complete SLB formation may no longer occur.[60, 61] This restricts the utility of SLBs created from vesicle fusion by limiting their compositional complexity to simple binary or tertiary lipid compositions containing little or no cholesterol. Cholesterol is often neglected or underrepresented in biomimetic SLBs because it can prevent vesicle fusion and subsequent SLB formation by increasing vesicle rigidity.[60] However, cholesterol is an essential component of plasma membranes, ranging from 15-50% of total lipid composition.[102] In native plasma membranes, cholesterol provides an important structural role by condensing acyl chains of unsaturated lipids in fluid lipid phases, and fluidizing saturated lipids that would otherwise form solid-like gel phases. Regions of cholesterol- and sphingolipid-enriched domains, termed lipid rafts,[103] are also believed to exist in plasma membranes, where they contribute to compartmentalizing cellular processes. Lipid rafts are associated with the function of many membrane proteins and are directly linked to important pathologies including those of the central

nervous system,[104, 105] viral infections,[106, 107] cardiovascular disease,[108] and certain types of cancer.[109]

Despite the difficulties in forming complex SLB systems, several vesicle fusion approaches have the capability to create SLBs with multiple lipid types and high cholesterol content on a range of substrates. In this chapter, we summarize two approaches to induce complex SLB formation: (i) optimizing experimental conditions, including temperature and buffer selection and (ii) the use of α-helical (AH) peptides acting as a vesicle fusion catalyst. These approaches were selected due to their potential to advance the use of biomimetic SLB platforms by easily achieving SLB formation on a range of substrates and under conditions that would otherwise be unfavorable.

3.3 Mechanism of Vesicle Fusion

The mechanism of vesicle fusion will be briefly discussed to understand the barriers to SLB formation and how they can be overcome. Although not completely understood, the mechanism of vesicle fusion is believed to be a two-step process that relies on membrane tension, vesicle-vesicle and vesicle-substrate interactions, as shown in Figure 3.1.[59, 110] Small unilamellar vesicles are first adsorbed to a substrate surface. Vesicle crowding ensues and after a critical concentration (θ_c) of surface-adhered vesicles is reached, vesicles will rupture and fuse with each other, forming SLB patches on the substrate. The energetically unfavorable edge of SLB patches can spread on the

surface and induce rupture of adsorbed vesicles to form a complete SLB (Fig. 3.1). Although one-step SLB formation by direct vesicle rupture is possible for certain combinations of vesicles, buffers, and substrates,[111] the surface-induced stress alone is often insufficient for vesicle rupture.

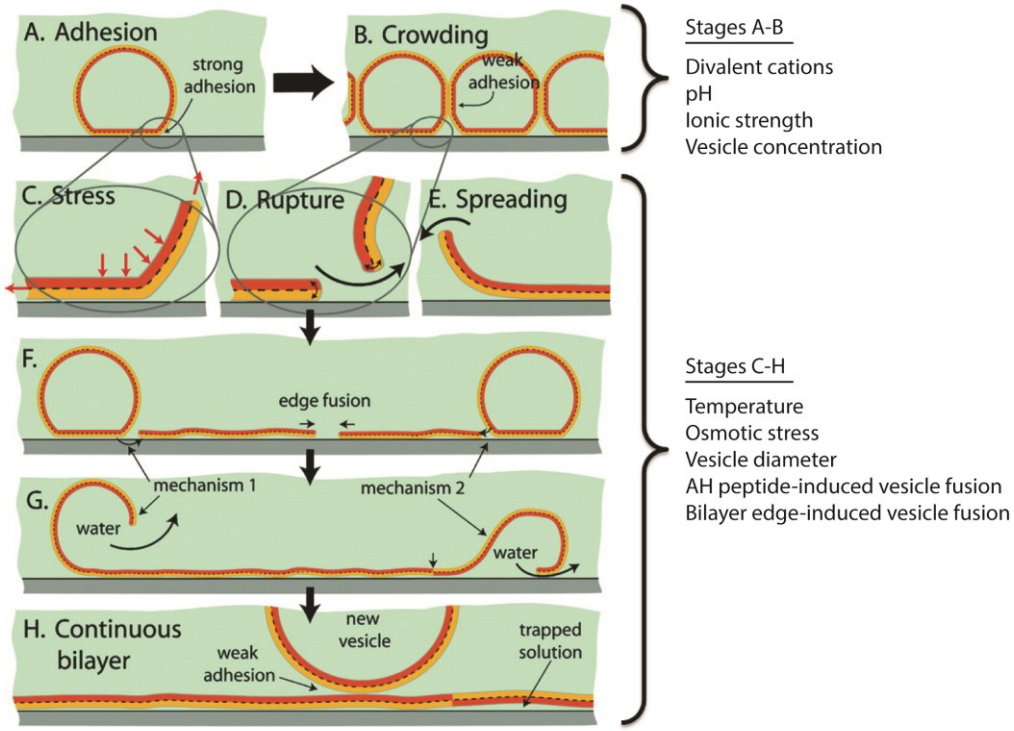

Figure 3.1: Stages of SLB formation: (A) adhesion, (B) crowding, (C-E) rupture and spreading of bilayer patches that can expose either leaflet by mechanism 1 or 2, (F, G) coalescence of high energy edges and release of water/excess lipid, and (H) completed SLB. Additional vesicle adsorption to the SLB is typically weak and does not lead to their rupture or spreading. Experimental conditions and techniques that generally have the most pronounce effect on respective stages of SLB formation are listed to the right of the figure. Substrate type and chemical surface modifications are omitted from classification since these conditions generally affect the entire SLB formation process. Adapted with permission from reference [112]. Copyright (2009) American Chemical Society.

The transition from vesicles to a SLB is most commonly observed with quartz crystal microbalance with dissipation monitoring (QCM-D).[113] In this chapter, QCM-D results will be used to discuss the effectiveness of vesicle fusion techniques. Additional mechanistic detail and description of the vesicle to SLB transformation can be found in Chapter 1, section 1.8.1.

3.4 Experimental Optimization Techniques to Achieve Vesicle Fusion

Although SLB formation via vesicle fusion is a reliable and easy technique for many vesicle compositions, it is still a complex, dynamic, and highly sensitive process. As researchers attempt to increase complexity of SLB platforms, additional steps or alternative techniques become necessary to induce SLB formation. Favorable SLB formation by conventional vesicle fusion largely depends on the substrate type and lipid composition of the vesicles, where lipid charge, polarity, head group size, acyl chain length, and degree of unsaturation ultimately all contribute to the ease of vesicle fusion and subsequent SLB formation. However, for researchers attempting to use SLBs to model native membranes the compositional ratios and lipid types of a vesicle are largely fixed. Yet, the experimental conditions in which vesicle fusion takes place can often be optimized to achieve SLB formation for a wide range of vesicle compositions. Conditions that are commonly manipulated include vesicle size,[57] vesicle

concentration,[101] temperature,[114] pH,[115] flow conditions (batch or flow system),[116] exposure to buffers of different ionic strengths,[117] the type of substrate material,[116] and chemical surface modifications.[59] It is commonly observed that experimental conditions that work for one vesicle composition, may fail to work as well for that of another vesicle composition. However, there are a few variables that are generally more important than others since they can be successfully applied to a wide range of vesicle compositions to promote vesicle fusion. These include temperature, buffer pH, buffer ionic strength, ion type, and osmotic stress.

3.4.1 Effect of Temperature

The critical surface coverage of vesicles required for SLB formation has been shown to be temperature dependent, thus indicating that vesicle rupture is a thermally activated process.[114] For example, Reimhult et al. have shown that a decrease in temperature requires a higher critical coverage (θ_c) of surface adhered vesicles (*i.e.*, an increase in vesicle-vesicle interactions) to induce fusion, and increases the time to transition from intact vesicles to SLBs.[98] Furthermore, temperature also affects the lipid phase, which can play a critical role for vesicle fusion. A phase change into a more fluid vesicle can promote SLB formation, especially when the temperature change involves passing through a chain melting temperature (T_m) of one of the lipid components.[101] The chain melting temperature defines the transition of a lipid from

one phase to another *i.e.*, from the gel to the liquid-disordered (L_d) phase. Vesicles with lipids in the gel phase contain higher order compared to the L_d phase and are believed to resist vesicle fusion due to decreased lipid mobility and vesicle-vesicle interactions. Thus, using vesicles in the liquid phase by raising the temperature approximately 15 °C above the highest lipid T_m is a common and successful strategy for achieving reliable SLB formation.[98, 114]

In addition to lipid structure, the presence of cholesterol and sphingolipids can also result in vesicle phase separations as they have the tendency to self-associate within the L_d phase to form highly ordered, tightly packed islands, known as liquid-ordered (L_o) domains or lipid rafts.[118] For instance, POPC:cholesterol (55:45) undergoes a phase transition in the temperature range between 15-35 °C.[53] At 15 °C the lipid bilayer is completely in the L_o phase while between 25-35 °C the L_o and L_d phases co-exist. With increasing temperature the L_d phase increases, resulting in shorter times to reach θ_c, peak Δf and ΔD amplitudes decrease, and final Δf and ΔD values approach those of pure POPC vesicles.[61] Thus, a temperature increase has been successful in achieving SLB formation from vesicles containing as much as 50 mol% cholesterol.[119] Without heating, vesicles may fail to consistently form SLBs when containing cholesterol compositions above 33 mol%.[120] Therefore, for vesicles containing cholesterol, raising the temperature to increase the L_d phase may assist in achieving reliable SLB formation.

Using elevated temperature to prepare SLBs via vesicle fusion is one of the most frequently used techniques. However, depending on the vesicle composition, the use of temperature alone can be insufficient to induce vesicle fusion. Furthermore, this technique is not appropriate when using temperature sensitive membrane components, such as membrane embedded proteins. In such instances, researchers are referred to alternative techniques discussed below.

3.4.2 Effect of pH

Initial vesicle-substrate interactions are often the limiting factor in determining whether successful SLB formation occurs. Whether these interactions are sufficient for SLB formation largely depends on electrostatic forces between the lipid vesicles and substrate surface.[111] Generally, to readily achieve vesicle fusion, electrostatic attraction between vesicles and the substrate surface should be enhanced. If attractive electrostatic interactions are not possible, then repulsive electrostatic forces should be minimized. This can allow van der Waals, steric, and hydration forces to dominate surface interactions which can be sufficient to promote bilayer formation.

Electrostatic forces play an important role in creating biomimetic SLBs because most native cell membranes contain negatively charged lipids (yielding a surface charge of ~ –0.05 C/m^2)[121] and SLBs are most commonly formed on negatively charged mica and silica substrates. This repulsive electrostatic interaction results in an increase in θ_c

required for vesicle rupture and, depending on the concentration of negatively charged lipid, may prevent SLB formation entirely.[116] An effective technique for tuning the electrostatic interactions between vesicles and the substrate surface is to adjust the buffer pH (under constant ionic strength). The buffer pH influences the state of lipid charge by affecting the degree of ionization, reflected in the lipid's pK_a. This pK_a is largely determined by the lipid head group acid-base chemistry.

Here, we present a general guideline for using buffer pH (with ionic strength ≈ 100 mM NaCl) to minimize the negative charge of common lipid types.[122] For example, common negatively charged lipid head groups include phosphatidylserine (PS), phosphatidylinositol (PI), phosphatidic acid (PA), and phosphatidylglycerol (PG). PS has pK_as at 2.6, 5.5, and 11.5, requiring a pH < 6 to diminish its charge of –1 and at pH < 4, PS will begin to have a net positive charge. PI, PA, and PG have a pK_a at 2.5, 3.0, and 3.5, respectively. Thus, each lipid type will begin to diminish its charge of –1 at pH < 4. Furthermore, common zwitterionic lipids include those with a phosphatidylcholine (PC) or phosphatidylethanolamine (PE) head group. PE has pK_as at ~1.7 and 9.8, resulting in a neutral charge between pH ≈ 3–9. PC has one pK_a at ~1.0 and will be neutral for any pH > ~3.[122] Positively charged lipids (at pH = 7) are not commonly used to model native cell membranes; however, when using negatively charged surfaces (*e.g.*, silica or mica) vesicle-substrate interactions can be enhanced by strategically incorporating positively charged membrane components (*e.g.*, peptides, lipids, or fluorescent probes) within the

vesicles. As little as 1 mol% of positively charged membrane probe can be effective at inducing SLB formation.[123]

Buffer pH can also affect the ionization of hydroxyl groups that exist on surface oxides commonly used for SLB formation (*e.g.*, mica, silica, and titanium oxide). At a certain pH, known as the point of zero charge (pzc), the surface charge is approximately zero. At a pH above its pzc value, a surface is generally negatively charged, while at a pH below the pzc the surface is generally positively charged. For silica and mica surfaces, the pzc is ~1.5 – 3.5, while the pzc of titanium oxide is ~6.5.[124] Thus, using a pH at or below the pzc value, can diminish repulsive vesicle-substrate interactions and enhance vesicle adsorption and subsequent SLB formation for negatively charged vesicles.

Cho et al. demonstrates how oxide surfaces are affected by pH and ultimately control successful vesicle fusion. SLB formation was monitored in various buffer pH (with 200 mM NaCl) using zwitterionic POPC vesicles on silicon and titanium oxide surfaces.[115] For POPC vesicles on silicon oxide at a pH ≥ 10.0 an irreversibly adsorbed vesicle monolayer is formed, with no subsequent vesicle fusion. At pH = 7.5, however, a SLB is formed, as expected, in two successive steps. At a pH ≤ 6.0, SLB formation approaches one-step behavior, indicating a decreasing role of vesicle-vesicle interactions required for rupture. POPC vesicles on titanium oxide, which showed weaker vesicle-substrate interactions than silicon oxide, form an irreversibly adsorbed vesicle

monolayer already at pH = 7.5, again with no subsequent vesicle fusion. However, at pH = 4.0 the vesicle-substrate interactions are strong enough to generate isolated SLB patches mixed with adsorbed vesicles, and at pH = 2.5, a complete bilayer finally forms. These results demonstrate that stronger vesicle-substrate interactions often occur at low pH and that oxide surfaces have titratable OH groups that control the surface charge density, which plays an important role in the adsorption and fusion of vesicles.

3.4.3 Effect of Ionic Strength and Ion Type

Closely linked to surface charge is the surface potential, which also needs to be considered when evaluating vesicle fusion interactions. The lipid surface potential is best approximated by the ζ potential, which describes the charge seen at a distance from the surface, where the Stern layer and diffuse layer meet. The ionic strength of the buffer plays an essential in role in determining the ζ potential and is likely the major reason why zwitterionic vesicles fail to adsorb to and fuse on substrates in deionized water. For example, Anderson *et al*. demonstrated that adhesion and fusion of DMPC vesicles on silica decreased with decreasing ionic strength, and below a critical ionic strength of about 1.5 mM no longer formed SLBs.[101] Even though DMPC is theoretically zwitterionic over a broad range of pH values, due to head group orientation[125] and hydration layers surrounding the head group surface,[126] PC has a negative ζ potential of ~ –12 mV in deionized water.[127] As the ionic strength increases, the ζ potential

increases because cations adsorb to the surface of the polar lipid head group. At a high ionic strength, the ζ potential of PC becomes positive and vesicles readily adsorb and fuse on negatively charged substrates.[127]

Presence of divalent ions can also influence the formation of SLBs, especially for vesicle compositions containing charged lipid head groups or charged membrane embedded peptides. Divalent cations stabilize vesicle-substrate interactions between the negatively charged lipid head groups and negatively charged substrates by charge bridging.[128] For example, calcium (Ca^{2+}) and magnesium (Mg^{2+}) ions are common divalent cations used to promote SLB formation with negatively charged vesicles.[117, 129, 130] Already at concentrations as low as 25 μM, Ca^{2+} ions contribute significantly to vesicle fusion.[123] It is important to introduce divalent cations only during the vesicle-substrate adsorption step. If introduced earlier, divalent cations can inhibit SLB formation by promoting vesicle-vesicle interactions, which leads to vesicle aggregation and an increase in vesicle polydispersity.

An example of how ionic strength and pH have a pronounced effect on SLB formation is given by Cremer and Boxer.[123] Using positively and negatively charged vesicles on borosilicate, SLB formation was monitored while varying the pH and ionic strength of a sodium phosphate buffer. For negatively charged vesicles, they observed that SLB formation occurred at high ionic strengths and low pH, but was inhibited at low ionic strength and high pH (Fig. 3.2A).[123] The low pH likely reduced negative

charge density of the substrate and the high ionic strength likely shielded repulsive vesicle-vesicle and vesicle-substrate electrostatic interactions. As the pH of the buffer is raised (or the ionic strength is lowered) electrostatic repulsion increases and eventually overcomes the attractive forces, thus inhibiting SLB formation.

However, SLBs formed from positively charged vesicles readily form on negatively charged substrates, often regardless of the pH and ionic strength used. Cremer and Boxer showed that positively charged vesicles formed SLBs at all pH values and ionic strengths measured (Fig. 3.2B).[123] Furthermore, with attractive electrostatic interactions, SLB formation can occur in one step, as the vesicle-substrate interaction alone can be sufficient to cause vesicle rupture.[58]

When using pH and ionic strength conditions conducive to vesicle fusion, it is important to realize that once a SLB has been formed, the buffer can be changed to one that more accurately mimics physiological conditions. This does not adversely affect bilayer adhesion or stability.[123] Thus, inducing vesicle fusion under low pH and high ionic strength conditions with a subsequent buffer change represents a practical technique to promote vesicle fusion.

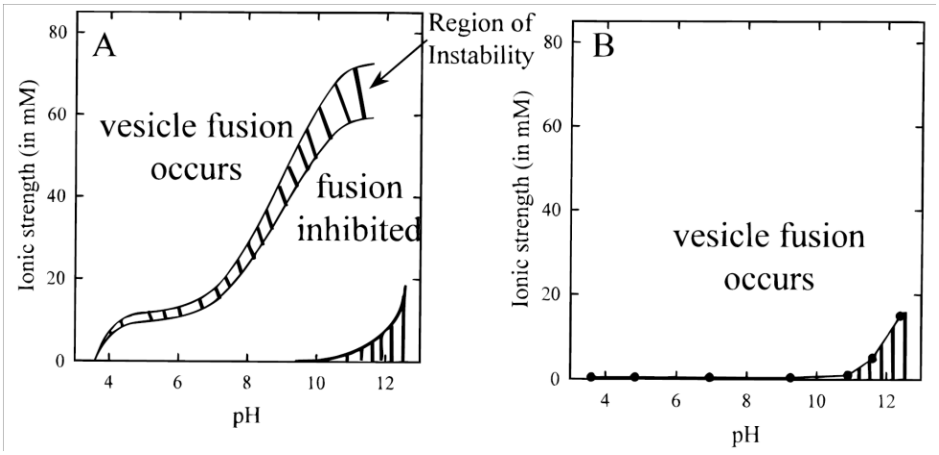

Figure 3.2: Vesicle fusion phase diagrams for egg PC vesicles containing: (A) 1 mol% of negatively charged lipid probe and (B) 1 mol% of positively charged membrane probe. Regions of vesicle instability and incomplete SLB formation are indicated by the crosshatched area in (A). The regions with vertical stripes in the lower right corner of both diagrams indicate conditions where buffer formation was not possible. Reprinted with permission from reference [123]. Copyright (1999) American Chemical Society.

3.4.4 Effect of Osmotic Stress

Increasing vesicle membrane tension is an important factor that can promote rupture of adsorbed vesicles. It is likely that the activation barrier against vesicle rupture is lowered for vesicles under high membrane tension. In addition to using small diameter vesicles between 50-100 nm (which can be controlled through vesicle extrusion), membrane tension can also be increased by creating a gradient in ionic strength across the vesicle membrane. The resulting osmotic pressure difference causes an osmotic stress that changes the volume of the vesicle, and thus creates membrane tension leading to rupture.[117] Reimhult *et al.* found that SLBs created from egg PC vesicles, with a fixed interior ionic strength of 150 mM, formed at all solution ionic

strengths tested (115–300 mM).[98] However, the θ_c decreased when the vesicles were osmotically stressed, *i.e.*, when the ionic strength of the buffer differed from that of the vesicle interior. This was also evident in the decrease of the Δf and ΔD peaks in QCM-D measurements, indicating that SLB formation occurred more quickly and required less surface adsorbed vesicles to induce vesicle rupture. For successful vesicle rupture via osmostic stress, it is thus common practice to introduce vesicles to substrates in buffers with ionic strengths between 150-500 mM NaCl (to maximize vesicle adsorption as discussed above) and to then induce an osmotic shock after their adsorption, by exchanging the buffer with deionized water. Once the SLB is formed, the deionized water can be replaced with standard buffer to maintain SLB stability.[131, 132]

3.5 Amphipathic α-Helical (AH) Peptide-Induced Vesicle Fusion

While adjusting experimental conditions provides a successful strategy for creating complex SLBs, the approach can be tedious since conditions are chosen based on the substrate type and vesicle composition. As substrates and lipid mixtures increase in complexity it can be difficult to anticipate which optimization techniques will promote vesicle fusion. To reliably create SLBs, it is likely that multiple experimental conditions will have to be optimized, including those not discussed above (*e.g.*, vesicle concentration, flow conditions, and chemical surface modifications). Furthermore, experimental optimization techniques can fail or become inconsistent when the vesicle

cholesterol content exceeds 30 mol%. To overcome these limitations, we summarize an alternative approach that uses amphipathic, α-helical (AH) peptides as a catalyst to promote vesicle fusion and that generates complex SLBs containing as much as 45 mol% cholesterol. While this approach can be used in combination with the optimization techniques discussed above, a unique and major advantage of AH peptide-induced vesicle fusion is that is sufficient to form SLBs independently of optimizing experimental conditions. With sufficient vesicle-substrate adsorption, it is generally recommended to introduce AH peptides under standard experimental conditions (room temperature, pH = 7, ionic strength ≈ 150 mM) regardless of the substrate and vesicle composition.

AH peptide is derived from hepatitis C virus's (HCV) nonstructural protein 5A (NS5A), which interacts with host cell membranes and is required for HCV replication. NS5A's membrane association is mediated by its N-terminal amphipathic α-helix, termed the AH peptide (Fig. 3.3B,C).[133] After realizing the AH peptide's ability to rupture intact adsorbed vesicles, Cho *et al*. created SLBs from simple POPC vesicles adsorbed on gold substrates (Fig. 3.3A).[134, 135] Without the use of AH peptide, gold substrates are limited to vesicle adsorption and do not induce vesicle rupture.[59] Previously, SLB formation from vesicle fusion was mainly limited to hydrophilic substrates (*e.g.*, mica, glass, and silicon oxide). This work thus established a technique that expanded the type of substrates amenable to easy SLB formation by vesicle fusion. Recently, our group has extended the value of AH peptide-induced vesicle fusion by

demonstrating a reliable and easy way to form SLBs that contain high cholesterol content (45 mol%) and multiple lipid types.[60] For the first time, this vesicle fusion technique enables researchers to form SLBs with complex lipid compositions and high cholesterol content, without the need to optimize experimental conditions such as temperature, pH, and ionic strength.

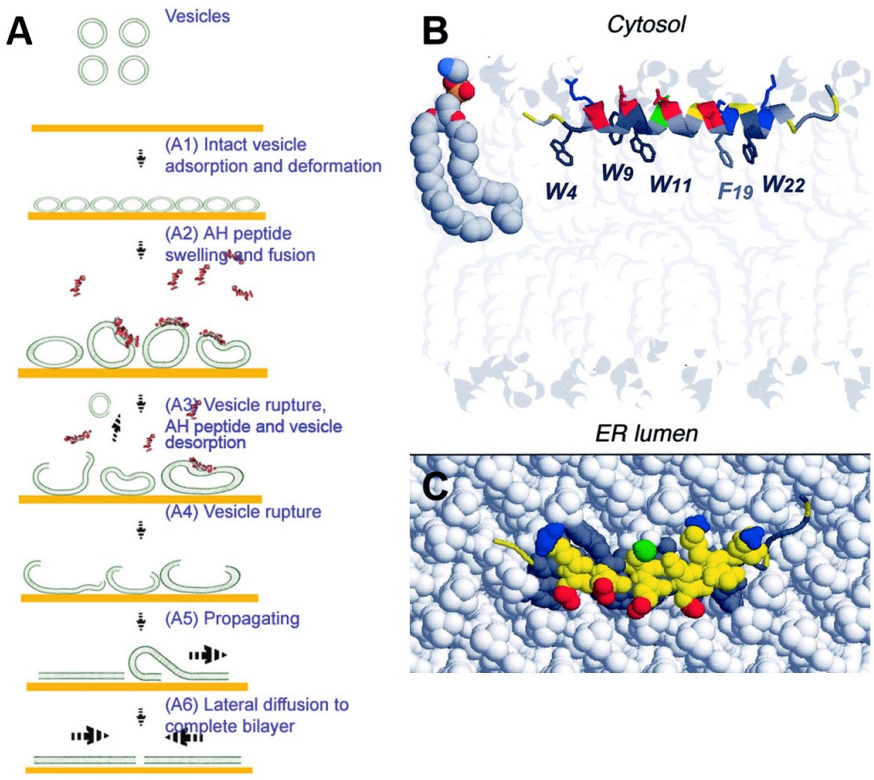

Figure 3.3: Membrane activity of the NS5A amphipathic α-helix (AH) peptide. (A) Potential mechanism of AH-peptide induced vesicle fusion on gold. (B) Expected positioning of the average structure of amphipathic α-helix membrane anchor domain of NS5A (PDB entry 1R7E) at the interface between phospholipid polar head groups and hydrophobic tails. The phospholipid bilayer was drawn using the phosphatidylethanolamine (PE) models reported in the Protein Data Bank entry 1BCC. Molecules are colored according to atom types (N, blue; O, red; P, yellow; C, H, gray). (C) Top view of AH peptide embedded in a model phospholipid membrane. Adapted with permission from reference [136] and [137]. Copyright (2009 and 2004) from the American Chemical Society and The American Society for Biochemistry and Molecular Biology, respectively.

3.5.1 Mechanism of AH Peptide-Induced Vesicle Fusion

The mechanism of AH peptide-induced vesicle fusion is not yet fully understood. It has been hypothesized that AH peptide membrane integration may cause

the vesicle membrane to swell and greatly expand, possibly into microvilli folds.[134, 138, 139] This hypothesis is supported by findings from Cho *et al*. who showed that the interaction of AH fusion peptides with POPC vesicles (~60 nm in diameter) on gold substrates caused vesicle swelling, which in turn enhanced vesicle-vesicle interactions and led to vesicle fusion and SLB formation.[138] However, this vesicle fusion activity was diminished for vesicles greater than 100 nm in diameter.[140, 141] Furthermore, at AH peptide concentrations that rupture vesicles, no peptide binding to planar bilayers was observed.[142] This functional dependence on vesicle diameter/membrane curvature is unique and suggests that the mechanism of AH peptide-induced vesicle fusion is not analogous to that of other membrane disruptive peptides interacting with large diameter membranes (*e.g*., cells, bacteria, and giant unilamellar vesicles). For these other membrane disruptive peptides, membrane disruption often occurs via pore formation by barrel-stave or toroidal pore mechanisms.[143-145]

To study the unique fusion mechanism of AH-peptide, Jackman and Cho studied the initial binding of the AH peptide to vesicles and found that binding saturation occurred before completion of vesicle swelling.[142] This lag time suggests that membrane association alone is insufficient to directly cause complete vesicle swelling. It is likely that associated peptides may first rearrange to achieve pore formation, which leads to solvent uptake and subsequent vesicle deformation and SLB formation. It was also observed that the onset of pore formation is almost a factor of 10 slower for larger

vesicles (~200 nm in diameter) compared to that of smaller vesicles (~70 nm in diameter), however, the rate of peptide binding had no significant dependence on the vesicle diameters studied.[140] Typically, pore formation increases with vesicle diameter due to an increase in the number of bound peptides per vesicle (given a constant peptide/lipid (P/L) ratio).[146] However, this is not the case for the AH peptide which suggests that pore formation, rather than the rate of peptide binding, is dependent on high membrane curvature.[140]

To investigate how AH peptide action depends on nanoscale membrane curvature, Tabaei *et al*. observed the release of encapsulated vesicle content, induced by AH peptide pore formation and membrane disruption.[140] They found that as little as four AH peptides per vesicle were required to cause pore formation, which translates into an unusually low effective P/L ratio of ~1/1000.[140] Furthermore, their results suggest that the inability of AH peptides to rupture large vesicles and planar bilayers is due to insufficient line tension, related to reduced or nonexistent membrane curvature. They also suggest that AH peptide's pore formation process may be facilitated by curvature-induced defects in lipid packing.

3.5.2 SLB Applications of the NS5A-Derived AH Peptide

While Cho and others are focused on realizing antiviral clinical benefits of this AH peptide[140, 141, 147, 148], our group is focused on promoting the use of AH

peptides to create SLB platforms under conditions that are generally unfavorable for vesicle fusion. Examples of such conditions include vesicles containing high amounts of cholesterol, the presence of membrane-embedded proteins, strong lipid-substrate interactions, and formation of SLBs on hydrophobic or irregular/patterned substrate surfaces. The extent to which AH peptides can overcome these and other barriers limiting SLB formation are subject to current investigation.

Using AH peptides, we report in Chapter 4 the formation of complex biomimetic SLBs that contain cholesterol concentrations of up to 45 mol% on mica and silica substrates.[60] Our chosen SLB system is a five-component lipid bilayer that models the native lipid envelope of human immunodeficiency virus-1 (HIV-1).[40] We chose to model this lipid envelope due to the membrane's significance in viral infection and its potential use as a target in next-generation vaccine designs.[17, 19, 73, 149] Furthermore, the native viral envelope is of interest as it contains a unique composition of heterogeneous membrane components that likely represents a mosaic of lipid rafts,[41] protein and antigen clustering,[150] and various gradients of lipid diffusivity.[151] Generating a complex SLB that models the native HIV-1 envelope also provides a proof-of-concept for modeling other complex native biological membranes. Complete details of this work are presented in Chapter 4.

3.6 Creating SLBs on Non-Siliceous Surfaces

In addition to the lipid composition of vesicles, the substrate also plays a crucial role in creating SLBs via vesicle fusion. Vesicle fusion is typically dominated by surface adhesion energy between vesicles and the substrate. Traditional substrates used for vesicle fusion include hydrophilic silica, glass, mica, and quartz. These siliceous substrates are commonly used because they provide the necessary balance between adhesion, repulsion, and hydration forces that results in vesicle rupture and a hydration layer between the substrate and SLB. This hydration layer allows SLBs to mimic the lateral fluidity of native cell membranes. However, as applications of SLBs continue to evolve, there is a need to create SLBs on a wider range of surfaces. Progress has been made to form SLBs on many solid non-siliceous surfaces including chrome,[152] indium tin oxide,[153] gold,[134] titanium oxide,[154] and alumina.[155] In many cases these surfaces have vesicle-substrate interactions that do not enable conventional vesicle fusion, and thus surface-specific techniques must be used to promote SLB formation.

Although optimization techniques, including surface functionalization[156, 157] and the use of charged lipids,[158] have been successfully applied to create SLBs on solid non-siliceous surfaces, these techniques are often specific to a particular substrate and not universally applicable. AH peptide-induced vesicle fusion may overcome this limitation as it can offer SLB formation on a broad range of substrates. For example, AH peptide-induced vesicle fusion was successfully used on gold and titanium oxide

surfaces.[134] Furthermore, our group is currently using AH peptides to create SLBs on chromium and experimenting with its use on a polymeric, Nafion surface.

While AH peptide-induced vesicle fusion may be harnessed to form SLBs under a range of conditions on a variety of substrates, it requires vesicle-substrate interactions that are strong enough to (i) form a monolayer of vesicles on the surface, and (ii) resist vesicle desorption upon a buffer wash. A vesicle monolayer is required to provide sufficient vesicle-vesicle interactions, while a buffer wash is required to remove excess vesicles from the surface and the bulk solution. Excess vesicles need to be removed from the system before AH peptide is introduced, so that it can interact exclusively with the surface adsorbed vesicles. For surfaces with especially weak vesicle-substrate interactions these requirements may not be met, and AH peptides may fail to form a complete SLB. In this case, the so-called bubble-collapse deposition (BCD) technique may overcome this limitation.[96]

BCD provides an innovative approach that requires a lower vesicle-substrate adhesion energy then traditional vesicle fusion. For example, Mager *et al*. use this technique to form a POPC SLB on alumina; a substrate which usually does not provide sufficient vesicle adhesion to induce fusion.[155] BCD uses an air bubble that is blown underwater at the end of a needle. This bubble is "inked" with a lipid monolayer by contacting it with a previously formed sacrificial bilayer. The bubble is then brought into contact with the substrate at the desired deposition site. The needle then withdraws air

from the bubble causing the bubble to shrink until the surface-supported monolayer folds back on itself, forming a bilayer patch on the substrate surface.

To date, BCD can form a SLB with simple lipid composition on substrates that otherwise are unable to induce vesicle rupture due to weak vesicle-substrate interactions. It is thus conceivable that if a complex SLB, created by one of the techniques discusses above, is used as the sacrificial inking bilayer, then BCD may be able to form SLBs with complex lipid composition on substrates that have weak vesicle interactions.

3.7 Vesicle Fusion Considerations

Many questions exist concerning how preparation methods affect properties of SLBs, and to what extent these properties accurately mimic native cell membranes. For the techniques discussed above, the conditions that are manipulated to induce vesicle fusion (*e.g.*, temperature, buffer type, fusion peptides, etc.) can be replaced with the desired experimental conditions once the SLB has formed. However, after the conditions have been changed, it is important to take into consideration the possibility of residual effects on SLB properties that originate from the SLB preparation conditions. For example, zwitterionic lateral lipid-lipid interactions are believe to be promoted by ions bound into the membrane. Strong interaction between Na^+ and Ca^{2+} ions and the carbonyl oxygens of the lipids form tight ion-lipid complexes.[127] This increases

membrane organization and can affect bilayer cohesion and lipid diffusivities. Thus, using high ionic strength for SLB formation, and then changing to a physiological ionic strength may have a lasting effect on lateral lipid-lipid interactions. Furthermore, temperature changes are known to affect the ζ potential and orientation of lipid head groups[126] and it is unclear if the resulting effects, both direct and indirect, are reversible.

Compositional asymmetry between the leaflets of the SLB must also be taken into consideration. Bilayer asymmetry is a common property in native cell membranes and is believed to contribute to many biological functions by mediating membrane protein distribution and functionality.[159] Thus, there is a large focus on controlling and characterizing asymmetry in deposited bilayers.[160, 161] Typically, Langmuir-Blodgett/Schäfer deposition offers the most control of SLB asymmetry since each leaflet can be deposited independently, allowing lipid selection of each initial leaflet composition. Asymmetry is harder to control with vesicle fusion techniques since it must originate from the vesicle or occur from lipid re-arrangement once the SLB has formed. However, it is possible to achieve and control bilayer asymmetry using vesicle fusion. Studies have suggested that the solid support can induce preferential distribution of certain lipid types. In the presence of Ca^{2+} ions, it has been observed that negatively charged DOPS preferentially resides in the leaflet closest to mica and titanium oxide surfaces.[128, 162] This suggests that lipid head group chemistry leads to

membrane asymmetry.[163] SLBs have also shown leaflet organizational asymmetry between gel- and fluid-phases[164] and with cholesterol induced domain formations.[165] Furthermore, it has been shown that SLB leaflet asymmetry can be controlled by vesicle deposition temperature and the salt concentration of the vesicle solution.[161]

This brief discussion is meant to demonstrate that details in preparation methods can affect SLB properties, and emphasizes that such details need to be considered and perhaps accounted for in experimental design and data interpretation.

3.8. Conclusions

Common criticism against SLB formation via vesicle fusion states that it is limited to few select surfaces and vesicle compositions. In this chapter, we have attempted to prove this criticism to be outdated by summarizing vesicle fusion techniques that are able to readily form SLBs with multiple lipid types, high cholesterol content, and on non-siliceous substrates. These techniques are simple and reliable, and thus maintain the major advantage of forming SLBs via vesicle fusion.

In the past, optimization of experimental conditions has been widely used to induce vesicle fusion and has provided a successful strategy for creating simple SLBs. With increasing SLB complexity and emerging applications for SLBs, such optimization techniques will play an even more important role for their formation. Here, we have

summarized the strategies that are used to tune the most important conditions to make vesicle fusion applicable to a larger range of SLB compositions and substrates. Important strategies include elevating the temperature, increasing buffer ionic strength, adding divalent cations, and lowering buffer pH. By optimizing these conditions it is possible to create SLBs from vesicles that ordinarily resist vesicle fusion, and to access substrates that are generally not amenable to SLB formation.

In cases where such optimization strategies fail to provide easy SLB formation, the optimization efforts can be supplemented with a novel vesicle fusion technique, AH peptide-induced vesicle fusion. Finally, bubble collapse deposition can be combined with these vesicle fusion techniques to create complex SLBs on surfaces with especially weak vesicle-substrate interactions. Together, these techniques allow researchers to easily create SLBs that contain high cholesterol content and multiple lipid types on a wide range of substrates. Thus, SLB formation via vesicle fusion is no longer restricted to a few select surfaces and a limited range of lipid compositions.

Chapter 4. Biomimetic Supported Lipid Bilayers with High Cholesterol Content Formed by α-Helical Peptide-Induced Vesicle Fusion

This research was performed in collaboration with Dr. Frank Heinrich (Carnegie Mellon University, NIST Center for Neutron Research) who analyzed and modeled the NR data.

4.1 Introduction

Chapter 4 presents a technique to create a complex, high cholesterol-containing supported lipid bilayers (SLBs) using α-helical (AH) peptide-induced vesicle fusion. Vesicles consisting of POPC:POPE:POPS:SM:CH (9.35 : 19.25 : 8.25 : 18.15 : 45.00) were used to form a SLB that models the native composition of the HIV-1 lipid envelope. In the absence of AH peptides, these biomimetic vesicles fail to form a complete SLB. We verified and characterized AH peptide-induced vesicle fusion by quartz crystal microbalance with dissipation monitoring, neutron reflectivity, and atomic force microscopy. Completion of this research was essential for establishing the basis of our SLB research platform and enabling the progression and utilization of this platform detailed in Chapter 5. The research presented within this chapter is published in the *Journal of Materials Chemistry*.[60]

4.2 Background

AH peptide is derived from hepatitis C virus's nonstructural protein 5A (NS5A). This AH segment within NS5A is responsible for the association between the hepatitis C virus and host cell membranes during viral infection.[166, 167] Using AH peptides we established SLB formation of complex biomimetic SLBs that contain concentrations of 45% cholesterol on mica and silica. Our chosen SLB system is a five-component lipid bilayer that models the native lipid envelope of human immunodeficiency virus-1 (HIV-

1).[40] The model HIV SLB consists of 1-palmitoyl-2-oleoyl-sn-glycero-3-phosphocholine (POPC), 1-palmitoyl-2-oleoyl-sn-glycero-3-phosphoethanolamine (POPE), 1-palmitoyl-2-oleoyl-sn-glycero-3-phospho-L-serine (POPS), brain sphingomyelin (SM), and cholesterol (CH) (Fig. 4.1) in a molar ratio of 9.35 : 19.25 : 8.25 : 18.15 : 45.00. SLB formation from vesicles modeling the HIV-1 lipid envelope does not occur by conventional spontaneous vesicle fusion. In part, this is due to the highly ordered model HIV vesicles. The high order arises from the high cholesterol content and presence of sphingomyelin. Furthermore, the negatively charged POPS and negatively charged silica give rise to repulsive lipid-substrate interactions that resist vesicle fusion. The use of AH peptide-induced vesicle fusion allows us to overcome these obstacles and to more accurately recapitulate the composition of the HIV-1 lipid envelope compared to simpler, lower cholesterol SLBs consisting of POPC:SM:CH (3 : 3 : 2).[168] To verify and characterize AH peptide-induced vesicle fusion of our model system, we used quartz crystal microbalance with dissipation monitoring (QCM-D), neutron reflectivity (NR), and atomic force microscopy (AFM) imaging.

The known mechanistic details of AH peptide-induced vesicle fusion is presented in Chapter 3, section 3.5. Cho and colleagues offer additional information on the proposed mechanism in previous publications.[137, 166, 169] Briefly, AH peptides first bind to a monolayer of intact vesicles on a substrate, creating a physical instability on the outer vesicle leaflet. This initial interaction leads to vesicle swelling and possibly

formation of microvilli-like extensions on the vesicle, which are believed to facilitate lateral vesicle-vesicle interactions.[137] Vesicles then start to rupture and spread on the substrate similar to that observed in the classical spontaneous vesicle fusion model. We note however, that the fusion mechanism for complex vesicles containing high concentrations of cholesterol with several lipid types has not been studied and the mechanism may differ from that observed from simple vesicles on gold.

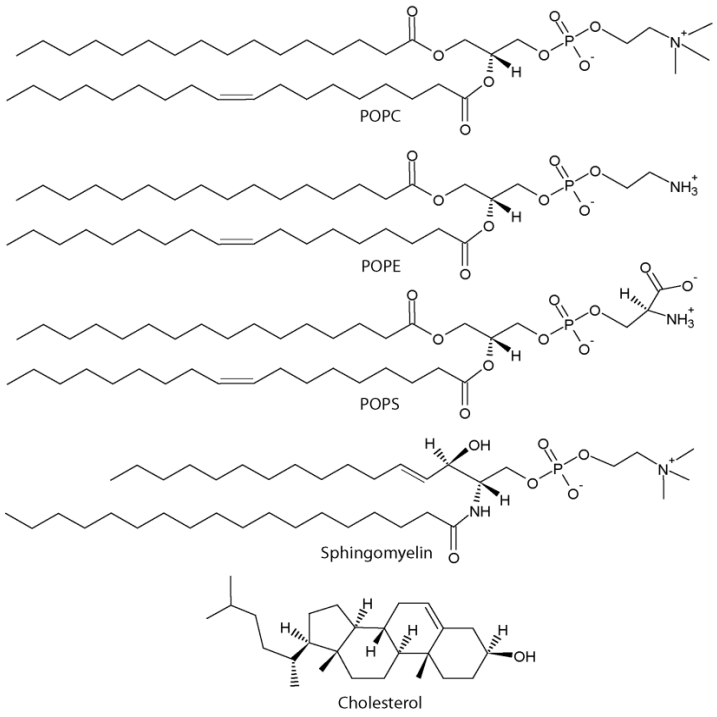

Figure 4.1: Chemical structures of membrane components used in this study. Biomimetic HIV-1 SLBs were formed from vesicles containing a lipid composition of POPC:POPE:POPS:SM:CH (9.35 : 19.25 : 8.25 : 18.15 : 45.00).[60] Reproduced by permission of The Royal Society of Chemistry.

4.3 Results and Discussion

4.3.1 AH Peptide-Induced Vesicle Fusion Observed by QCM-D.

We used quartz crystal microbalance with dissipation monitoring (QCM-D) to observe the characteristics of AH peptide-induced vesicle fusion and lipid bilayer formation. Figure 4.2A shows SLB formation from POPC vesicles by spontaneous vesicle fusion. This is a two-step process that relies on membrane tension,[110, 170] vesicle-vesicle, and vesicle-substrate interactions.[170] First, POPC vesicles are sparsely adsorbed onto the silica surface, resulting in a large frequency drop due to the increase in associated mass from the large amount of solvent trapped within and between the intact vesicles. Concurrently, the adsorbed vesicles contribute to an increase in dissipation due to their viscoelastic properties. Once the vesicle surface coverage reaches a critical concentration, the vesicles spontaneously rupture and fuse to form a continuous SLB.[55-58] The frequency increases due to released solvent from within the vesicle interior. Consistent with previous literature,[98] our final Δf and ΔD values for homogenous POPC SLBs are -27.1 ± 0.1 Hz and 0.19 x 10^{-6}, respectively (Table 4.1).

However, when vesicles were used that reflect the high cholesterol content and complex membrane of the HIV-1 envelope, complete spontaneous vesicle fusion does not occur (Fig. 4.2B). As the model HIV vesicles are added, vesicles adsorb to the silica surface resulting in a monolayer of un-ruptured vesicles. The leveled-off frequency

response (Δf = -150 Hz) demonstrates that vesicles adsorb until a vesicle monolayer is reached, as there is no vesicle fusion, which would provide a release of associated solvent. The frequency response here closely resembles that of a POPC vesicle monolayer on a gold substrate.[137]

Figure 4.2C demonstrates the ability of AH peptides to induce SLB formation from a monolayer of model HIV vesicles (as shown in Fig. 4.2B). Vesicles are first added to achieve monolayer saturation, then excess vesicles in the QCM-D chamber are removed by three successive buffer washes. AH peptides (15 μM) are then added and cause vesicle fusion, which is reflected in the increase in frequency. After the frequency becomes stable, the peptide is washed away from the bilayer leaving behind the final SLB. Since the wash step of a complete SLB formed by spontaneous vesicle fusion does not remove surface-associated mass, we conjecture that when using AH peptide-induced vesicle fusion, the observed frequency rise after the final wash step is due to decoupled mass associated with the removal of AH peptides from the SLB. The associated mass removed after the AH peptide wash was calculated to be 346.0 ± 22 ng cm^{-2} (n=5), using the Sauerbrey equation.

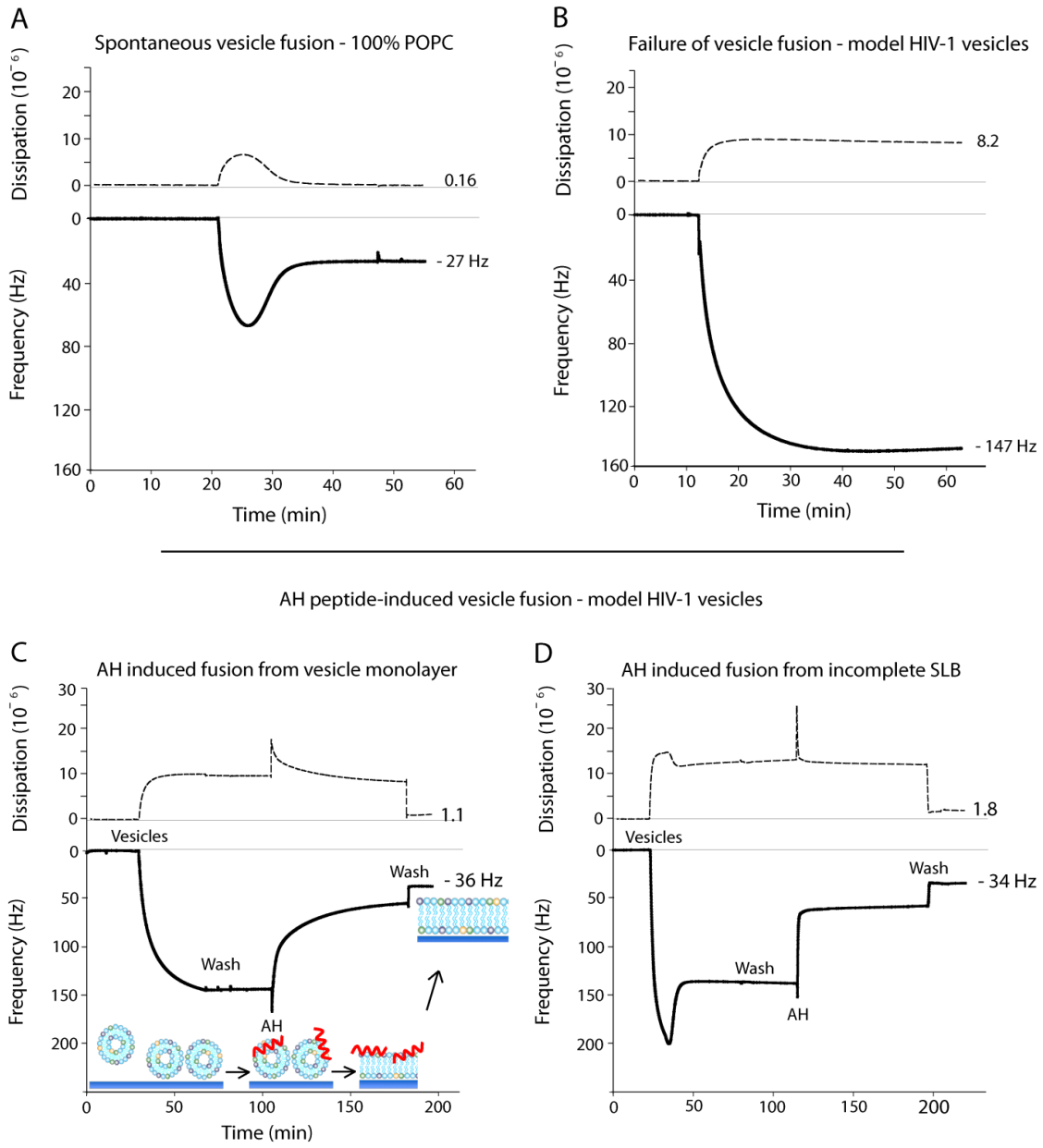

Figure 4.2: Representative QCM-D plots. Energy dissipation (dashed) and third overtone frequency (solid) plotted versus time. (A) SLB formation of 100% POPC by spontaneous vesicle fusion. (B) Failure of model HIV vesicles to undergo spontaneous vesicle fusion. (C) Successful model HIV SLB formation by AH peptide-induced vesicle fusion. (D) AH peptides create a SLB from a partially formed bilayer amongst un-fused vesicles.[60] Reproduced by permission of The Royal Society of Chemistry.

In most experiments, there was no spontaneous vesicle fusion when using model HIV vesicles (Figs. 4.2B,C). However, as seen in Figure 4.2D, there were instances when partial spontaneous vesicle fusion occurred. Figure 4.2D shows that even when AH peptides are added to a partially formed bilayer amongst un-fused vesicles, complete SLB formation is still achieved. This suggests that AH peptides are able to integrate preformed SLB areas with areas of intact vesicles to form a complete SLB with minimal defects. This is further corroborated by the close agreement in the final Δf value for SLBs formed from different starting conditions and shows that variations in the starting condition do not compromise the ability of AH peptides to form complete SLBs.

The final Δf of the model HIV SLB was -35.4 ± 0.8 Hz with a ΔD of 1.91 ± 0.23 x 10^{-6}. These values are significantly larger than the final Δf and ΔD values of SLBs formed by spontaneous vesicle fusion using 100% POPC vesicles (Table 4.1). The frequency difference between these SLBs corresponds to about a 32% apparent mass increase for the model HIV SLB. It is unclear, however, if this apparent mass increase arises from an increase in lipid packing density due to the presence of cholesterol and sphingomyelin, or from an increase in SLB-associated solvent, or from an incomplete bilayer with areas of intact vesicles. Our NR and AFM data suggest, however, that our SLB is complete with no intact vesicles remaining on the surface. The SLB preparation for NR and AFM experiments is not identical to that for the QCM-D experiments, and thus, we cannot

definitively conclude that our final Δf value reflects a 100% complete SLB. Our QCM-D results agree closely, however, with a previous publication that reports the final Δf and ΔD of a POPC:CH (55:45) SLB formed at 25 °C on silica to be 32 ± 0.7 Hz and 2.00 ± 0.4 x 10^{-6}, respectively.[30] Although the SLB lipid composition is simpler compared to the model HIV SLB, the cholesterol content is identical and the final Δf and ΔD values closely agree. Therefore, we speculate that the increase in lipid packing density due to high cholesterol concentration is likely a factor contributing to the observed mass increase of the model HIV SLB.

However, there is also an increase in the final dissipation value compared to the POPC bilayer formed by spontaneous vesicle fusion. This suggests that the model HIV SLB is more viscoelastic, which is contrary to a more rigid and denser SLB. Thus, it is unlikely that the increased packing density accounts for the entire increase in mass. The higher final Δf and ΔD could indicate that there are intact vesicles on the surface. There is also a possibility that upon AH peptide-induced vesicle fusion, the amount of liposomes present on the surface before the introduction of the AH fusion peptide, exceeds the lipid content necessary to form a planar SLB. This could give rise to small undulations in the SLB, which would contribute to higher final Δf and ΔD values.

Table 4.1: QCM-D data showing mean and SE of Δf and ΔD at the maximum and final values for SLB formation from model HIV vesicles (formed by AH peptide-induced vesicle fusion) and from POPC vesicles (formed by spontaneous vesicle fusion).

Vesicle Composition	$\Delta f_{max,3}$ 3^{-1} /Hz	$\Delta D_{max,3}$ (10^{-6})	$\Delta f_{final,3}$ 3^{-1} /Hz	$\Delta D_{final,3}$ (10^{-6})
Model HIV SLB (n=6)	-172 ± 17	38 ± 8	-35.4 ± 0.8	1.91 ± 0.23
POPC (n=3)	-65 ± 6	5.7 ± 0.7	-27.1 ± 0.1	0.19 ± 0.02

4.3.2 SLB Characterization by Neutron Reflectivity

Neutron reflectivity (NR) is a surface-sensitive technique that provides molecular-scale information about the structure of interfacial layers perpendicular to the interface.[171] NR measurements were used to characterize the membrane structure (to identify membrane defects), to determine SLB thickness, and to determine if there were residual AH peptides embedded within or associated with the SLB after washing. Fit parameters and 95% confidence intervals were determined using a Monte Carlo re-sampling analysis of the reflectivity data. The reflectivity curves obtained from NR (Fig. 4.3) give rise to the modeled NR scattering length density (nSLD) profiles (Fig. 4.3, inset) that provide a depth profile of the chemical constituents of the model bilayer with Ångstrom resolution. The NR results confirm that the SLB is 100 $^{+0.0}_{-0.1}$% complete. The nSLD value of the hydrocarbon core of the bilayer ϱ_n = 0.42 $^{+0.07}_{-0.07}$ 10-6 Å^{-2} shows the absence of peptide material in this region with an uncertainty of approximately 3 vol%. The volume fraction of head group material in the head group layers was 78 $^{+0.1}_{-0.3}$%. This falls, within confidence limits, into the expected range of 40%-60% for a bilayer void of

additional peptide material, but the high uncertainties do not permit a quantification of residual amounts of peptide in the narrow head group region. However, from the NR data the presence of any peptide material beyond the outer lipid head group can be excluded. We conclude therefore, that the AH fusion peptides are completely removed from the SLB surface after washing, which is in agreement with previous studies.[137, 172] Finally, the hydration layer between the silicon wafer and the SLB was 4.8 $^{+1.0}_{-1.4}$ Å, the average total bilayer thickness was 49.9 $^{+1.9}_{-1.5}$ Å. A similar bilayer composition (DOPC:SM:CH 1:1:1) measured by X-ray diffraction results in a bilayer thickness of approximately 54 Å[46] and is in close agreement to our bilayer thickness of our model HIV SLB measured by NR. The thickness of the inner head group, each hydrocarbon leaflet, and outer head groups were 12.3 $^{+0.9}_{-0.8}$, 14.8 $^{+1.0}_{-0.8}$, and 8.0 $^{+0.8}_{-0.5}$ Å, respectively. We expected the inner and outer lipid headgroups to have a similar thickness, yet the inner head group was measured to be approximately 4.3 Å thicker than the outer headgroup. This suggests asymmetric leaflet organization or that there is an error in the experimental modeling of the NR curves. To detect asymmetry in our SLBs it is possible to use sum frequency generation (SFG) spectroscopy, which is a highly surface sensitive characterization method that emits sum frequency light at interfaces.[173] This inherent interface specificity can be used to probe the molecular leaflet arrangements in our SLBs and can help determine if the lipid headgroup thicknesses of our SLBs were modeled

accurately. Deuterated lipids may also be used with NR to more accurately model thicknesses of the SLB structure.

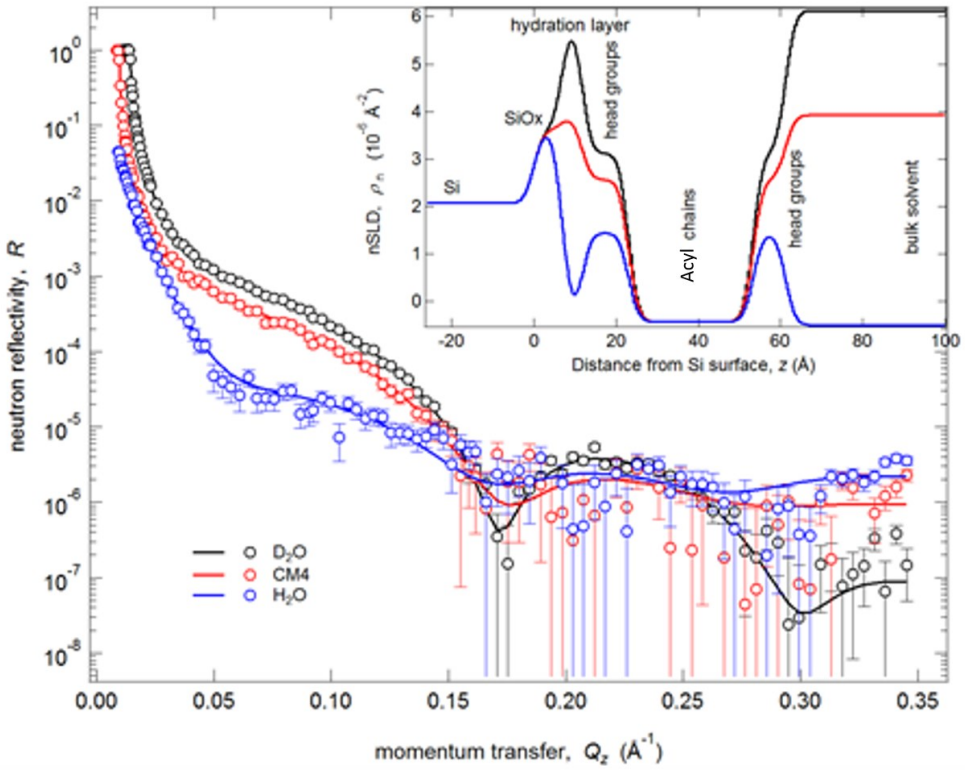

Figure 4.3: Neutron reflectivity curves, best-fits, and best-fit nSLD profiles for the measurements of the model HIV SLB. Inset: Best-fit nSLD profiles of reflectivity curves.[60] Reproduced by permission of The Royal Society of Chemistry.

4.3.3 AFM Visualization of the Model HIV SLB.

We used AFM[174] imaging to visualize lipid domains that are expected to form in SLBs with high concentrations of cholesterol and to visualize potential SLB surface defects. Due to the packing characteristics of phospholipids, two domain types typically

form, (i) gel domains and (ii) liquid-disordered (L_d) domains. Gel domains are characterized by tightly packed lipids that have limited lateral mobility compared with liquid-disordered domains, in which lipids are more loosely packed and have a higher degree of lateral mobility. The phase transition from the gel domain to an L_d domain is determined by the T_m of the lipids that constitute the domain. Furthermore, cholesterol and sphingolipids have a tendency to associate with lipids to create the L_d domain where they stiffen the lipid's acyl chains into a more upright position. This organization facilitates a high lipid packing density, resulting in highly ordered, tightly packed islands, known as liquid-ordered (L_o) domains or lipid rafts.[47, 48] A height difference between lipids within L_o and L_d domains ensues because lipids are in a more upright position within L_o domains compared to lipids within L_d domains. These height differences can be visualized using high-resolution AFM imaging (Figs. 4.4A,B).

Three visually distinct lipid domains can be seen in the model HIV SLB (Figs. 4.4A,B). Ordered membrane domains are taller and appear brighter compared to the more disordered membrane domains which are lower and appear darker. Domain height differences were analyzed from several AFM images after a wash step, which removed SLB-associated AH peptides (Fig. 4.4B). We also completed experiments where SLBs were imaged before and after the final wash step (Fig. 4.4A contrasted with Fig. 4.4B). Thus, AH peptides are still associated with the SLB in Figure 4.4A as observed from QCM-D results (Fig. 4.2). Within the limit of detection, AFM imaging did not

reveal the presence of AH peptide aggregates on the membrane surface. Additionally, no differences in domain heights were observed before or after AH peptides were washed from the SLB.

The height differences between the lowest and middle domain (*i.e.* domains 1 and 2) was 10.3 ± 0.6 Å, and between the middle and tallest domain (*i.e.* domains 2 and 3) was 2.4 ± 0.7 Å. The thickness of domains 1, 2, and 3 were 40.9 $^{+1.9}_{-1.6}$, 51.2 $^{+2.0}_{-1.7}$, and 53.7 $^{+2.1}_{-1.8}$ Å, respectively. These thicknesses were determined using the average thickness of the SLB obtained from NR measurements, the relative height differences between domains, and the fractional surface area occupied by each domain (obtained from several AFM height images).

Considering the transition temperature of each lipid type, it is likely that the most fluid domain (lowest height, domain 1) predominantly contains POPC (T_m = -2 °C) and POPS (T_m = 14 °C), while the more ordered domains, 2 and 3, likely contain a mixture of POPE (T_m = 25 °C), sphingomyelin (T_m = 37 °C), and cholesterol. Since domain 3 is the thickest, and thus, the most ordered, cholesterol is likely to be at the highest concentration in this domain.

Furthermore, Figure 4.4C shows a 64 μm^2 image, which offers a more global view of a complete SLB. Within imaged regions of the bilayer, cross-sections revealed that there were neither hole defects (expected to be ~ 5 nm deep *i.e.*, the bilayer thickness) nor intact vesicles on the substrate surface (expected to be ~ 100 nm tall). We

note that the resolution of AFM imaging depends on many variables including tip size, imaging parameters, and tip-substrate interactions. It is therefore possible that there are defects on the molecular scale that were not resolved by AFM imaging. Furthermore, it is possible that AFM imaging can smooth out membrane undulations, and potentially rupture surface-adhered vesicles.[129, 175]

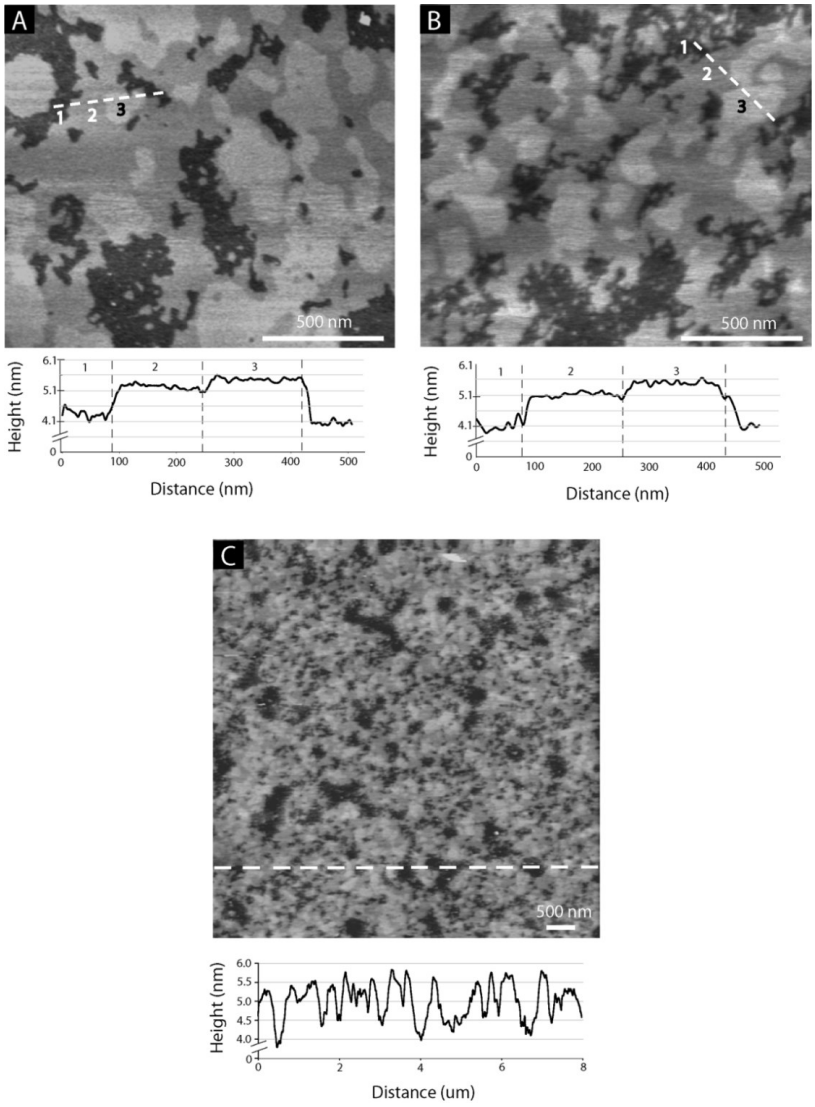

Figure 4.4: AFM height image of model HIV SLB on mica (imaged in buffer, 18° C, ± 1.6 nm height scale). (A) 1.8 x 1.6 μm image showing SLB topography before AH peptides were washed from the surface. Height cross-section was taken along the three domains indicated by the position of the dashed line. The three domains labeled in the height cross-section correspond to the numbers labeled on the AFM height image. (B) 1.8 x 1.6 μm image showing SLB topography after AH peptides were washed from the surface. (C) Height image demonstrating a complete, defect free SLB over a larger, 8 x 8 μm, area.[60] Reproduced by permission of The Royal Society of Chemistry.

4.4 Conclusions

This work introduces AH peptide-induced vesicle fusion as a reliable and facile technique to form a SLB that contains a high cholesterol content and multiple lipid types. The utility of this technique to form biomimetic SLBs was exemplified by forming SLBs from vesicles that recapitulate the native HIV-1 envelope. Without the use of AH peptides, model HIV vesicles fail to form a complete SLB. The SLB formation was characterized by QCM-D and NR measurements, and AFM imaging. AH peptides were able to induce SLB formation from adsorbed vesicles, and also from areas of partially formed bilayer amongst un-fused vesicles. NR results show that the formation of the SLB using AH peptides is complete and that peptides are completely removed from the SLB surface after washing. AFM imaging provided a topographical map of the SLB and revealed three distinct membrane domains. Furthermore, AFM imaging showed that imaged SLB areas did not have major hole defects, did not contain intact vesicles, and did not show AH peptide aggregates.

Given the success reported here and by Cho and coworkers in using AH peptide-induced vesicle fusion, there is potential for this technique to form SLBs under a range of conditions and surfaces that are generally unfavorable for spontaneous vesicle fusion. Examples may include, fusion of vesicles that contain large membrane-embedded proteins, and SLB formation on polymeric substrates.

4.5 Materials and Methods

4.5.1 Vesicle Preparation

All lipids used, palmitoyl-2-oleoyl-sn-glycero-3-phosphocholine (POPC), 1-palmitoyl-2-oleoyl-sn-glycero-3-phosphoethanolamine (POPE), 1-palmitoyl-2-oleoyl-sn-glycero-3-phospho-L-serine (POPS), brain sphingomyelin (SM), and cholesterol (CH), were dissolved in chloroform (Avanti Polar Lipids) and brought to room temperature for 1 h, dried under nitrogen for 5 min, and then dried under vacuum for 3 h. The lipid film was reconstituted in 37 °C PBS without Ca^{2+} and Mg^{2+}, pH 7.4 (Gibco Invitrogen, Grand Island, NY) vortexed, sonicated, and extruded 11 times through a 0.4 μm filter and then through a 0.1 μm filter (Whatman, Florham Park, NJ).[176] The concentrated lipid solution was then diluted to 0.6 mg/mL in buffer and vortexed immediately before use. Lipid solutions were used within 10 h of extrusion.

4.5.2 AH Peptide-Induced Vesicle Fusion

Amphipathic α-helical (AH) peptide was synthesized by Anaspec Corporation (San Jose, CA). The sequence of the AH peptide is H-Ser-Gly-Ser-Trp-Leu-Arg-Asp-Val-Trp-Asp-Trp-Ile-Cys-Thr-Val-Leu-Thr-Asp-Phe-Lys-Thr-Trp-Leu-Gln-Ser-Lys-Leu-Asp-Tyr-Lys-Asp-NH_2. Peptide powder was dissolved in dimethyl sulfoxide and diluted to 15 μM in buffer. AH peptide-induced vesicle rupture was achieved by first depositing a

solution of 100 nm vesicles on substrates using a fluid cell (for QCM-D and NR experiments) or pipetted onto substrates (for AFM experiments). After washing non-adhered vesicles from solution, AH peptide (15 μM) was added and allowed to incubate on the sample between 15-45 min. Finally, samples were washed to remove AH peptides and excess lipids unless otherwise noted.

4.5.3 Quartz Crystal Microbalance with Dissipation Monitoring

Experiments were performed using a D300 Q-Sense QCM-D with silicon oxide crystal sensors (Biolin Scientific, Gothenburg, Sweden). Before each QCM-D experiment, all crystals were first treated with ultraviolet light and ozone for 5 min and then cleaned in 2% sodium dodecyl sulfate (SDS) solution for 30 min, rinsed with ultrapure water, and blown dry under N_2 flow. The crystals were then treated with ultraviolet light and ozone for 10 min before being sonicated in acetone for 3 min. Finally, the crystals were rinsed excessively with ultrapure water, blown dry under N_2 gas, and immediately mounted into the QCM-D chamber. 10 mM Tris, 150 mM NaCl, pH 7.4 was used to equilibrate the crystal, and then vesicles in buffer were introduced into the chamber until a stable frequency level was obtained.

4.5.4 Neutron Reflectivity

Neutron reflectivity (NR) measurements were performed at the NG1 reflectometer at the NIST Center for Neutron Research (NCNR)[177] using neutrons of a wave length λ = 4.75 ± 0.10 Å. A momentum transfer, q_z, range between 0 and 0.35 $Å^{-1}$ was used for all measurements. The bilayer sample was measured while being immersed subsequently using three distinct solvent isotopic contrasts: aqueous buffer prepared from D_2O, H_2O, and from a 2:1 mixture of D_2O and H_2O by volume (CM4). For each contrast, sufficient counting statistics were obtained after 6-9 h. The NCNR flow cell allows for in situ isotopic solvent contrast exchange on the instrument. Therefore, all measurements were performed on exactly the same sample area. The entire flow cell was maintained at room temperature.

Analysis of NR data was performed using the GARefl software package.[178] Reflectivity is computed from a slab model[179] that represent the scattering length density (SLD) profiles using the optical matrix method[180] for computing the reflectivity. Optimization of model parameters is achieved by the combined use of a genetic algorithm and a simplex amoeba algorithm for efficient searching of parameter space and a Levenberg-Marquardt non-linear least square algorithm to refine the fit. All reflectivity curves measured on the same wafer during an experiment were fitted simultaneously, sharing fit parameters, for example, for the solid substrate.

A Monte Carlo error analysis procedure[181] was used to determine the SLD confidence limits by multiple generation of synthetic reflectivity consistent with the measured data based upon the original data set and the statistical uncertainties of the individual data points. Synthetic reflectivities were subsequently fitted to the same model. Using a statistic analysis of the obtained set of parameter values, a bias free estimate of the uncertainties of the resulting SLD profiles is obtained.

4.5.5 Atomic Force Microscopy

Visualization of the SLB was performed using a commercial atomic force microscope (Nanoscope V, Bruker, Santa Barbara, CA) at room temperature. All images were obtained in buffer and imaged in tapping mode using triangular Si_3N_4 cantilevers (Digital Instruments) with a spring constant of 0.06 N m^{-1} operating at 5% offset from the cantilever resonance frequency. Formation of SLBs was achieved by depositing 200 μL of 100 nm vesicle solution (10 mM HEPES, 150 mM NaCl, pH 7) on a freshly cleaved mica surface taped to a circular Teflon puck. Prepared surfaces were then washed with buffer and then incubated with AH peptides (Anaspec, San Jose, CA) at room temperature for at least 30 min. Prior to imaging, surfaces were rinsed by successive 50 μL buffer exchanges 7 times unless otherwise noted. High-resolution (512 x 512 points) topographical images were collected. The height differences between lipid domains were determined from cross-sectional analysis of six different locations from two

different SLB samples. Error propagation was used to calculate the standard error of absolute domain thicknesses, which were determined from NR and AFM measurements.

Chapter 5. HIV-1 Antibodies and Vaccine Antigen Selectively Interact with Lipid Domains

This work was in collaboration with Kara Anasti (Duke Human Vaccine Institute) who performed the SPR experiments.

5.1 Introduction

Chapter 5 applies the SLB research platform developed in Chapter 4 to help determine how lipid domains contribute to 2F5/4E10 membrane interactions and antigen presentation in supported lipid bilayers. To this end, we have engineered biomimetic supported lipid bilayers and use atomic force microscopy to visualize membrane domains, antigen clustering, and antibody-membrane interactions. Our results contribute to vaccine design considerations by determining the optimal lipid phase that should be used in vaccine liposomes to elicit 2F5/4E10 membrane-interactions. This research is currently under preparation for submission to the *Proceeding of the National Academy of Sciences*.

5.2 Background

Understanding the role of the lipid membrane in 2F5/4E10's neutralization mechanism can help select important lipid components to be used in the synthesis of vaccine liposomes. We posit that vaccine liposomes that contain the MPER antigen and an optimized lipid environment are more likely to induce the desired, polyreactive NAbs. The research presented here ultimately provides information on lipid selection when developing new immunogen designs.

Several spectroscopy-based techniques have been used to help understand the role of lipids in 2F5/4E10 HIV-1 neutralization and vaccine design.[73, 182] Although

these established techniques are sensitive, they lack lateral resolution and cannot visualize how membrane morphology, such as lipid domains, contribute to NAb- and antigen-membrane interactions. Currently, it is believed that the viral envelope will organize highly ordered lipid domains (*i.e.*, lipid rafts) and that these lipid domains influence lipid-NAb interactions. Due to the high concentration of cholesterol (CH) and sphingomyelin (SM) in the native HIV-1 envelope, the L_o domain is expected to dominate HIV-1 domain structures. With proper lipid selection, lipid domains can also be created in vaccine liposomes and potentially influence antibody binding and antigen presentation. To help understand how lipid domains influence NAb- and antigen-membrane interactions we have created supported lipid bilayers (SLBs) that can phase separate into lipid domains (Fig. 5.1A). To visualize NAb- and antigen-membrane interactions, we used atomic force microscopy[183] (AFM) to produce high-resolution, topographical images of three different types of SLBs: a single-phase SLB, a two-phase SLB, and a complex, five-component SLB composition that mimics the lipid composition of the native HIV-1 lipid envelope. Unlike many surface-sensitive, spectroscopy techniques, AFM can visualize how antibodies and antigens spatially interact with lipid domains. We show that AFM reveals the height mismatch between lipid domains and surface-associated proteins with Ångstrom vertical resolution and approximately 5-10 nm lateral resolution.

5.2.1 Domain Formation and 2F5/4E10's Lipid Reactivity

A comprehensive discussion of domain formation and 2F5/4E10's lipid-reactivity is given in Chapter 1. A brief description will be given here. Generally, lipid domains are defined as areas of a membrane that have a different composition from their surroundings, *i.e.*, an enrichment or depletion of certain membrane components. Lipid domains typically form when there is more than one lipid phase in the same bilayer. There are two main phase types: a solid and a liquid phase. The solid or "gel" phase is characterized by highly ordered, tightly packed lipids that have limited lateral mobility compared with the liquid phase (Fig. 5.1B). The liquid phase can be further divided into the liquid-disordered (L_d) and liquid-ordered (L_o) phase (Fig. 5.1C). The L_d phase exists when lipids have melted from the gel to liquid phase (defined by the transition temperature, T_m) while the L_o typically forms when CH and SM exist in L_d membranes. CH and SM will co-localize within the L_d phase resulting in highly ordered, tightly packed islands known as L_o domains or lipid rafts.[47, 184].

The interaction between lipids and 2F5/4E10 is likely mediated by the NAb's unique complementary determining region (CDR) H3 loop.[20] The CDR H3 regions contain an unusually large number of hydrophobic and membrane-reactive residues, suggesting that they can embed in the viral membrane and position the NAb to encounter and bind its antigen.[21, 185] Mutations in these CDR H3 antibody regions allow 2F5/4E10 to bind MPER's linear and conformational epitopes, but prevent the

NAb's lipid reactivity, which results in the inability to bind membrane bound MPER antigen.[186] This phenomenon may explain why simple peptide immunogens that mimic neutralizing epitopes on gp41 do not elicit NAbs *in vivo,*[187, 188] and it is clear that antigen sequence is not the sole determinant of neutralizing ability. To mimic 2F5 and 4E10's *in vitro* neutralizing ability, *in vivo* immunogens must elicit antibodies that also react with the HIV-1 lipid envelope. How to design immunogens to do this remains largely unknown.

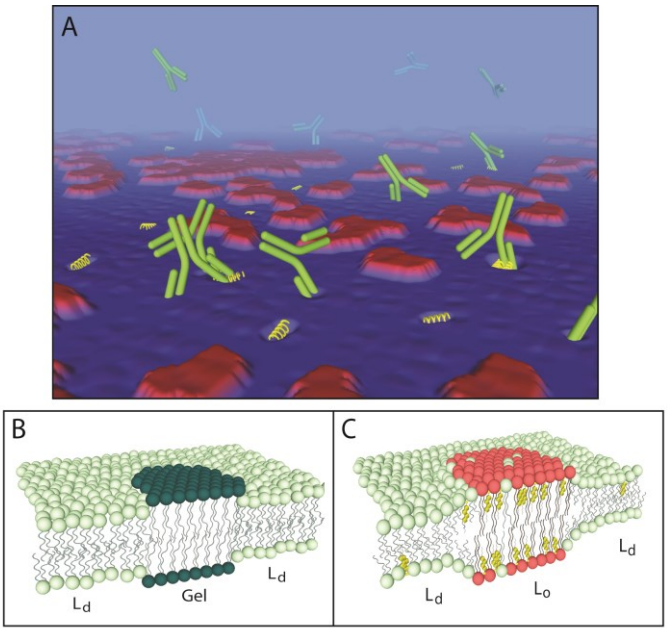

Figure 5.1: Schematic representations of NAbs, antigen, and lipid organization in SLBs. (A) Proposed SLB environment interacting with NAbs (green) and MPER656 (yellow). NAbs and MPER656 only interact with the Ld phase (blue) and avoid Lo and gel domains (represented collectively in red). (B) Lipid organization expected from the POPC:POPE SLB. Gel domain (dark green) surrounded by Ld phase (light green). (C) Lipid organization expected from the model HIV SLB. Lo domains consisting of sphingomyelin (red) and cholesterol (yellow) in a Ld phase (light green).

5.2.2 Model Membrane Research Platform

The three SLBs tested here contain the L_d, L_o, and gel phase. The POPC SLB contains a homogenous L_d phase. POPC:POPE (1:1) SLB contains a gel and L_d phase, and the model HIV SLB (POPC:POPE:POPS:SM:CH, 9.35 : 19.25 : 8.25 : 18.15 : 45.00) contains an L_d and L_o phase, and depending on the temperature, may also contain a gel phase. To reliably create the model HIV SLB, we used amphipathic, α-helical (AH) peptides (detailed in Chapter 4) as a catalyst to generate complex SLBs containing high cholesterol content with multiple lipid types.[60]

5.3 Results

5.3.1 Antibody and Antigen Interactions with Liquid-Disordered SLBs

AFM height images of 1-palmitoyl-2-oleoyl-sn-glycero-3-phosphocholine (POPC) SLBs are shown in Figures 5.2A-D. In these, and all following AFM height images, increasing topographical feature heights are represented by increasing brightness. The POPC SLB appears smooth, with no observable height differences in the membrane organization (Fig. 5.2A). This smooth topography reflects the presence of a homogenous lipid phase with no observable domain formation. Since the T_m of POPC is -2 °C, the SLB exists in the L_d phase at room temperature.

2F5 and 4E10 were each separately added to the POPC SLBs. After NAb addition, the AFM height images (Figs. 5.2B,C) reveal bright spots (*i.e.*, topographical peaks) over the entire membrane surface; we attribute these peaks to the presence of NAbs that have interacted with the top leaflet of the SLB. The surface-associated NAbs cover approximately 3% of the SLB surface (Table 5.1). Based on topographical feature size distributions, the surface-associated NAbs are distributed between 0.5-1.5 nm above the SLB with few feature counts at 2 nm and greater. Features exceeding 2 nm in height likely reflect clusters of antibodies bound to the SLB. In solution, antibodies such as 2F5 and 4E10 have a radius of gyration of approximately 7 nm.[189] The small heights of the topographic peaks suggest that in most instances individual antibodies are bound to the SLB surface. We attribute the apparent size difference (i.e., height of NAbs on the SLB surface *vs.* Ab size in solution) to the tapping force exerted by the AFM cantilever during imaging. This force compresses the antibody against and possibly into the SLB, which results in the smaller observed heights.

$MPER_{656}$ consists of a hydrophobic GTH1 membrane anchor tag and the binding epitope for both 2F5 and 4E10.[190] While the GTH1 anchor resides within the hydrophobic core of the SLB, the NAb binding epitopes are likely positioned parallel with the top lipid leaflet, *i.e.*, at the interface of the lipid bilayer and bulk solution.[191] Based on the size of the MPER binding epitope (3.3 kDa), the folded length is approximately 2 nm. When $MPER_{656}$ is included in the POPC SLB (Fig. 5.2E), 0.5 nm

high topographical peaks appear evenly distributed over the SLB surface. This subtle, antigen-induced height difference between the POPC and POPC:$MPER_{656}$ SLB is further confirmed by the root mean squared (RMS) surface roughness. Over a 1 μm^2 area, the RMS roughness of the POPC:$MPER_{656}$ SLB is 2.7 ± 0.2 Å, while that of the neat POPC bilayer is significantly smaller, with 1.6 ± 0.05 Å. This difference in SLB surface roughness can also be seen by comparing the height cross-sections from Figures 5.2A and 5.2E, presented below the topography images.

When NAbs are incubated on these SLB surfaces, they bind preferentially to regions that contain $MPER_{656}$ antigen (Figs. 5.2F,G). NAb binding to the SLB and to $MPER_{656}$ can be seen by the appearance of "bright spots", *i.e.*, peaks 2-4 nm in height, in the SLB height images. The locations of these peaks are evenly distributed across the SLB surface, suggesting that $MPER_{656}$ is also evenly distributed. 2F5's surface coverage is 42 ± 6%, while addition of 4E10 results in a surface coverage of 47 ± 5% (Table 5.1).

A murine monoclonal antibody, 13H11, was incubated on all SLB surfaces as control. 13H11 has no lipid reactivity and while it does bind to the soluble form of the MPER-antigen peptide, it cannot bind to membrane-embedded MPER.[17] As expected, there is little to no 13H11 interactions with the POPC SLB (Fig. 5.2D) nor with POPC SLB containing MPER (Fig. 5.2H), thus confirming that NAb-membrane interactions are specific to 2F5 and 4E10.

Table 5.1: Average percent surface coverage of L_d area and NAb binding for all SLBs tested (calculated from AFM topographical images). (--) indicates NAb coverage was unable to be determined.

SLB	L_d coverage (%, n=4)	2F5 coverage (%, n=3)		4E10 coverage (%, n=3)	
		L_d area	Total area	L_d area	Total area
POPC	100 ± 0	3 ± 0.3	3.0 ± 0.3	2.7 ± 0.3	2.7 ± 0.3
POPC:MPER$_{656}$	100 ± 0	42.0 ± 5.5	42.0 ± 5.5	46.7 ± 4.7	46.7 ± 4.7
POPC:POPE	41.2 ± 4.1	2.8 ± 0.7	1.1 ± 0.4	3.4 ± 0.3	1.4 ± 0.3
POPC:POPE:MPER$_{656}$	38.7 ± 2.3	26.1 ± 7.0	10.1 ± 3.3	19.3 ± 1.9	7.5 ± 1.2
Model HIV	39.1 ± 3.0	--	3.7 ± 0.9	--	1.9 ± 0.2
Model HIV:MPER$_{656}$	3.1 ± 0.4	--	2.1 ± 0.5	--	1.7 ± 0.1

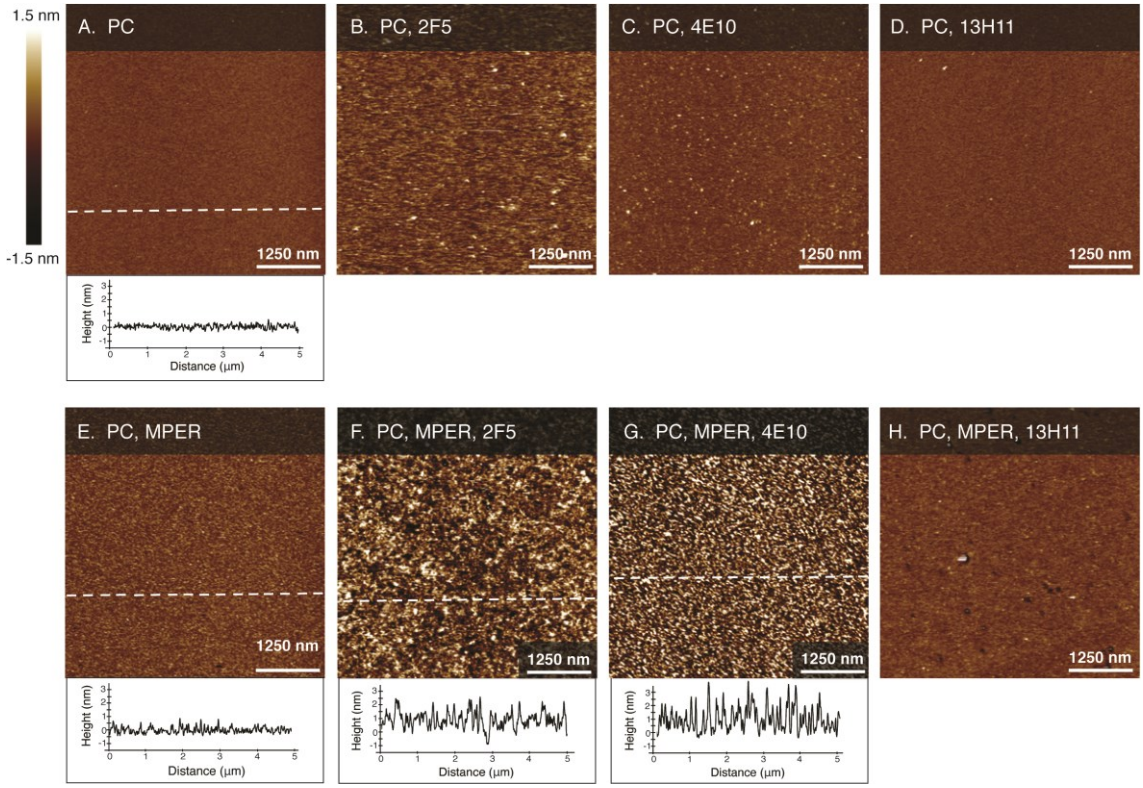

Figure 5.2: AFM height images of the POPC and POPC:MPER$_{656}$ SLBs with and without antibody addition (imaged in liquid at 24 °C). Height cross-section given for select images. (A) POPC SLB. (B-D) 2F5, 4E10 and 13H11 added to the POPC SLB, respectively. (E) POPC:MPER$_{656}$ SLB. (F-H) 2F5, 4E10, and 13H11 added to the POPC:MPER$_{656}$ SLB, respectively.

5.3.2 Antibody/Antigen Interactions with Gel/Liquid-Disordered SLBs

While NAbs and MPER$_{656}$ are apparently evenly distributed throughout the L_d phase of the unary POPC SLB, we next tested their distribution in a binary, phase-separated SLB, consisting of POPC:1-palmitoyl-2-oleoyl-sn-glycero-3-phosphoethanolamine (POPE) (1:1). POPC:POPE SLBs, imaged at 18-20 °C (Fig. 5.3A), revealed a gel domain consisting of predominantly POPE (T_m = 25 °C) and an L_d phase

consisting of predominantly POPC (T_m = -2 °C). Gel domains are taller and appear brighter compared to the L_d phase, which is lower and thus appears darker. The taller POPE gel domains extend 4.8 ± 0.4 Å above the surrounding POPC L_d phase. When NAbs were incubated on this phase-separated SLB surface, they interacted only with the L_d phase (Figs. 5.3B,C), resulting in a surface coverage on the L_d phase of 3 ± 1% for 2F5 and 3 ± 0% for 4E10, respectively (Table 5.1). The tallest NAb peaks were approximately 1.5 nm above the L_d domain surface.

Next, POPC:POPE:$MPER_{656}$ SLBs were prepared. AFM images (Fig. 5.3E) revealed that $MPER_{656}$ exclusively localized to the L_d domain. While the antigen peak heights ranged from about 0.5 nm to 2.0 nm, the peak widths ranged from about 15 to 30 nm, *i.e.*, much wider than expected for single $MPER_{656}$ peptides. This observation suggests that $MPER_{656}$ aggregated in the L_d phase.

When NAbs were added to the POPC:POPE:$MPER_{656}$ SLB, they bound to the SLB and to $MPER_{656}$, indicated by the presence of 1-2 nm peaks in the AFM images (Figs. 5.3G,I). These images also show that NAbs only bound to the L_d phase and were excluded from the taller, gel phase. 2F5's L_d surface coverage was 26 ± 1%, while 4E10 addition resulted in an L_d surface coverage of 19 ± 2% (Table 5.1). A second addition of NAbs (4.0 μM) resulted in large clusters (3-7 nm tall) of L_d-localized NAb (Figs. 5.3H,J) reaching close to 100% coverage of the L_d phase. No antibody binding peaks were found

in the gel domains, which suggest that gel domains are either void of $MPER_{656}$, or the antigen is presented in a conformation that is not accessible to NAb binding.

As expected, 13H11 showed no interactions with neither the POPC:POPE (Fig. 5.3D) nor the POPC:POPE:$MPER_{656}$ SLB (Fig. 5.3F).

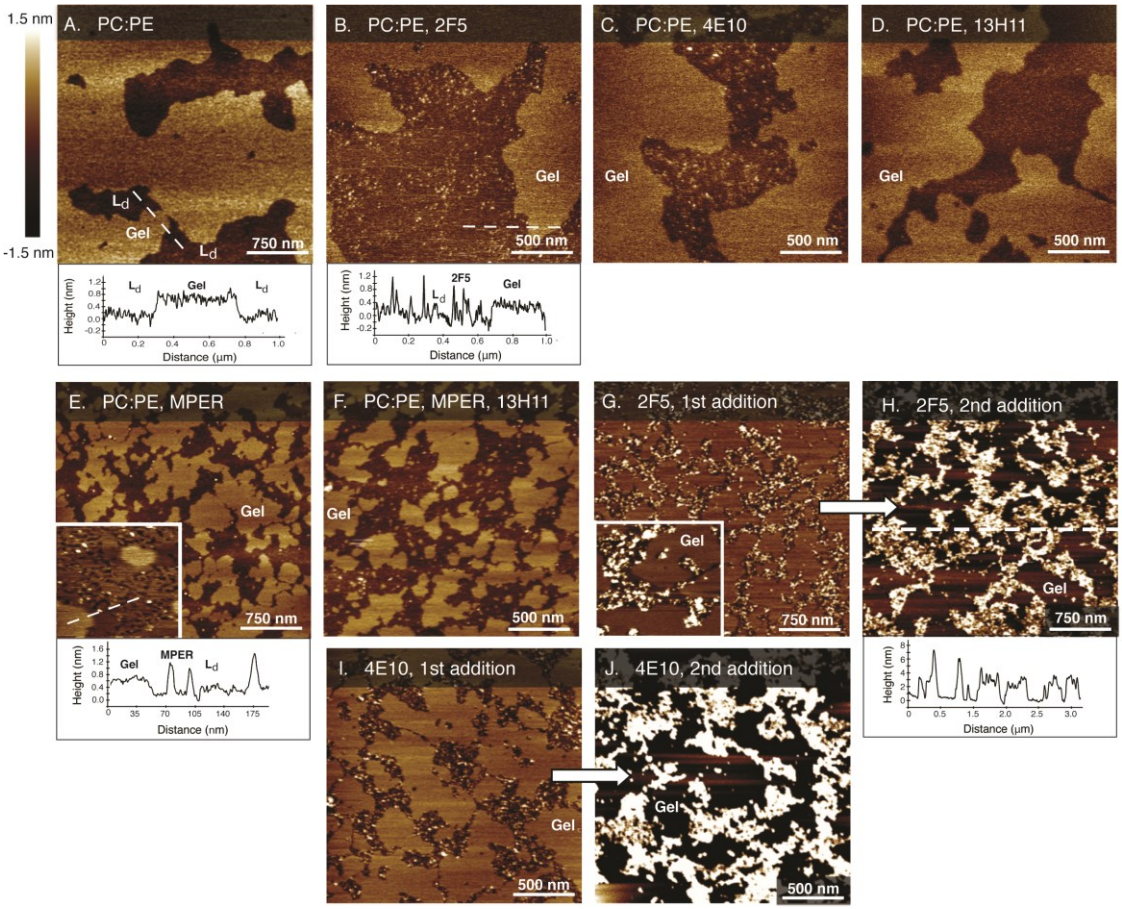

Figure 5.3: AFM height images of the POPC:POPE and POPC:POPE:MPER$_{656}$ SLBs with and without antibody addition (imaged in liquid at 18-20 °C). Height cross-section given for select images. (A) POPC:POPE SLB. The bright area is the taller, gel domain, while the darker area is the lower, L_d phase. (B-D) 2F5, 4E10, and 13H11 added to the POPC:POPE SLB, respectively. (E) POPC:POPE:MPER$_{656}$ SLB. Inset: 250 x 250 nm height image from a replicate sample showing MPER$_{656}$ in the L_d phase. (F) 2F5 added to the POPC:POPE:MPER$_{656}$ SLB. Inset: 250 x 250 nm image from a replicate sample (G) Image (F) with a second addition of 2F5 (4.0 μM). (H,I) Repeated conditions from image (F,G) with 4E10. (M) 13H11 added to POPC:POPE:MPER$_{656}$ SLB.

5.3.3 NAb and Antigen Interactions with Complex, HIV-1 Mimetic SLB

A common SLB model of the HIV-1 envelope is a ternary composition consisting of POPC, SM, and CH.[168, 192] Here we use a more physiologically relevant SLB model

of the HIV-1 envelope[193] to study NAb and antigen interactions. Our model HIV SLB composition consists of POPC, POPE, 1-palmitoyl-2-oleoyl-sn-glycero-3-phospho-L-serine (POPS), brain SM, and CH in a molar ratio of 9.35 : 19.25 : 8.25 : 18.15 : 45.00. This composition was previously used to make liposomes for SPR binding assays in vaccine studies.[12, 186]. To create SLBs with this model HIV composition, we have previously developed a vesicle fusion technique that uses amphipathic, α-helical (AH) peptides as a catalyst to generate complex SLBs containing high cholesterol content.[194] Here, for the first time, we imaged with AFM to visualize NAb and antigen interactions with this model HIV SLB.

Figure 5.4 demonstrates the significant morphological changes that occur in the model HIV SLB when imaged at 18 °C compared to 37 °C. At 18 °C there are three distinct domains visible (Fig. 5.4A) with a height difference of 10.3 ± 0.6 Å between the lowest and medium height domain, and a height difference of 2.4 ± 0.7 Å between the medium height and tallest domain. At 37 °C (Fig. 5.4B), however, only two distinct phases exist, with a height difference of 8.2 ± 0.4 Å.

Regardless of temperature, the addition of 2F5 resulted in 2F5-membrane interactions only in the most disordered (*i.e.*, lowest height) lipid phase (Figs. 5.4C,D). To mimic physiological conditions, comprehensive measurements were conducted on model HIV SLBs at 37 °C. We found that 2F5 had a surface coverage of 4 ± 1%, and that 4E10 behaved like 2F5, by binding only to the most disordered lipid phase (Fig. 5.4E),

reaching a surface coverage of 2 ± 0% (Table 5.1).

When $MPER_{656}$ was incorporated in the model HIV SLB (37 °C), the prominent, two-phase SLB no longer existed (Figs. 5.4G-J). Rather, a more homogenous lipid phase, with small, about 7 Å deep, narrow depressions appeared in the bilayer (Fig. 5.4G). We surmise that these depressions consist largely of the L_d phase, likely containing also $MPER_{656}$. The surface coverage of these L_d features is 3 ± 0%, *i.e.*, significantly less than the surface coverage of the L_d area on the model HIV SLB without antigen (39 ± 3%). Upon addition of NAb, the antibodies only bound to these depressions (Figs. 5.4H,I), resulting in a NAb total surface coverage of 2 ± 1% and 2 ± 0% for 2F5 and 4E10, respectively (Table 5.1). The taller, homogenous lipid phase is void of any antigen or antibody binding. Addition of 13H11 resulted in little to no interactions with the HIV SLB in absence (Fig. 5.4F) and presence (Fig. 5.4J) of $MPER_{656}$.

Surface plasmon resonance (SPR) experiments (Fig. 5.5) revealed that NAb binding was significantly higher on the POPC:$MPER_{656}$ membrane compared with binding on the model HIV:$MPER_{656}$ membrane (Figs. 5.5A,B *vs.* 5.5D,E). The R_{max} (maximum binding capacity) for POPC:$MPER_{656}$ was 65 ± 9 and 214 ± 10 response units (RU) for 4E10 and 2F5, respectively. For the model HIV:$MPER_{656}$ membrane, the R_{max} dropped to 9 ± 2 RU for 4E10 while binding of 2F5 was even weaker, and no reliable R_{max} values could be determined. These results qualitatively agree with our surface coverage (*i.e.*, binding) measurements by AFM imaging, which showed NAb coverage to be

between 42 and 47% for the POPC:$MPER_{656}$ SLB compared to only 2 to 4% for the model HIV:$MPER_{656}$ SLB. For the POPC and the model HIV membrane, 4E10 resulted in an R_{max} of 7 ± 2 and 5 ± 0 RU, respectively, while 2F5 resulted in an undetectable R_{max}. SPR measurements showed no detectable interactions of 13H11 for all membrane compositions tested (Figs. 5.5C,F).

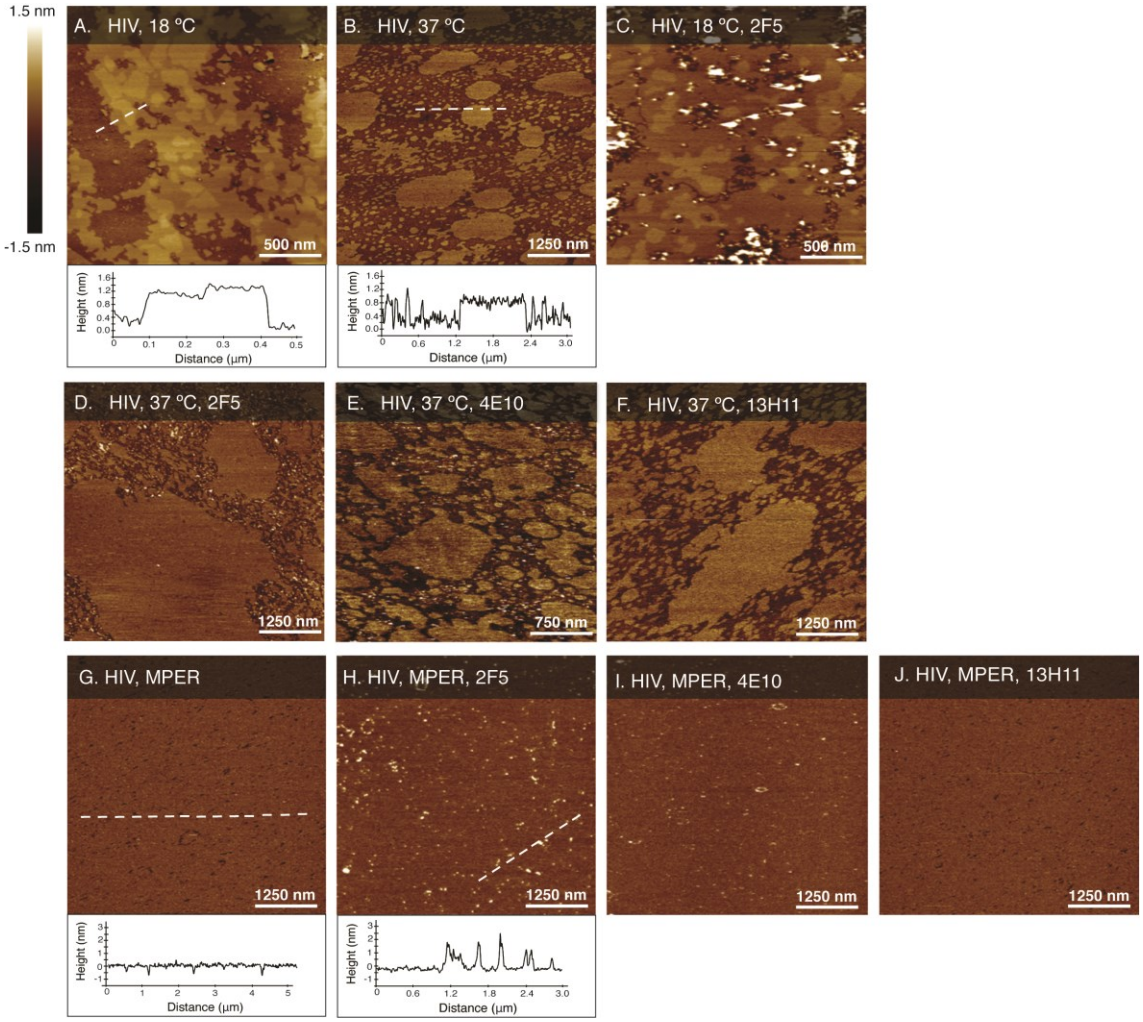

Figure 5.4: AFM height images of the model HIV and model HIV:MPER$_{656}$ SLB with and without antibody addition. Height cross-section of SLBs given below select images. (A,B) Model HIV SLB imaged at 18 °C and 37 °C, respectively. (C,D) 2F5 added to the model HIV SLB at 18 °C and 37 °C, respectively. (E,H) 4E10 and 13H11 added to the model HIV SLB at 37 °C, respectively (G) Model HIV:MPER$_{656}$ SLB at 37 °C. (H-J) 2F5, 4E10, and 13H11 added to the model HIV SLB:MPER$_{656}$, respectively (at 37 °C).

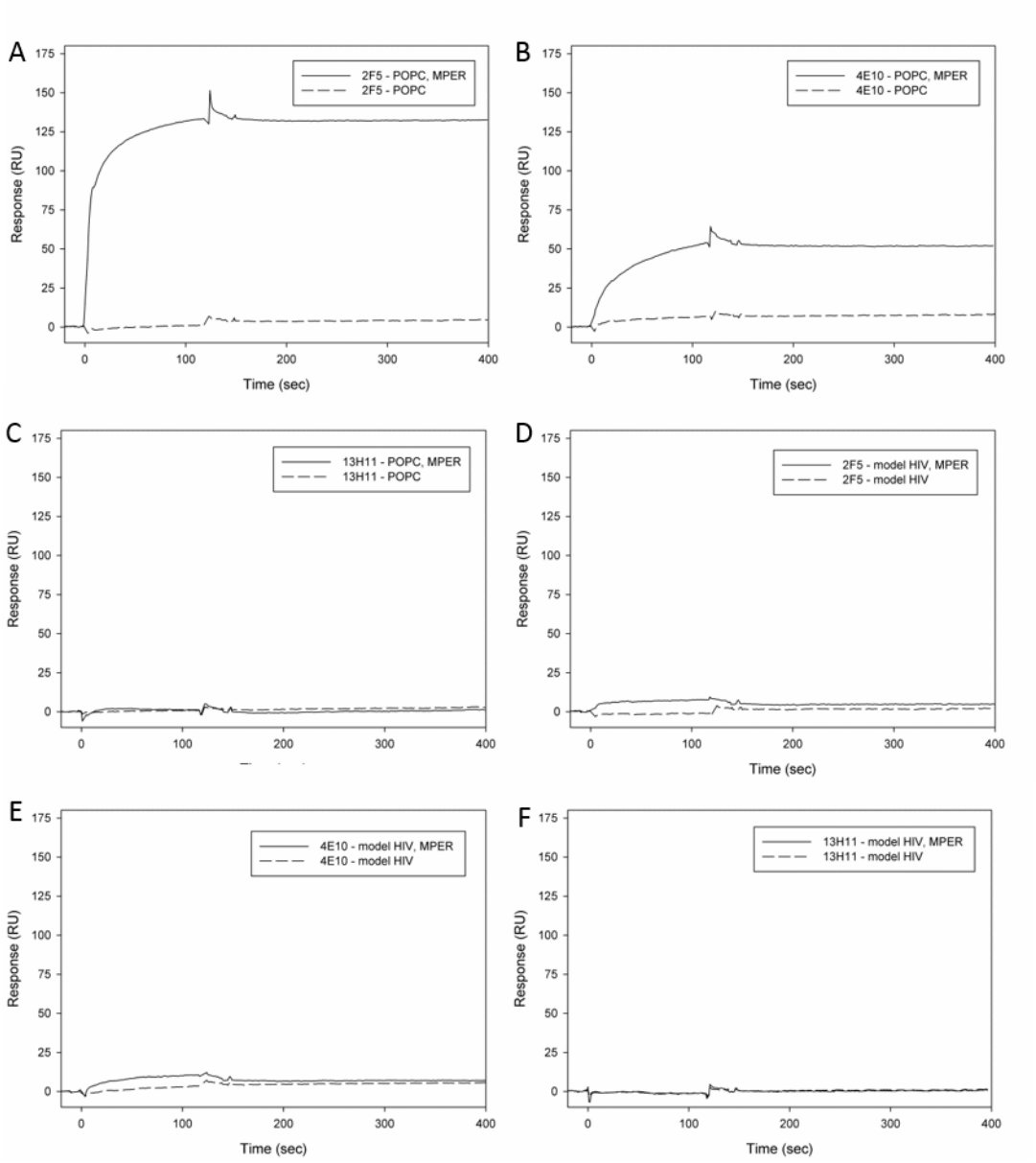

Figure 5.5: Surface plasmon resonance (SPR) curves of NAbs and 13H11 interacting with POPC and model-HIV membranes (with and without $MPER_{656}$). Antibodies added at 0 sec and washed from surface at 120 sec (resulting in response spike). (A-C) Antibodies interacting with POPC:$MPER_{656}$ (solid line) and POPC (dashed line) membranes. (D-F) Antibodies interacting with model HIV:$MPER_{656}$ (solid line) and model HIV (dashed line) membranes.

5.4 Discussion

5.4.1 NAb Interactions with SLBs

AFM imaging of NAbs interacting with the POPC and POPC:POPE SLB revealed that 2F5 and 4E10 exclusively interacted with the L_d membrane phase. For the POPC SLB the L_d phase made up 100% of the SLB area, while for the POPC:POPE SLB, the L_d area was 41 ± 4%. Despite the difference in L_d area, NAb binding coverage was about 3% on both SLBs. NAb coverage on the L_d area for the model HIV SLB could not be determined accurately due to the dispersed nature and small size of the L_d phase. Instead, we report NAb coverage relative to the total area of the model HIV SLB (Table 1). NAb binding on the model HIV SLB was similar to that on the POPC and POPC:POPE SLBs. NAbs exclusively interacted with the lipid phase with the lowest height and therefore the lowest lipid packing density, the largest membrane disorder, and the highest lipid diffusivity.[195-197] This result is in agreement with a previous AFM study completed by Franquelim et al.[168] The lipid diffusivity in the L_o phase is approximately a factor 2-10 smaller than in the L_d phase, depending on experimental details.[50-52] The presence of cholesterol is a major contributor to the physical properties of lipid domains. It has been shown that the force required to break the intermolecular lipid interactions in a cholesterol-rich L_o phase is greater compared to that in a cholesterol-depleted L_d phase.[197] This supports the hypothesis that the high order of L_o and gel domains prevented NAb insertion into these SLB areas.

Given the overall compositional and structural complexity of the model HIV SLB, the detailed lipid compositions of individual domains are unclear, but can be estimated considering the T_m values of the lipids. At 18 °C, the domain with the lowest height likely contains the highest concentration of POPC (T_m = -2 °C) and POPS (T_m = 14 °C). The middle and tallest domains likely contain the highest concentration of POPE (T_m = 25 °C), SM (T_m = 37 °C), and CH. When the temperature is increased from 18 °C to 37 °C, the SLB transitions from three to two phases. To create this two-phase system, it is likely that CH and SM have redistributed to form discrete L_o–L_d domains. At 37 °C, an L_o–L_d forming bilayer of the model HIV SLB agrees with the phase diagram of a similar bilayer composition, *i.e.*, POPC:PSM:CH (1:1:1).[53] X-ray diffraction experiments of another, similar bilayer composition, *i.e.*, DOPC:SM:CH (1:1:1), confirm the absence of a gel phase. This suggests that our model SLB also lacks a gel phase, and thus contains a L_d and L_o phase instead.[46] Furthermore, at 37 ºC, our model HIV domain height difference is 8.2 ± 0.4 Å, which agrees with expected L_o–L_d height differences. For example, Rinia *et al.* report similar height differences observed by AFM for DOPC:SM:CH bilayers that phase separate into L_o–L_d domains.[198] Thus, we believe that a L_d phase exists in our model HIV SLB, and since the L_d phase contains the highest lipid disorder, that it should reside in the domains of lowest SLB height, *i.e.*, the same domains to which NAbs bind. This suggests that NAbs interact exclusively with the L_d phase in the model HIV SLB.

Collectively, our experiments on the three SLB systems tested, demonstrate that NAbs 2F5/4E10 bind exclusively to the L_d phase and do not interact with the ordered gel and L_o domains. This also suggests that these NAbs likely target L_d regions on the native virus before binding to their MPER antigen on gp41. To elicit antibodies that can recognize and interact with the L_d phase, vaccine liposomes likely should also contain lipids that organize into a dominant L_d phase. However, as discussed below, vaccine antigens may adversely contribute to L_d formation.

5.4.2 Antigen/NAb interactions with SLBs

On the POPC SLB (L_d), antigen presentation and NAb binding was uniformly distributed across the entire SLB surface. This indicates that the L_d phase does not restrict or hinder antibody/antigen membrane interactions and facilitates high antibody to antigen binding. In the POPC:POPE:$MPER_{656}$ SLB (gel-L_d), $MPER_{656}$ resided exclusively in the L_d phase. Gel domains not only excluded NAb interactions, but also prevented $MPER_{656}$ membrane integration. The presence of $MPER_{656}$ also inhibited gel domain coalescence. This is seen in Figure 5.3 where, in presence of antigen, smaller gel domains still exist (Fig. 5.3E) when compared to the gel domains in absence of antigen (Fig. 5.3A). However, the overall L_d area remains relatively constant, *i.e.*, 41 ± 4% without and 39 ± 2% with $MPER_{656}$. The presence of $MPER_{656}$ in the model HIV SLB, decreased the total L_d area substantially. Without $MPER_{656}$, the model HIV SLB had an L_d coverage

of 39 ± 3%, and with $MPER_{656}$ the L_d area decreased to 3 ± 0%. When comparing the morphology between the model HIV SLB without and with $MPER_{656}$ (Fig. 5.4B *vs.* 5.4G), the presence of antigen resulted in a more homogenous lipid phase that is void of antigen-NAb binding. Large L_d areas fail to form, and the antigen is likely limited to the location of small (~30-60 nm in diameter) L_d pockets. This antigen distribution is in stark contrast to that in the POPC:$MPER_{656}$ (Fig. 5.2E) and POPC:POPE:$MPER_{656}$ (Fig. 5.3E) SLBs, where antigen is evenly distributed across the entire L_d phase. The NAb binding coverage is the lowest in the model HIV:$MPER_{656}$ SLB (2 ± 0% for both 2F5 and 4E10) compared to that on POPC:$MPER_{656}$ and POPC:POPE:$MPER_{656}$ SLBs.

SPR experiments confirmed that there is substantially less NAb-$MPER_{656}$ binding when $MPER_{656}$ is included in the highly ordered model HIV SLB when compared to the more fluid POPC SLB. Since both SLBs were prepared with an equal amount of $MPER_{656}$, we believe that the reduced NAb binding to the model HIV:$MPER_{656}$ SLB arises from the membrane structure and the organization of $MPER_{656}$ in the SLB. AFM topography images suggest that an ordered phase dominates in the model HIV membrane (~97% surface coverage). Either this ordered phase is completely void of $MPER_{656}$ or the antigen is buried in such an orientation that it cannot be detected by NAbs (or by the AFM cantilever during imaging). AFM images also show that $MPER_{656}$ appears to be restricted to the small pockets in the SLB that contain the L_d phase (~3% surface coverage). Only a limited number of NAbs can bind $MPER_{656}$ in these areas (Fig. 5.4H,I), before steric

restrictions likely prevent unbound NAbs from accessing unbound antigens, thus severely limiting NAb-antigen interactions.

5.5 Conclusion

Our results on SLBs demonstrate that NAbs 2F5/4E10 do not interact with the highly ordered gel or L_o phase but exclusively bind to the L_d phase. Using vaccine liposomes that mimic the high order of the HIV-1 envelope to induce antibodies that can recognize and bind to the viral envelope, may thus not be advantageous for 2F5/4E10 based vaccine strategies. Rather, vaccine liposomes that contain an L_d phase may provide optimal selection of 2F5- and 4E10-like antibodies.

In the context of liposomal antigen presentation, our results suggest that the presence of the $MPER_{656}$ peptide may severely limit the L_d area available for antibody interactions. Subsequently, this reduces the amount of $MPER_{656}$ that is accessible for 2F5/4E10 binding, since $MPER_{656}$ preferentially localizes to the L_d area. If L_d forming lipid components are used in vaccine liposomes, it is important to ensure that the presence of antigen does not inhibit large-scale L_d formation.

5.6 Materials and Methods

5.6.1 Antibodies and Antigen

Anti-HIV-1 gp41 (anti-membrane proximal) NAbs 4E10 and 2F5 were purchased from Polymun, Inc., Vienna, Austria. Mouse mAb 13H11 was produced from splenocytes from a mouse immunized with HIV Env oligomer CON-S [86], as described [84]. SLBs containing embedded HIV antigen, $MPER_{656}$-GTH1 (CPC Scientific Inc., San Jose, CA) were prepared by first dissolving antigen in chloroform and then adding to lipid mixture before being dried under nitrogen.

5.6.2 Lipid Preparation

1-palmitoyl-2-oleoyl-*sn*-glycero-3-phosphocholine (POPC), 1-palmitoyl-2-oleoyl-*sn*-glycero-3-phosphoethanolamine (POPE), 1-palmitoyl-2-oleoyl-sn-glycero-3-phospho-L-serine (POPS), brain sphingomyelin, and cholesterol in chloroform (Avanti Polar Lipids, Alabaster, AL) was brought to room temperature, dried under nitrogen, and then dried under vacuum for three hours. The lipid film was reconstituted in 37 °C PBS without Ca^{2+} and Mg^{2+}, pH 7.4 (Gibco Invitrogen, Grand Island, NY), vortexed, sonicated, and extruded 11 times through a 0.4 μm filter (Whatman, Florham Park, NJ), and then through a 0.1 μm filter.[88] The concentrated lipid solution was then diluted to 0.4 mg/mL in PBS buffer and vortexed immediately before use. After lipid extrusion, vesicle solutions were used within eight hours.

5.6.3 Atomic Force Microscopy

The AFM images presented are the highest quality images that are representative of the observations obtained from image replicates (n=3 for SLBs containing antibodies and n≥4 for all other SLBs). In all AFM experiments, 2F5 and 4E10 were tested individually; however, no significant differences between the NAbs were observed. Unless otherwise noted, NAbs were added at approximately 4.7 μM for SLBs without $MPER_{656}$ and 2.0 μM for SLBs with $MPER_{656}$. Control antibody, 13H11 was added at 4.7 μM for all membranes tested.

AFM imaging was performed using a commercial AFM (Nanoscope IV, Digital Instruments/Bruker, Santa Barbara, CA) operating at room temperature. Images were obtained in buffer with tapping mode using triangular Si_3N_4 cantilevers (Bruker, SNL-10) with a spring constant of 0.06 Nm^{-1}. Between AFM experiments, cantilevers that were previously exposed to NAbs were soaked in ethanol in an attempt to remove NAbs that were adhered to the cantilever tip. This was necessary, because we observed that adhered NAbs from previous experiments could transfer from the cantilever tip to the SLB during AFM scanning.

Formation of SLBs for AFM imaging was achieved by α-helical (AH) peptide-induced vesicle fusion.[60] First, 200 μL of 100 nm vesicle solution was added to a freshly cleaved mica surface taped to a Teflon puck. Samples were then washed with

buffer and incubated with AH peptide (Anaspec, San Jose, CA) at room temperature for at least 30 min. Stock AH peptide was prepared in dimethyl sulfoxide and diluted to 15 mM in buffer. Prior to AFM imaging, surfaces were rinsed by successive 50 μL buffer exchanges. High resolution (512 x 512 points) topographical images were then collected. Antibodies were added to SLB samples between AFM scans by pipetting 20-50 μL of buffer containing antibodies to the water meniscus on the mica sample (ranging from 60-120 μL). For experiments at 37 °C, a Thermal Applications Controller (Bruker, Santa Barbara, CA) was used to heat the sample. DI water was added to samples to compensate for water loss due to evaporation. Percent coverage of lipid domains and bound antibodies to SLB surfaces was calculated using height images analyzed with ImageJ software. Images were converted to grey scale and percent coverage was measured based on color thresholds. SLB RMS values (n=4) were calculated with NanoScope Analysis software.

5.6.4 Surface Plasmon Resonance

Surface plasmon resonance (SPR) measurements were performed on a BIAcore 3000 (BIAcore Inc., Uppsala, Sweden) instrument. Antibody binding (100 ug/mL) was monitored in real-time at 25 ^{o}C with a continuous flow of PBS, pH 7.4 (Gibco Invitrogen, Grand Island, NY) at 20 μL/min for 2 min. For lipid surfaces, approximately 500 RU of liposomes were captured on a BIAcore SPR L1 chip. A blank in-line reference surface

was used to determine non-specific or bulk responses. Bound protein was removed from the liposome sensor surfaces following each cycle of antibody binding by octyl β-D glucopyranoside, and 5 s injections each of 5 mM HCl then 5 mM NaOH. BIAevaluation 3.0 software (BIAcore Inc.) was used to determine R_{max} values. A bivalent analyte model was used to fit the binding curves of 2F5/4E10-POPC:MPER interactions and a Langmuir 1:1 model was used to fit the binding curves of all other antibody-membrane interactions.

Chapter 6. Conclusions and Future Research

6.1 Conclusions

The research activities reported in this dissertation have advanced the design and synthesis of model membrane systems in an effort to contribute to HIV-1 vaccine development. By using substrates functionalized with thiol self-assembled monolayers (SAMs), we were able to mimic lipid surface chemistry, and identify functional groups that contribute to specific antibody-lipid interactions. We found that a hydrophobic SAM surface enables the distinction between neutralizing and non-neutralizing antibodies, both lipid reactive and non-lipid reactive, and thus is well suited as a screening platform for identifying antibodies that can replicate 2F5 and 4E10's lipid reactivity. The unique hydrophobic reactivity of 2F5 and 4E10 supports the hypothesis that these NAbs embed into the hydrophobic membrane core, and suggests that immunogens designed to elicit 2F5/4E10-like antibodies may require an accessible hydrophobic lipid component.

Since the accessibility of the hydrophobic membrane core is largely controlled by lipid type and membrane organization, we next tested NAb binding in the context of supported lipid bilayers (SLBs). To this end we developed a technique to create complex, high cholesterol-containing SLBs, using α-helical (AH) peptide-induced vesicle fusion. Specifically we used vesicles consisting of POPC:POPE:POPS:SM:CH (9.35 : 19.25 : 8.25 : 18.15 : 45.00) to form a SLB that reflects the native composition of the human immunodeficiency virus-1 (HIV-1) lipid envelope. In the absence of AH peptides, these

biomimetic vesicles fail to form a complete SLB. We verified and characterized AH peptide-induced vesicle fusion by quartz crystal microbalance with dissipation monitoring (QCM-D), neutron reflectivity (NR), and atomic force microscopy (AFM). This vesicle fusion technique gives researchers access to complex SLB compositions with high cholesterol content and thus the ability to work with model systems that recapitulate the native HIV-1 lipid membrane.

This SLB research platform was then used to visualize membrane domains, HIV antigen presentation, and HIV antibody-membrane interactions. Our results demonstrate that NAbs 2F5/4E10 do not interact with the highly ordered gel or L_o phase, but rather bind exclusively to the L_d phase. Thus, vaccine liposomes that contain a dominant L_d phase may provide improved selection of 2F5- and 4E10-like antibodies. However, our results also showed that the presence of vaccine antigen, $MPER_{656}$ peptide, can severely limit the L_d area available for antibody interactions. Subsequently, this reduces the amount of $MPER_{656}$ that is accessible for 2F5/4E10 binding, since $MPER_{656}$ preferentially localizes to the L_d area. If L_d forming lipid components are used in vaccine liposomes, it is important to ensure that the presence of antigen does not inhibit large-scale L_d formation.

In summary, this research has helped to advance the design and synthesis of model membrane systems, and has helped to gain a more complete, mechanistic understanding of the interaction of HIV-1 neutralizing antibodies 2F5 and 4E10 with

lipid membranes. Ultimately, this information can help guide HIV-1 vaccine development efforts. More broadly, this research contributes to the understanding of native lipid organization and progresses the understanding of more physiological relevant multi-component lipid membranes.

6.2 Future Research

There are two main areas of future work: (i) application and characterization of SLB model lipid systems, and (ii) continued HIV-1 vaccine related research.

6.2.1 Application and Characterization of the SLB Model Lipid System

There are many membrane properties and characteristics that have yet to be determined for phase-separated SLBs with multiple lipid types and high cholesterol content. Those of high importance include the effect of the membrane curvature on domain organization, and the effect of transmembrane proteins on lipid organization, and identifying physical properties of domains, including composition, thickness, and diffusivity.

While planar SLBs are essential for quantitative surface-characterization techniques, they do not recapitulate the local and global curvature of the native HIV-1 envelope, which could influence lipid organization.[199] To remedy this potential concern, it will be important to explore SLB formation on wrinkled oxidized

poly(dimethylsiloxane) (PDMS) surfaces.[200] The separation and height of the wrinkles can be precisely controlled from tens to hundreds of nanometers, which would allow the determination of protein-membrane interactions as a function of local substrate curvature. Such PDMS surfaces are ideally suited for SLB formation,[201] and are compatible with AFM imaging and fluorescence microscopy.[200]

SLB research platforms often include important membrane proteins. As seen with the MPER antigen, inclusion of proteins in SLBs can have a dramatic effect on membrane organization. Although the SLBs used for this research were all formed on solid substrates (silica, gold, and mica), these substrates do not readily allow the inclusion of transmembrane proteins. A typical, solid-supported SLB has a hydration layer of 1–3 nm that separates the SLB from the substrate. This is often insufficient space for SLBs containing transmembrane proteins. The cytosolic domain of the protein could thus easily contact the substrate which would result in adhesion, deformation, and eventually denaturation. The use of polymer cushioned SLBs can overcome this problem by providing a low friction spacer layer that accommodates transmembrane proteins. To make the transition from complex solid supported SLBs to polymer supported SLBs it is necessary to first test the use of AH peptide-induced vesicle fusion on polymer substrates.

With phase-separated SLBs is it important to understand the physical properties of each domain type. NanoSIMS, confocal microscopy in conjunction with fluorescently

tagged lipids, and force volume imaging using chemically functionalized AFM cantilevers, are important techniques that we have not yet utilized to provide structure-function relationships. A high priority is also the identification of lipids within specific lipid domains when creating SLBs from multiple lipid types. While lipid domains inherently contain a composition different from that of the surrounding membrane, it is also likely that the lipid compositions in the upper and lower bilayer leaflet will differ.[161] This composition difference may be significant since only the upper leaflet is available to directly interact with antibodies. To detect asymmetry in our SLBs one can use sum frequency generation (SFG) spectroscopy, which is a highly surface sensitive characterization method.[202, 203] While the bulk phase of most materials does not emit sum frequency light, the asymmetry of a lipid bilayer will produce sum frequency signals. This inherent interface specificity can be used to probe the molecular leaflet arrangements in our SLBs.

6.2.2 Continued HIV-1 Related Research

There are many remaining questions on how lipid composition contributes to HIV neutralization and vaccine design. Open questions include:

1. How does the density of MPER antigen contribute to domain organization? We observed that at 0.216 mol %, the presence of MPER

significantly reduced the L_d area in the model HIV SLB. Will this also occur at a lower concentration of antigen?

2. Does the antigen disrupt domains in the model HIV SLB without cholesterol? If cholesterol is titrated into the SLB composition, at what concentration does MPER inhibit domain formation?

3. Instead of localizing MPER to the L_d phase, can MPER's membrane anchor be changed so it localizes to the L_o phase? Will NAbs then bind to MPER when it is surrounded by the L_o phase? What effect will CD4-MPER binding have on domain localization?

4. Can an SLB form large L_d areas while containing large amounts of cholesterol and antigen? Cholesterol is likely needed in vaccine liposomes to create sufficient liposome shelf-life and mechanical stability, while MPER antigen is required to elicit relevant antibodies. However, we showed that both cholesterol and antigen can inhibit L_d phase formation, the phase for which 2F5/4E10 exclusively bind. Thus, it should be a priority to discover a lipid composition that is able to contain cholesterol and antigen, but also large-scale L_d phase formation.

5. Can SLB compositions be created that more accurately mimic current vaccine liposomes and the native HIV-1 envelope? Membrane components that could be added to our SLBs may include lipid A, native

lipid rafts, glycosylated lipids, and full length gp41 or gp160 peptides. To include, transmembrane HIV proteins within SLBs, it is likely that SLBs will need to be created on polymeric cushions. This provides further motivation to establish SLB formation techniques on polymer substrates.

6. Neutralizing antibody, 10E8, interacts preferentially with the cholesterol-rich, HIV-1-like membrane and has a weaker interaction to host membranes.[204] Will 10E8 interact with L_o domains?

It is also a priority to use our research platform and methods to study not only 2F5/4E10-viral membrane interactions but also other promising HIV-1 NAbs for which their epitopes are optimally expressed in the context of cell membranes.[205, 206] Potent neutralizing antibodies, VCRO1, PG9, and PG16, all have optimal antigen binding when their antigen is expressed within a cell membrane. Our SLB platform would allow us to extend our biophysical surface characterization techniques to help determine how and why these antibodies prefer membrane bound antigens. This information is significant for designing vaccine liposomes that could contain these membrane bound antigens for immunization studies.

Finally, in order to validate current results and substantiate future research, it is essential to complete the following aim: Demonstrate that vaccine liposome compositions can contribute to antibody specificity.

This aim will validate that lipid compositions can dictate and contribute to antibody specificity. The research presented here provides the foundation for answering questions about which lipids should be used in vaccine liposomes for animal immunization studies, *i.e.*, the transition from *in vitro* to *in vivo* experiments.

Appendix A. Membrane Screening Platforms Fabricated by Dip-Pen Nanolithography

A.1 Introduction

Appendix A details progress towards fabricating a high-throughput phospholipid screening platforms using dip pen nanolithography (DPN). This research seeks to expand our SLB systems by writing lipid islands using DPN to generate a high-throughput, array-based antibody screening platform. Currently, nanopatterned arrays of SLBs that contain different and complex lipid compositions cannot be achieved by vesicle fusion. The proposed screening platform will ultimately enable the efficient testing of multiple variables contributing to HIV-1 membrane organization, antigen distribution, and antibody binding in a single experiment under controlled conditions.

Our approach is to first characterize high cholesterol containing lipid arrays prepared by lipid dip-pen nanolithography (DPN) in both liquid and in air. We also utilize α-helical (AH) fusion peptide to attempt to create HIV-1 mimetic domains within SLB islands created from dip pen nanolithography (DPN). This appendix will summarize progress achieved toward these objectives from research completed at Karlsruhe Institute of Technology under the guidance of Dr. Dr. Michael Hirtz. The results presented are preliminary and provide a basis for continuing these research objectives.

A.2 Background

Dip pen nanolithography (DPN),[207] is a scanning probe based, parallel patterning technique. DPN can be used to pattern lipid bilayers and will thus enable the fabrication of combinatorial, high-throughput SLB screening platforms, amenable to testing membrane organization and NAb-lipid reactivity. Unlike other lithographic techniques, DPN is a direct-write "constructive" method that allows soft and hard materials to be printed from scanning probe tips on a surface from tens of nanometers to many micrometers in size. The technique works by delivering chemical or biological reagents ("inks") to a substrate with nanometer precision. The tip, usually an AFM cantilever, is coated in ink and brought into contact with the substrate as a fluid meniscus forms between the tip and the surface. Ink molecules move through this meniscus to deposit onto the surface (depicted in Fig. A.1). Importantly, it is not necessary to modify the surface and DPN can be used to deposit multiple compounds, sequentially or in parallel, in a precise and exclusive manner. During the last decade, DPN has been developed to pattern a wide variety of inks, including small organic molecules[207, 208], polymers[209, 210], DNA[211, 212], proteins[212-214], antibodies[215], nanoparticles[216], and metal ions[217] which result in many diverse applications. The ability to pattern such biomolecules with nanometer precision is essential for a variety of biological applications including: studying cell surface binding

events[218], immobilizing antibodies for pathogen screening[215, 219], and deposition of therapeutic drugs on implantable biomaterials.[220]

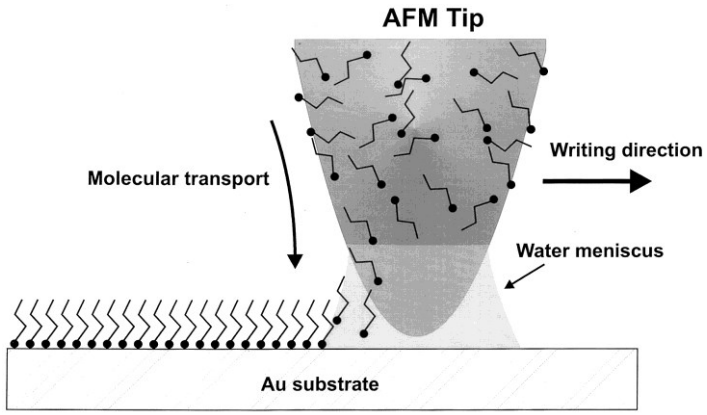

Figure A.1: Conventional dip-pen nanolithography. An AFM cantilever tip is coated with molecules in solution. As the tip travels across a substrate molecules are deposited through the fluid meniscus. Adapted with permission from reference [221]. Copyright (1999) Science.

Our research will focus on using DPN's ability to print lipids on substrates with nanoscale resolution to create monolayer and bilayer assemblies. Previous lipid DPN[222] research has mainly targeted applications toward biosensing[223-226] with a focus on analyte detection, functionalization, and quality control. This past research fails to characterize and control the structure and organization of lipid patterns in liquid. The ability of lipids to organize into domains and dictate membrane associated protein clustering is essential to the native cellular bilayer. Thus, it is crucial to create membrane

domains and achieve protein integration into SLBs upon DPN patterning if DPN is to be utilized as a research platform to model native membranes.

SLBs formed from classical vesicle fusion are the standard for modeling cellular membranes. However, this classical SLB formation is inherently limited since it is difficult to control nanoscale patterning of the SLB or the ability to easily define different lipid composition on the same substrate. Thus, it is the focus of lipid DPN to be able to overcome those limitations. A DPN array-based lipid platform also eliminates experimental variations that typically arise when comparing results from substrates that use classical SLB formation. Since a DPN array of SLB compositions are tested on the same substrate, they are exposed to identical experimental variables such as temperature, protein concentrations, and washing conditions. SLBs are extremely sensitive to such experimental variations and the ability to eliminate these confounding variables insures any differences observed between tested variables are not influenced by experimental deviations.

Although patterning domain-containing SLB islands with DPN is a relatively new concept, there are other, more established, methods of patterning SLBs. These techniques include robotic spotting,[227] ink-jet printing,[228] and microcontact printing.[201] While these techniques are established, they have many disadvantages compared to DPN, including limited reproducibility, residue transfer from stamps to substrates, molecular denaturation, and limited size resolutions. Importantly, these

techniques cannot obtain the lateral resolution of DPN. DPN lipid islands can range from tens of nanometers to micrometers in diameter. Spotting, ink-jet printing, and stamping can only achieve resolution on the order of tens of micrometers.[229] DPN's nanometer resolution is essential since a major focus of lipid patterning is for cellular and viral interactions. Cell diameters are in the range of tens of micrometers and enveloped viruses are in the range of hundreds of nanometers. Thus, to target localized areas of cell and viral membranes, nanometer scale patterning of molecules (*i.e.*, ligands) is required. Previous research has established that optimal spacing of cellular ligands that influence stress fiber formation, focal adhesion, cell motility, proliferation, and differentiation range from 10 nm to 500 nm.[230-232]

To gain access to DPN capability and expertise, we have established a collaboration with Michael Hirtz (KIT, Karlsruhe, Germany). Dr. Hirtz is an expert in DPN and has already begun to focus on SLB formation from lipid DPN. Hirtz and colleagues have successfully patterned lipid islands consisting of a combination of an assembled lipid monolayer and bilayers (Fig. A.2). The schematic depiction of lipid assemblies in Figure A.2 can be seen in Figure A.3.

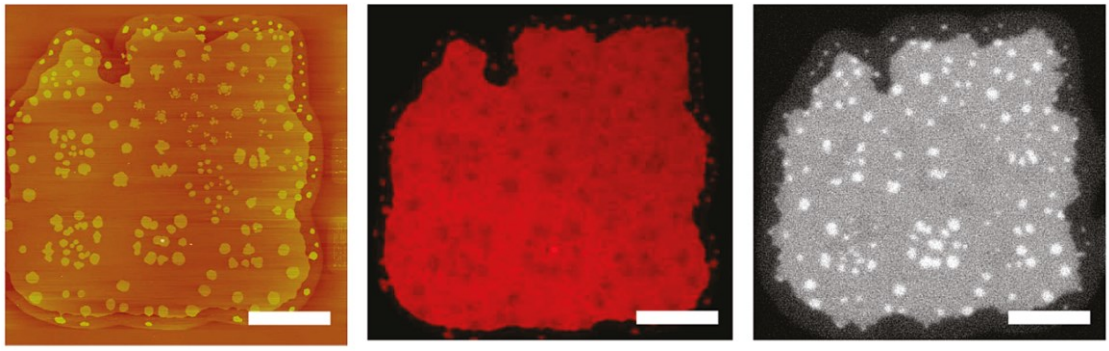

Figure A.2: Images of lipid stack structures in air with 20 mol % admixing of DNP Cap PE to DOPC as carrier ink obtained by AFM, FM, and SEEC microscopy (left to right, respectively). Scale bars = 20 μm. Adapted with permission from reference [233]. Copyright (2011) American Chemical Society.

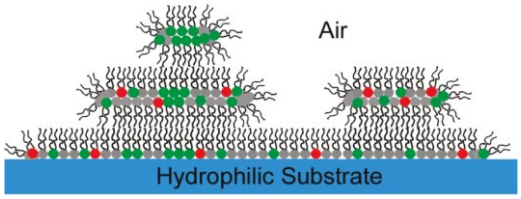

Figure A.3: Structural model for lipid membrane stacking. The three-layer membrane stack consists of a single monolayer as wetting layer and two bilayers. Adapted with permission from reference [233]. Copyright (2011) American Chemical Society.

AFM, fluorescence microscopy (FM), and surface-enhanced ellipsometric contrast (SEEC) imaging revealed (i) a flat silicon oxide surface of the substrate, (ii) a first lipid layer approximating the height of a monolayer, (iii) a second lipid layer with a height of a single bilayer and (iv) a third lipid layer with a height of a single bilayer. The SEEC image profile shows optical thicknesses of 2.5 nm for the first layer, 5.0 nm for the

second layer, and 4.8 nm for the third layer. These images were taken in air, however, the dehydrated lipid structure is expected to be conserved upon exposure to water.[234, 235] This research has initiated the effort to characterize and control the structure and organization of lipid DPN patterns. Further research is necessary, however, to enable lipid DPN to write biomimetic, domain containing SLBs in liquid.

A.3 Results and Discussion

To model the high concentration of sphingomyelin (SM) and cholesterol (CH) in the native HIV-1 envelope, the main lipid composition tested was DOPC:SM:CH with two different ratios of cholesterol, 18.25 and 30.00 molar %. The lipid ink wells and the multiplexed AFM cantilever array can be seen in Figure A.4. Sphingomyelin remained constant at 18.25 molar percent, which is the molar ratio recommended to mimic the amount of sphingomyelin in the native HIV-1 envelope. DOPC was used as a carrier ink and constituted the remaining molar percent of lipid. Thus, the molar ratios of lipid mixtures tested was DOPC:SM:CH (63.5 : 18.25 : 18.25) and DOPC:SM:CH (51.75 : 18.25 : 30.00). All presented results are for these compositions unless specifically stated. Primary characterization of lipid DPN will be from atomic force microscopy (AFM) height and phase imaging in air and in liquid. Fluorescent imaging will be used to gain a macroscopic perspective on lipid DPN islands.

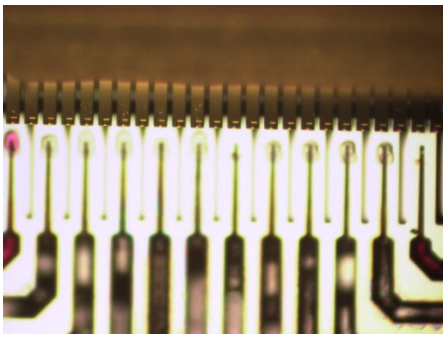

Figure A.4: Lipid ink well (lower half of image) and dip pen nanolithography cantilever array (upper half of image).

A.3.1 Optimization of Lipid DPN Parameters

Optimal lipid DPN writing on glass for both compositions occurs between 60 – 70% writing humidity with 2.3 nm writing density for square patterns between 5-10 micrometers in length. These parameters helped achieve uniform pattern coverage while minimizing lipid spreading and maintaining as few lipid multilayers as possible. See the Methods section for complete details.

Mica substrates were tested for lipid DPN in an attempt to minimize substrate effects on lipid organization (as seen with glass substrates, Fig. A.9), however, this was abandoned because, (i) it is difficult and time consuming to define an accurate plane when writing lipid patterns due to the highly curved mica samples, and (ii) the increased hydrophilicity of mica compared to glass requires different writing parameters to prevent mulitlayers and lipid spreading. Mica writing parameters for the lipid mixtures of interest have not been determined.

A.3.2 AFM Characterization of Lipid DPN in Air

After imaging DOPC:SM:CH (63.50/51.75 : 18.25 : 18.25/30.00) islands in air there are three major results observed from AFM height and phase images; (i) height cross-sections, (ii) halo effect, and (iii) the influence of cholesterol on lipid DPN writing.

(i) Height Cross-sections: Lipid DPN islands, in air, result in a base layer of lipids approximately 5 nm in height (Fig. A.5). Figure A.5 shows that there can be additional lipids on top of the base coverage that form a 5 nanometer height addition to the top of the base layer. When optimizing DPN writing parameters, it was the goal to achieve uniform coverage of only a 5 nm height difference between the lipids and the substrate. Within the base layer, small height differences, just less than 1 nm, can be observed at both the edges (Fig. A.6) and interior of the base layer (Fig. A.5D). It is possible that these areas indicate domain formation, however, this inference has not been proven or linked to the presence of sphingomyelin or cholesterol.

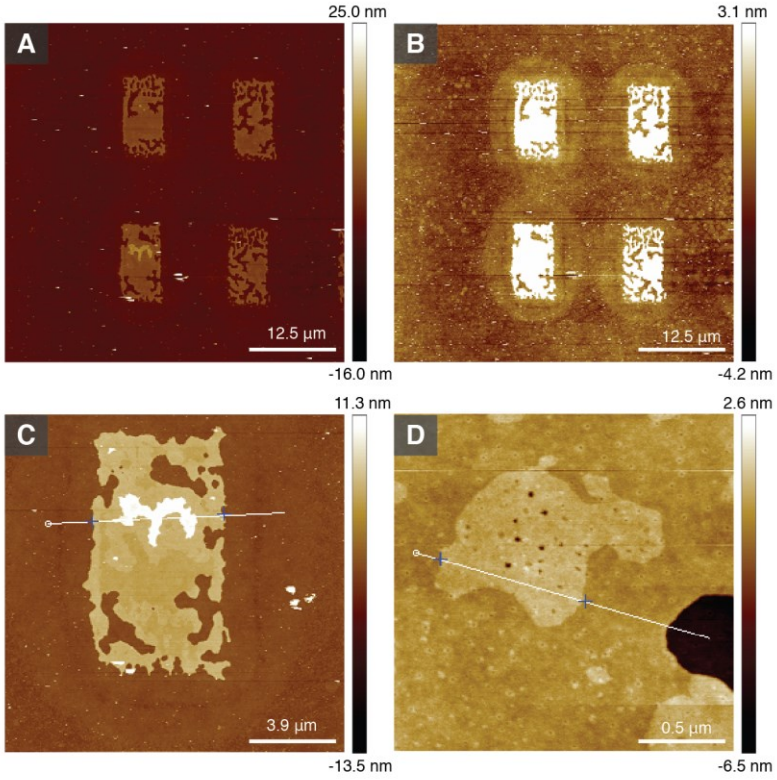

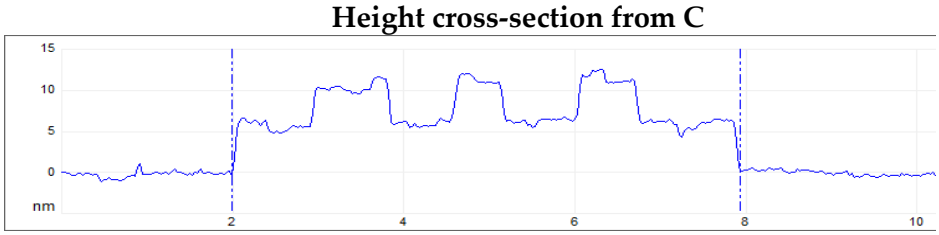

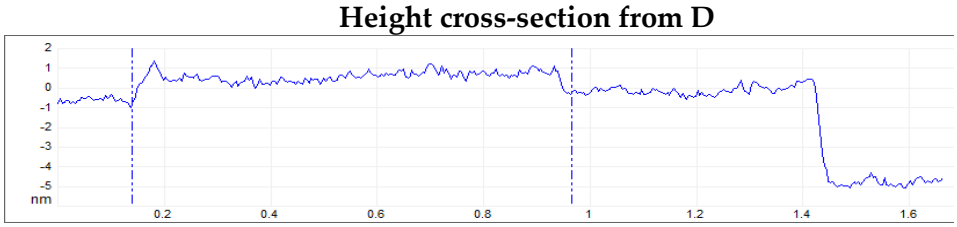

Figure A.5: AFM height images of lipid DPN islands in air. DOPC:SM:CH (51.75 : 18.25 : 30.00) written at 60% humidity.

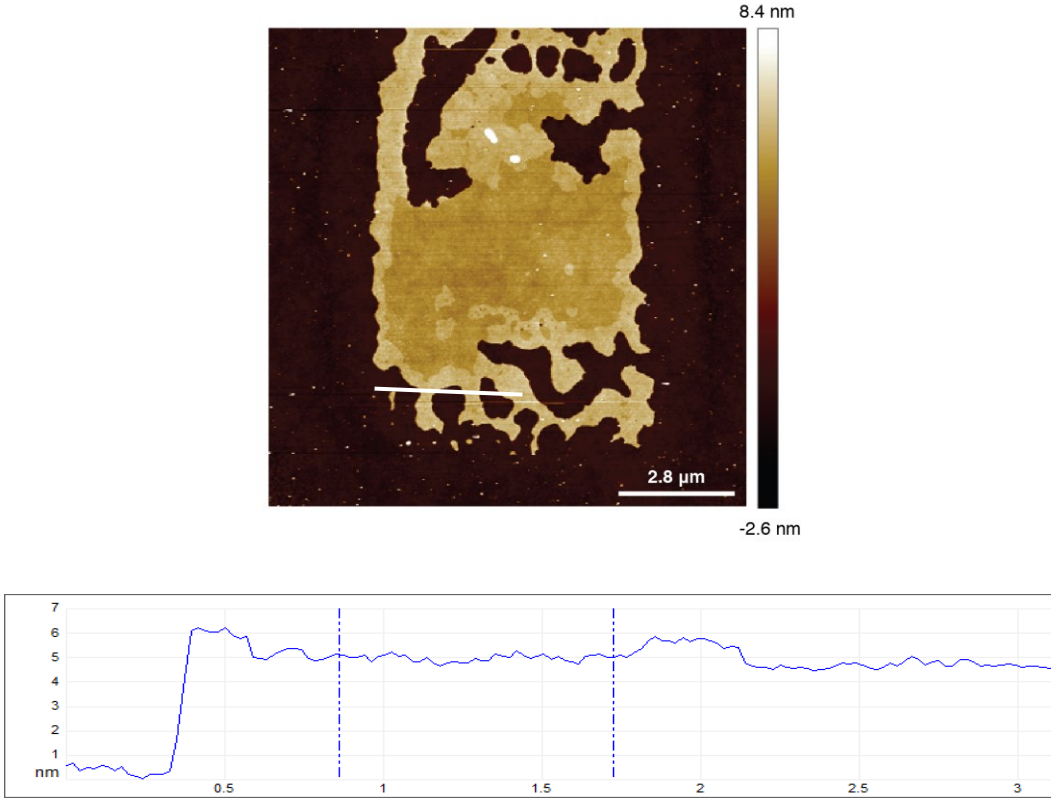

Figure A.6: AFM height image showing the height elevation on outer edge of DPN islands and patches of elevated lipids within the interior of DPN island. Height cross-section given below the image.

(ii) *Halo effect:* There is a presence of a faint circular ring, termed a halo, which appears to originate from DPN islands. This halo can be observed in both AFM height and phase images (Fig. A.7). This halo appears to be specific for islands that contain cholesterol since it is not observed in island containing solely phospholipids (images not shown). This halo may be important because if it contains cholesterol, then it suggests that the composition of the base layer lipid pattern contains less cholesterol then the original molar ratio of the lipid ink. The halo also appears to take the shape of the base

layer lipid island. In Figures A.7D,E the top of the island projects upwards into a small line of lipids. The phase image of Figure A.7E shows the halo wraps around this projection with the same width (lateral spread) as the main square island.

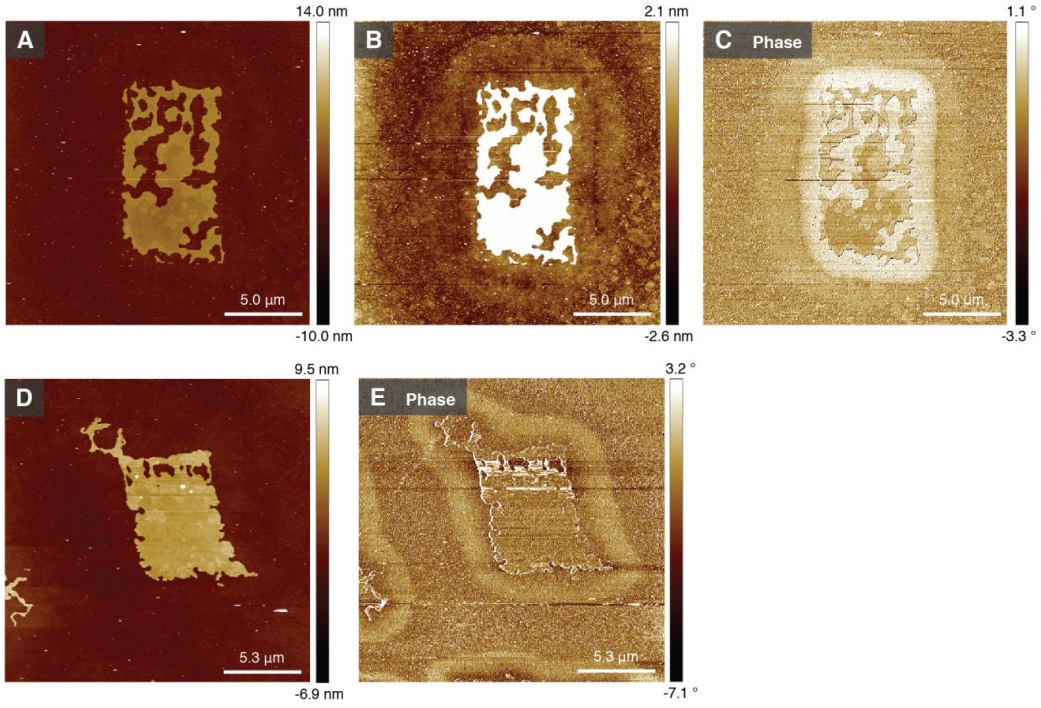

Figure A.7: AFM height (A,B,D) and phase images (C,E), in air of lipid DPN islands demonstrating the halo effect.

(iii) *Influence of cholesterol on lipid DPN writing:* As expected, the presence of cholesterol in lipid inks effects the transfer of lipids mixtures from the AFM tip to the substrate. As the molar ratio of cholesterol increases, the ink transfer from tip to the substrate decreases. This relationship can be observed in Figure A.8.

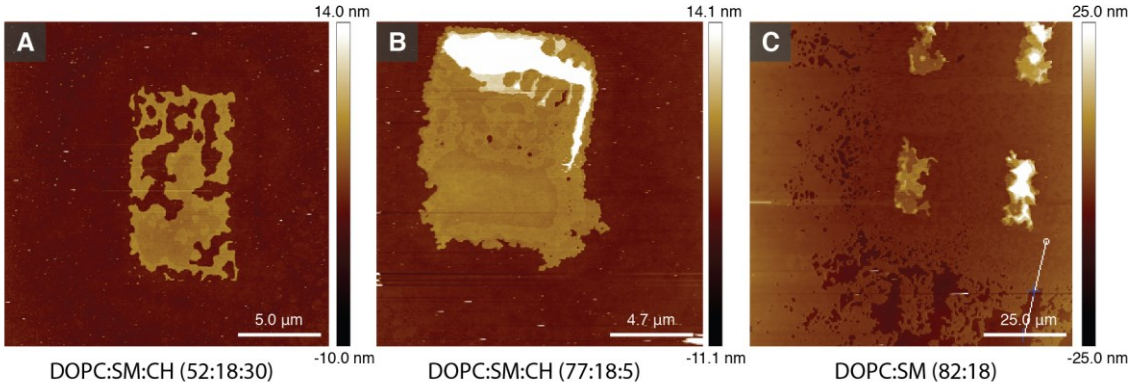

Figure A.8: AFM height images of DPN islands consisting of 30, 5, and 0 molar % of cholesterol (A,B, and C respectively). As the molar ratio of cholesterol increases, the lipid ink transfer from tip to the substrate decreases. All lipid compositions were written at 60% humidity, on glass.

Remaining questions to test and answer: Is the appearance of the 1 nm height differences due to domain formation? Is the presence of cholesterol in the lipid mixture responsible for the formation of this height difference? What is responsible for the appearance of the halo? Does the halo contain cholesterol?

A.3.3 AFM Characterization of Lipid DPN in Liquid

Characterization of lipid DPN islands in liquid resulted in eight major observations; (i) surface of bare glass in liquid, (ii) lipid smear from AFM imaging, (iii) dimples within base layer coverage, (iv) lipid DPN topography- with and without AH

fusion peptide, (v) blocking lipid DPN islands, (vi) antibody addition to DPN substrates, (vii) vesicle fusion versus DPN, and finally, (viii) lipid DPN island stability.

(i) Clean, bare glass in liquid: AFM height images of bare glass substrates in liquid are first considered. As seen in Figure A.9, the glass surface results in patches with a height difference of approximately 1 nm. These patches resemble domains seen in planar supported lipid bilayers (SLBs), however, it is believed these patches do not contain lipids. Height images from a fresh AFM tip (Figs. A.9A,B) were compared to height images from a heavily used AFM tip (Figs. A.9C,D) which likely had lipids adhered to the surface of the tip. This comparison was made to confirm that lipid transfer from the tip to substrate was not responsible for creating the topography observed. Both test conditions give similar height images of bare glass. It should be noted that when clean, bare glass is imaged in air, a smooth surface is observed with no topographical features.

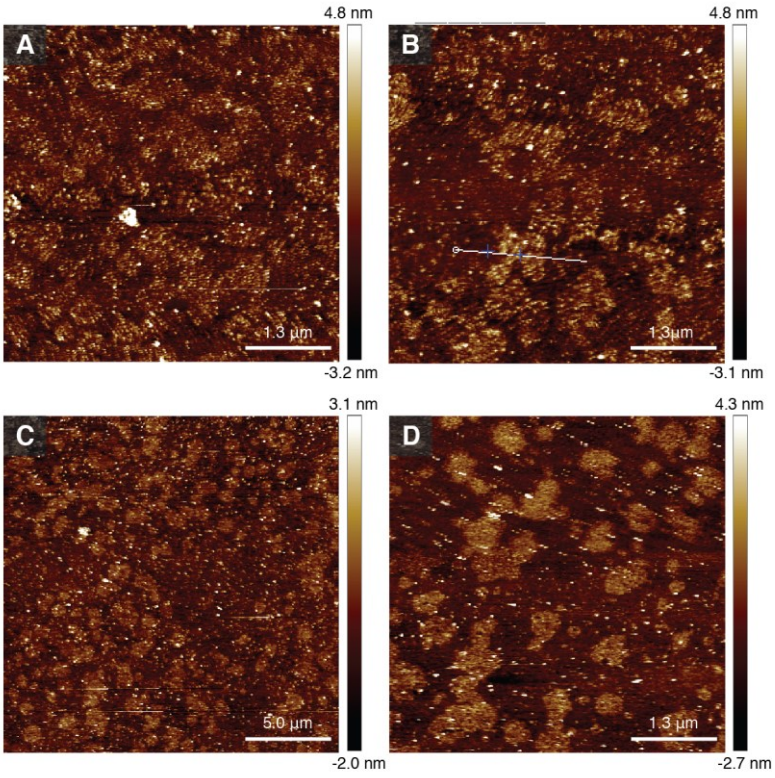

Figure A.9: (A,B) AFM height images from a fresh tip, imaging fresh glass in buffer (tapping mode). (C,D) AFM height images from a heavily used tip, imaging fresh glass in buffer (tapping mode).

(*ii) Lipid smear from tapping mode:* While imaging the edges of lipid DPN islands it was observed that lipids, with a very irregular height profile, occupied the area directly adjacent to the boundaries of the lipid DPN islands. It was determined that lipid smearing from the AFM tip contributed to the placement of these lipids adjacent to lipid islands. Using fluorescently tagged lipids (1 molar %) smearing could be observed only on islands imaged by the AFM (indicated by the red arrows in Fig. A.10). Lipids are transferred from the main DPN island to the surrounding glass substrate by the AFM

tip. There is no fluorescent smearing observed from islands that have not been imaged with the AFM (islands with no red arrow).

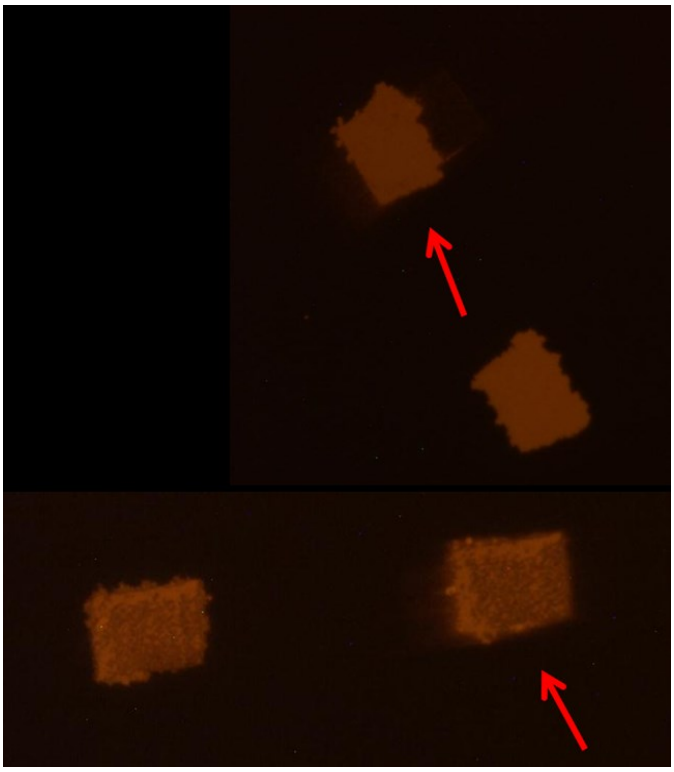

Figure A.10: Fluorescent images of lipid DPN islands, DOPC:SM:CH (63.50 : 18.25 : 18.25) with Rho-PE dye, taken at 63 x in liquid. The red arrows indicated islands that have been imaged by AFM tapping mode which results in lipid smearing. Lipids are transferred from the main DPN island to the surrounding glass substrate by the AFM tip.

(iii) Dimples within base layer coverage: Small holes, or dimples, about 20 nm in diameter regularly populate the base layer lipid coverage (Fig. A.11). Figure A.11A, is an image from a lipid mixture containing a 1:1 mixture of DOPC and POPE. Due to the small diameter of the holes, an accurate depth profile of the holes could not be determined. Currently, it is believed that these holes are a result of the underlying glass substrate. It is also noteworthy, that upon addition of AH fusion peptide, the holes still remained. Figure A.11B, was taken after AH fusion peptide was added and washed away.

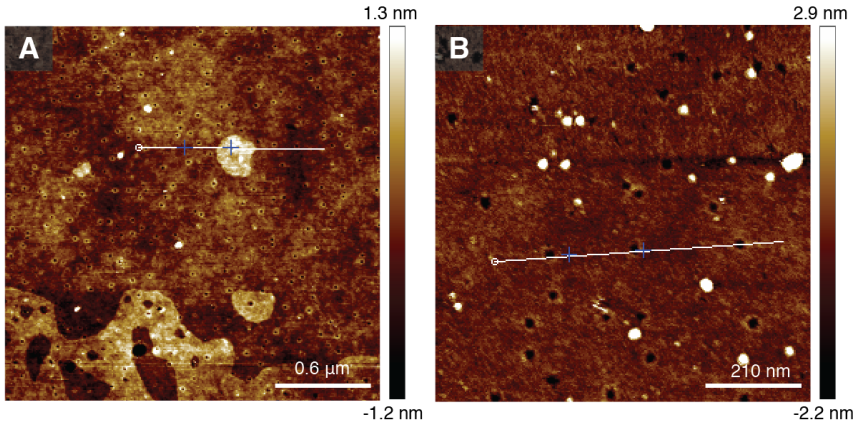

Figure A.11: (A) AFM height images showing regular arrangement of dimples on DPN island surfaces (DOPC:DOPE 1:1). (B) Height image of dimples after introduction and wash of AH fusion peptide.

(iv) Lipid DPN topography- with and without AH fusion peptide: The topography of lipid DPN islands in liquid can be seen in Figures A.12 - A.15. Often the surface contains

holes from 5-15 nm deep, striations from the raster pattern of the AFM tip during written can be observed, and the area directly adjacent to the lipid DPN pattern often contains an irregular surface approximately the same height of the written DPN island. Upon addition of AH fusion peptide, the holes are closed and the irregular lipid organization adjacent to the written DPN island is merged with the main island to create a smoother, more uniform lipid surface (Fig. A.12). After AH peptide addition, patches within the main SLB are observed to be 1.5 nm tall (Fig. A.14).

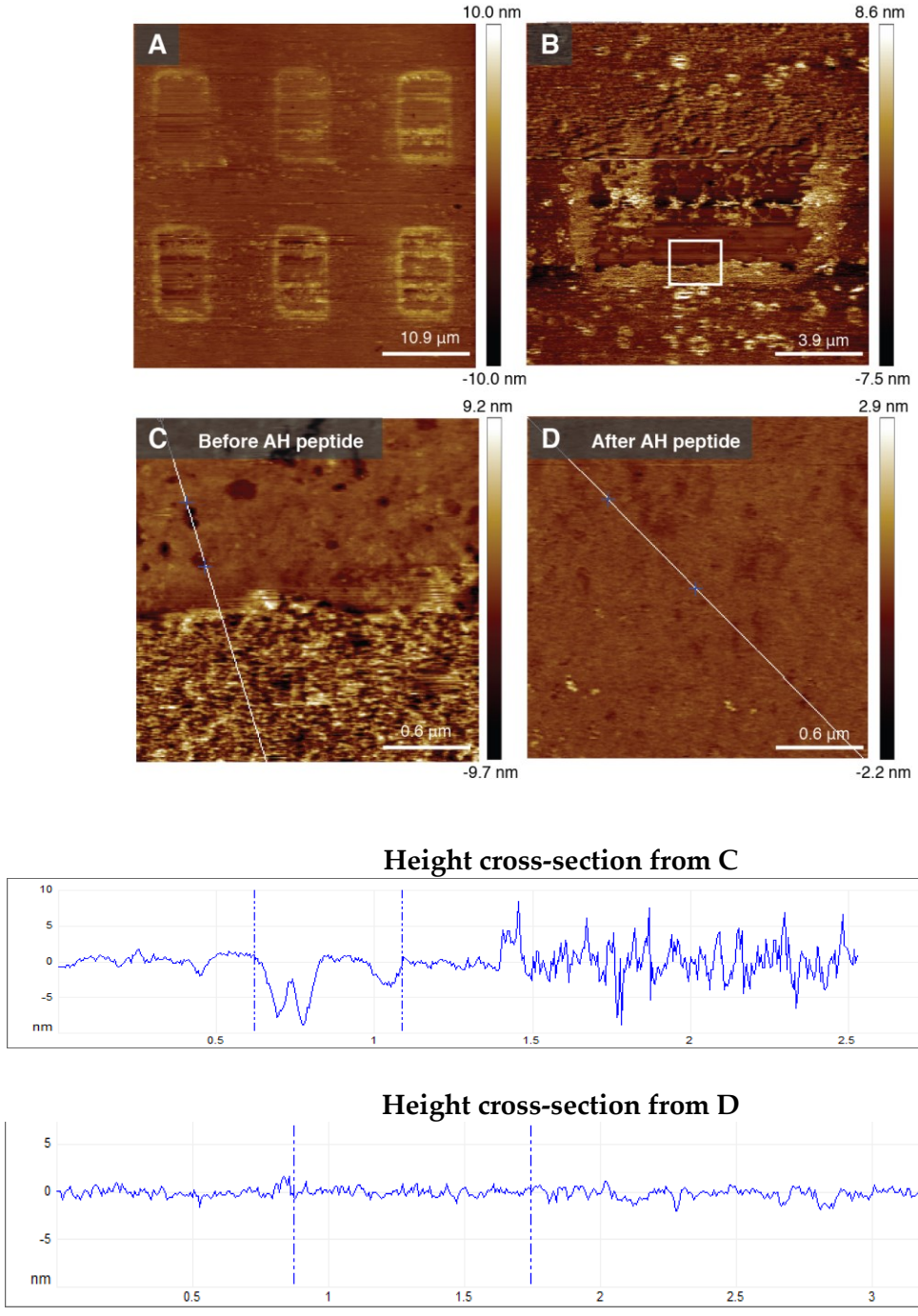

Figure A.12: AFM height image of lipid DPN islands in buffer. DOPC:SM:CH (51.75 : 18.25 : 30.00), 60% writing humidity. Before and after images of AH fusion peptide addition from the zoomed in region from B. The corresponding height profiles are given below the height images. DOPC:SM:CH (51.75 : 18.25 : 30.00)

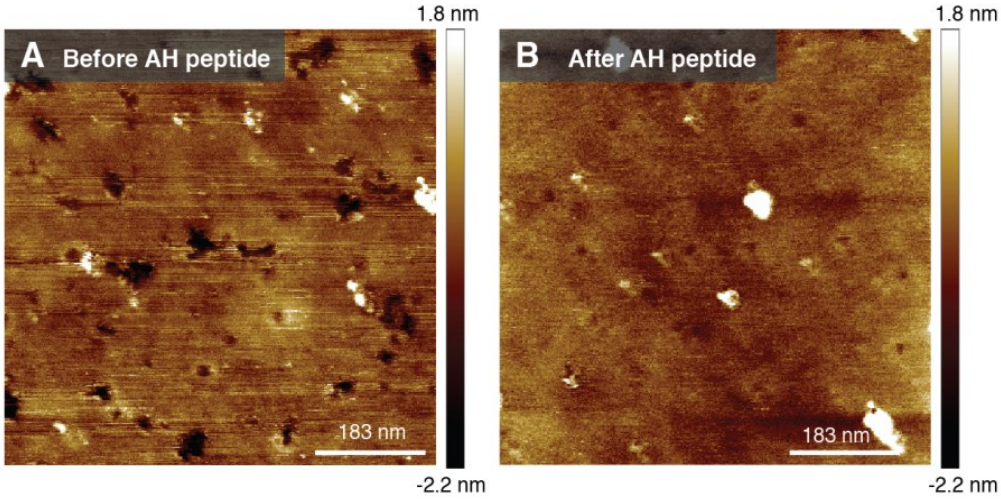

Figure A.13: AFM height images before (A) and after (B) introduction of AH fusion peptide.

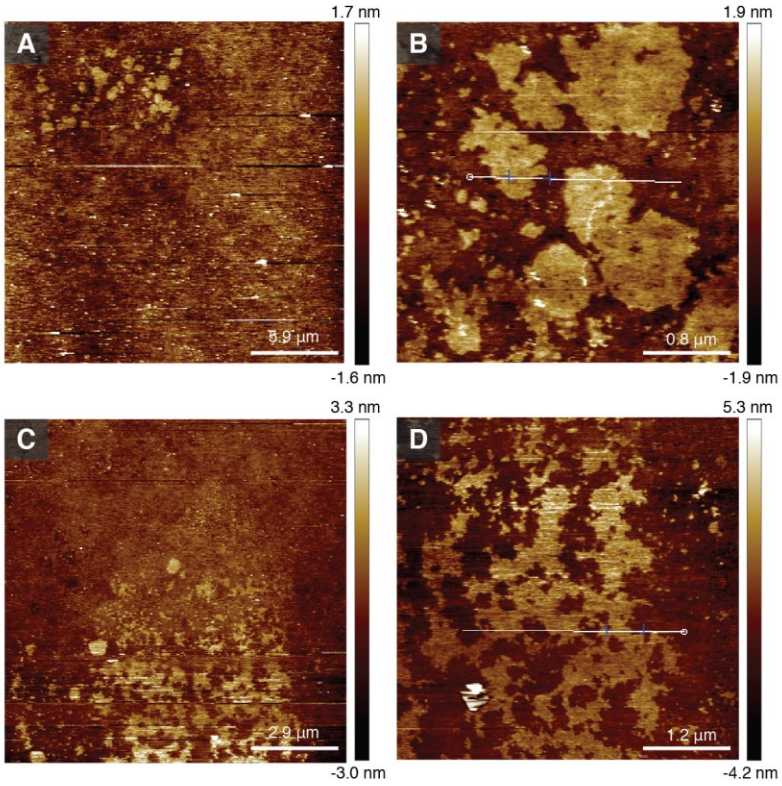

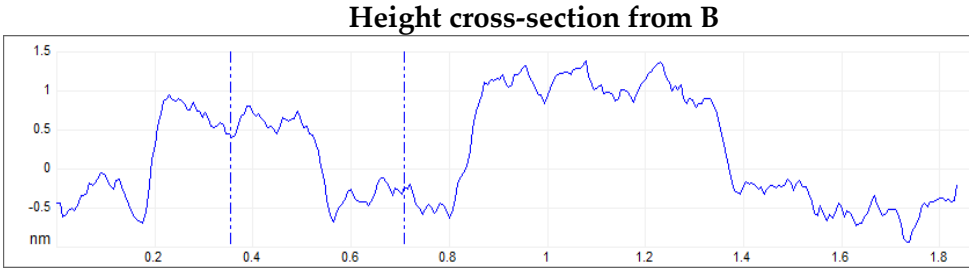

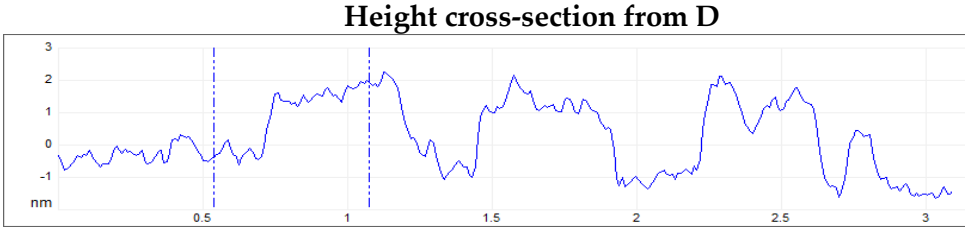

Figure A.14: (A-D) AFM height image of DPN islands in liquid after addition of AH fusion peptide, DOPC:SM:CH (51.75 : 18.25 : 30.00).

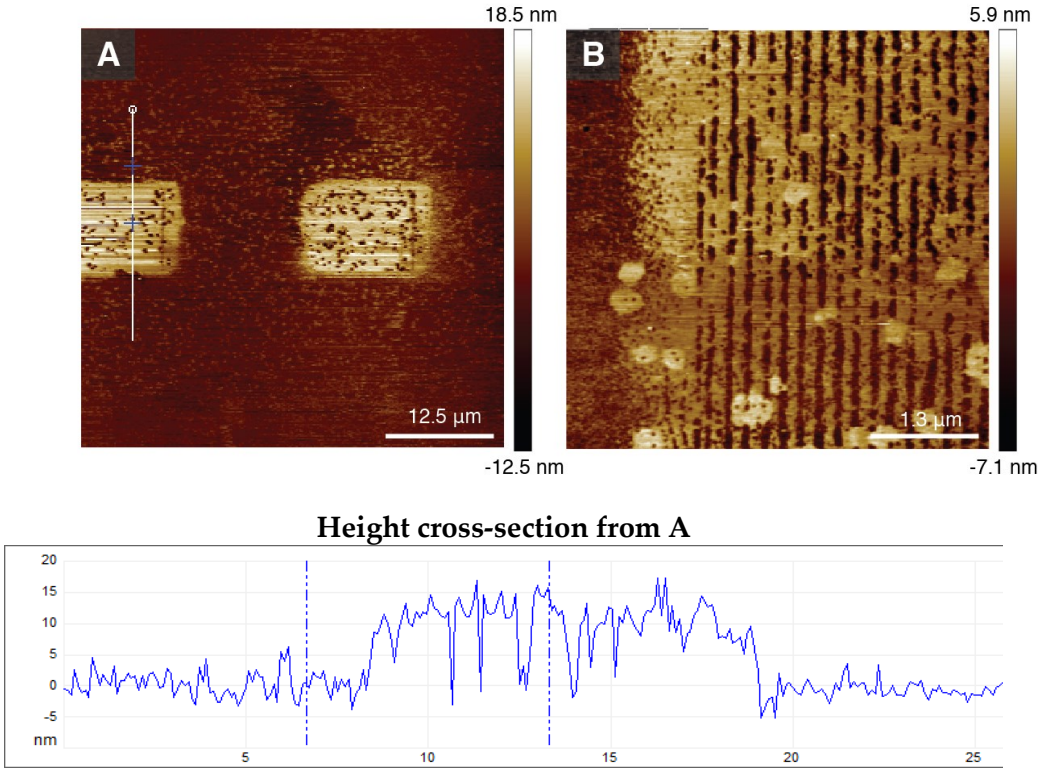

Figure A.15: AFM height images of lipid DPN islands in liquid. Height cross-section given below image.

(v) Blocking lipid DPN islands: Blocking lipid DPN samples with bovine serum albumin (BSA) was performed to experiment with preventing lipid smearing and non specific binding of antibodies and AH fusion peptide to the glass substrate (Fig. A.16). While using height images to search for and image lipid DPN islands it was difficult to identify the location of the islands. The BSA blocking created a layer on the glass substrate that closely matched the height of the lipid DPN islands, thus, creating very

little height contrast between the lipid island and the background. The lipid islands could only be clearly identified in phase contrast (Fig. A.16B).

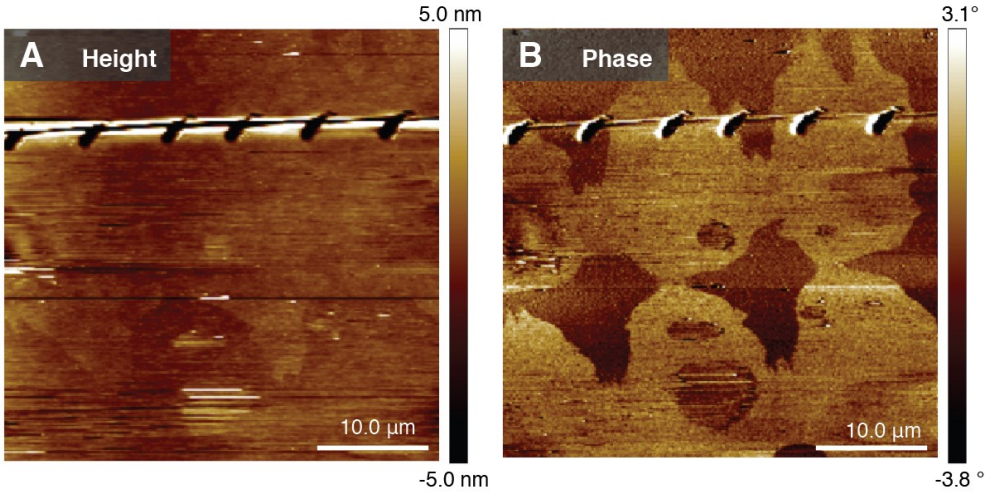

Figure A.16: (A) AFM height image, and (B) phase image of lipid DPN islands that have been blocked with 5% bovine serum albumin (BSA).

(vi) Antibody addition to DPN substrates: Figures A.17A-E shows the progression of added the AH fusion peptide, then 4E10 to DPN patterned surfaces. The image after the addition of AH fusion peptide (Fig. A.17B) has a reduced height contrast compared to the neat DPN island (Fig. A.17A) which suggests that the fusion peptide adheres to the glass substrate, raising the background height. Addition of 4E10 (Fig. A.17C) appears to adhere to the surrounding substrate since the image contrast is inverted when compared to the island with AH peptide (Fig. A.17B). As more 4E10 is added to the sample (Figs. A.17D,E), the height of the background grows taller and provided further height

contrast with the DPN island. No antibody addition to the DPN island can be detected (Fig. A.18). It should be noted that the concentration of antibody used in this experiment started at 4.6 μM, and raised to 46 μM, ten times the amount used to detect antibody-lipid binding in SLBs created from vesicle fusion.

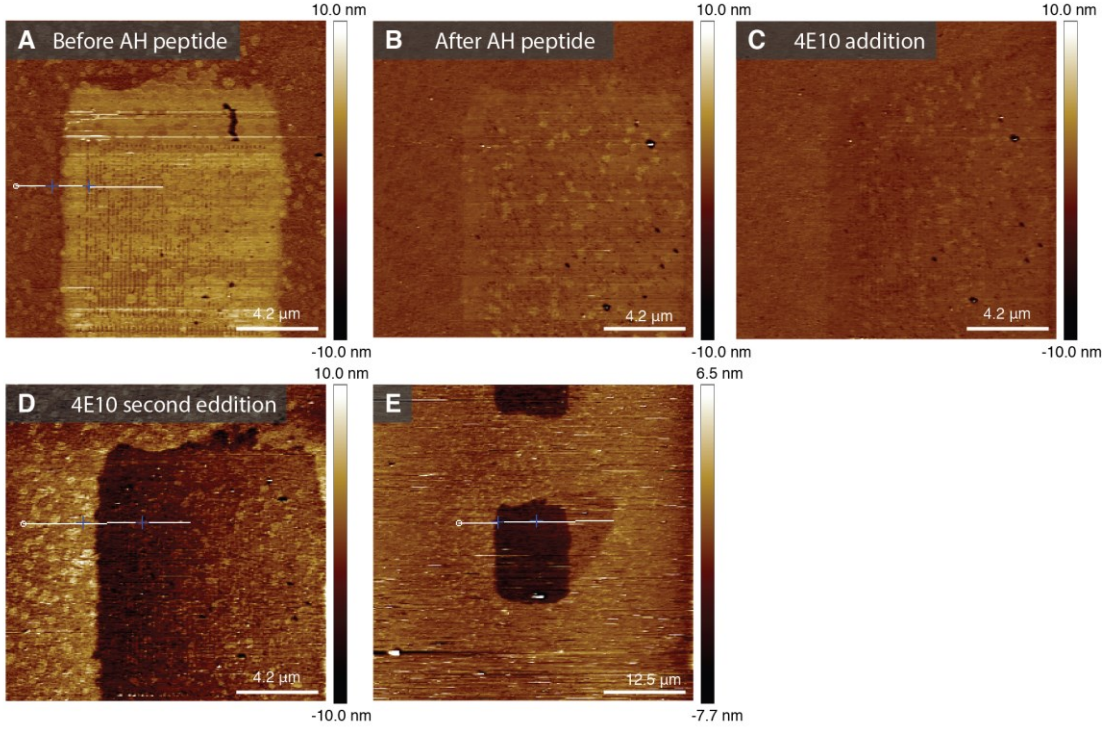

Figure A.17: AFM height images showing the result of AH fusion addition (A to B) and antibody, 4E10, addition. (C) one dose of 4E10 (0.3 mg/mL), and (D) after three doses of 4E10 (0.3 mg/mL). Each scan is about 15 minutes apart. Scan takes 8:30 minutes to complete, with about 7 minutes for the addition of antibody, incubation, and AFM setup to scan again. DOPC:SM:CH (51.75 : 18.25 : 30.00), written at 70% humidity.

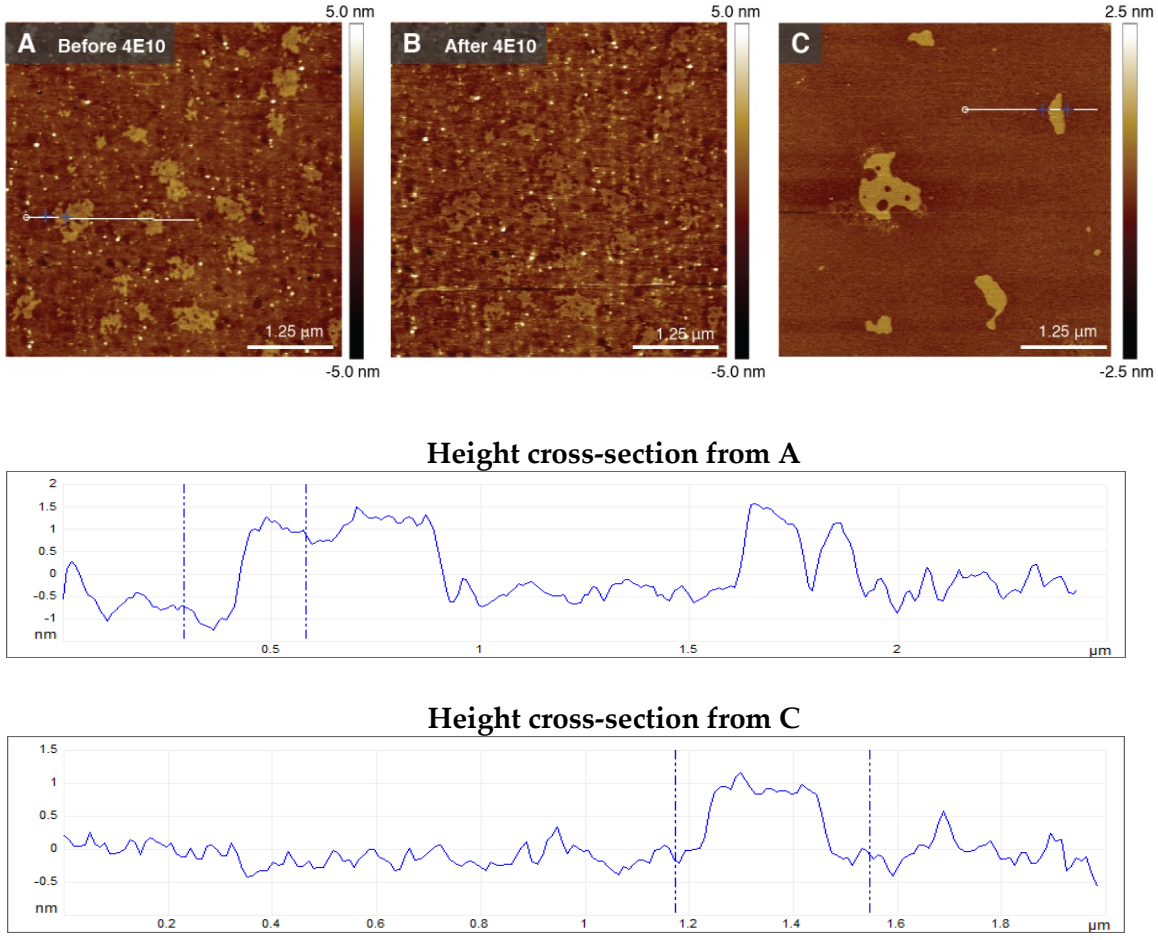

Figure A.18: Height image of the interior of DPN island before and after addition of antibody 4E10. Topography comparison of SLB created from vesicle fusion (left image) with lipid island created from DPN (Right image). Both techniques used a lipid composition of DOPC:SM:CH (63.50 : 18.25 : 18.25). Antibody was added in four dosages of 0.6 mg/mL each. The difference in color of the taller patches between the before and after image is due to a decreased set point (harder tapping force) when the "after" image was taken.

Figure A.18 shows images of before and after 4E10 addition. No addition of antibody to the island can be detected. Antibody, 2F5, was also tested and the antibody was not detected on the DPN islands (images not shown). To confirm that the batch of

antibodies used had lipid reactivity, planar SLBs were created from vesicle fusion and screened for interactions with both 2F5 and 4E10. Both antibodies were observed to bind to the SLBs demonstrating the lipid reactivity of the antibodies.

(vii) Vesicle fusion versus DPN: Figure A.18 compares the topology between supported lipid bilayers (SLBs) created from vesicle fusion (Fig. A.18C) and lipid islands created from DPN (Fig. A.18A). It is the goal of lipid DPN to create a lipid bilayer identical to the lipid bilayer created from vesicle fusion. However, major topological differences exist between the lipid structures resulting from each technique.

(viii) Lipid DPN island stability: To test if the islands written from lipid DPN are stable and can resist washing (which occurs upon protein introduction to the sample) the interior region of a DPN patterned area was imaged, washed vigorously with a pipette, then re-imaged in the same location. No changes to the topology occurred, indicating that the patterned lipids are relatively stable in liquid.

Remaining questions to test and answer:

1) Is the regular appearance of the small holes, or dimples, in the base layer due to the glass substrate? Does a glass surface that is cleaned with a more aggressive technique (*i.e.*, ozone or RCA solution) also result in these holes?
2) Are the patches observed before/after AH peptide introduction domains? Are they dependent on the presence of sphingomyelin/cholesterol?

3) Can blocking with BSA prevent antibody adhesion to the glass substrate?
4) Do antibodies adhere to a BSA substrate?
5) Is there a more efficient way to correlate/identify which lipid islands were written with which AFM tips (pens) from the array of tips?
6) What is the organizational structure of lipid DPN patterns? Why do they not resemble SLBs?
7) What are diffusivities of lipid DPN patterns? - FRAP

A.4 Conclusions

While progress has been achieve towards understanding lipid DPN patterns in liquid, additional research needs to be completed to use lipid DPN platforms as an array platform for screening antibodies with lipid structures that mimic native cell membranes. Lipid DPN structures need to achieve a continuous bilayer formation and currently it is unclear what the resulting structures of lipid DPN patterns are. From these results, there are two major obstacles that must be overcome: (i) lipid DPN islands do not resemble the topology and domain formation of supported lipid bilayers (SLBs), a standard platform used for screening membrane-protein interactions, and (ii) lipid reactive antibodies that bind to SLBs have no detectable interactions with lipid DPN islands.

A.5 Materials and Methods

For experiments using DPN, tip arrays were used to write lipid patterns ranging from 0.5 x 0.5 μm to 90 x 90 μm. Lipids were written on hydrophilic glass to facilitate SLB formation. Membrane components used for DPN ink included combinations of; POPC, DOPE, POPS, cholesterol, and sphingomyelin. Cholorform was used as a solvent to ink the DPN wells with lipids and antigen. Lipid DPN was written on glass samples using Nano Ink DPN 2000. DPN tips were inked at 70% humidity for 15 minutes. Optimal lipid DPN writing for both compositions occurs between 60 – 70% humidity with 2.3 um writing density for squares between 5-10 micrometers in length. Glass samples were cleaned by successive 5 minute sonication in chloroform, isopropanol, and water. Characterization of lipid DPN included fluorescent imaging, AFM imaging in air, and AFM imaging in liquid.

Appendix B. Protocols

B.1 AFM Parameters for Imaging Lipids Bilayers

Imaging in Air:

- Best cantilevers for tapping mode: Tap300 AI-G (NSC 15 and AIBS from μmasch was recommended by KIT but were not tried.)
- Spring constant: 40 N/m
- Resonance: about 298 kHz
- Set point: around 388 mV
- Target amp: 500 mV
- Nanoscope V controller
- Mulitmode 8 with scan assist
- J scanner

Imaging in Liquid:

- Best cantilevers for tapping mode: SNL-10 Bruker
- Resonance: 33-34 kHz
- Set point: 70-130 mV
- Target Amp: 200 mV
- Peak offset: 5%
- Nanoscope V controller
- Dimension Icon head with scan assist

For SLB samples that will be used for both fluorescent and AFM analysis black double-sided tape must be used to secure glass samples to metal puck. When yellow double-sided tape was used the background illumination from the tape (Rhodamine) overpowered any fluorescent signal from the lipids.

B.2 AFM Fluid Cell and Sample Preparation

This protocol is used to prepare samples being imaged in liquid. Take note that syringes, fluid ports, and o-ring assembly of the AFM liquid cell will not be used.

1. Use a circlular Teflon puck, with an insert on the bottom to house metal disk (which is normally used for sample mounting).
2. Clean Teflon puck in 2% SDS to maximize hydrophobicity of the Teflon surface.
3. Use double sided sticky tape to mount the substrate (*e.g.*, mica) to the Teflon surface. Insure the substrate is fully contained on the Teflon puck.
4. Add sample (in liquid) to be imaged onto substrate surface. Add enough liquid (100-200 μL) to observe a rounded bead of liquid on the sample surface. The liquid should be contained to the substrate and should not spill onto the Teflon.
5. Mount sample onto AFM scanner stage.
6. Mount AFM cantilever to the fluid cell of the AFM. Place a small drop (20-50 uL) of liquid on the tip of the cantilever and mount inside the AFM head.
7. Merge the liquid drop on the cantilever with the liquid on the sample by raising the sample until the liquid meniscus merge together. Continue to raise the sample until a stable liquid interface is formed.
8. Locate laser and center on cantilever. Then tune the cantilever and approach surface to begin imaging.
9. Due to the small amount of liquid, be aware of water loss due to evaporation, especially when the heater is used. Add distilled H_2O (instead of buffer) to conserve salt concentrations.
10. To add liquid (*e.g.*, pure H_2O or liquid containing proteins) separate the cantilever and sample surface without breaking the water meniscus. Then add liquid using a standard pipette. Monitor the total volume and be sure the liquid is not spilled off the substrate surface and onto/over the Teflon surface. Large Teflon surfaces better protect from spills.

B.3 Quartz Crystal Cleaning

This protocol was used to prepare quartz crystals for QCM-D experiments with bilayers (silica) and monolayers (hydrophobic gold). It was adapted from the Q-Sense D300 cleaning methods.

New SiO_2 crystal:

1. UV/ozone 5 min
2. Incubate in 2 wt % SDS for 30 min
3. Sonicate in SDS for 3 min, power 3
4. Rinse with ultrapure H_2O, dry with N_2
5. UV/Ozone 10 min
6. Sonicate in acetone 3 min, power 3
7. Rinse excessively in ultrapure H_2O, dry with N_2. Use immediately.

Used SiO_2 Crystal:

1. Start at step 2 in cleaning procedure above.

Au Crystal:

1. Clean as per SiO_2 crystals.
2. Place cleaned crystals in heated solution of 5:1:1 ultrapure H_2O: NH_3OH:H_2O_2 (14 ml in a beaker on a hot plate set to 190 °C to reach 70-75 °C in beaker). (5 parts H_2O : 1 part Hydrogen Peroxide : 1 part Ammonium Hydroxide) for 5 minutes.
    - Rinse with DI H_2O, dry with N_2
3. UV/Ozone 5 minutes. Rinse with acetone and ultrapure H_2O. Dry under N_2.
4. Submerge immediately into 1 mM solution of octadecanethiol in ethanol. Incubate at least 12 hours in the dark.
5. Sonicate 3 min at power 3 in thiol solution.
6. Rinse with ethanol, dry under N_2, and mount immediately into QCM-D chamber.

B.4 Lipid Film and Vesicle Preparation

This protocol was adapted from David Boren (Duke Human Vaccine Institute). It was used to prepare lipid films and extruded lipid solutions for SLB experiments.

Lipid Film Preparation:

1. Take lipids out of -20 °C freezer for 45 minutes to equilibrate to room temperature (lipids should be clear when at room temperature).
2. Pipette solutions in desired ratio into new test tube.
3. Place test tube in holder in hood, and flow nitrogen over top until there is no visible liquid in vial. N_2 pipette should not touch lipid solution.
4. Fill ice bucket with dry ice.
5. Submerge Erlenmeyer flask in dry ice and hook up to vacuum.
6. When chloroform is mostly evaporated, turn off N_2 flow and place lipid vial in vacuum spinner. Place balance vial opposite.
7. Start rotation, then turn on spinner.
8. Turn on vacuum pump.
9. Wait at least 3 hours for lipids to dry.
10. Turn off centrifuge and vacuum pump, then pull plug from flask to release vacuum seal on centrifuge.
11. Remove lipid vial, cap with N_2, and store at 4 °C. Use within a few weeks.

Lipid Extrusion:

1. Turn on water bath to 37°C, and place vial of lipid film filled with buffer in the water bath for 30 minutes.
2. Vortex to help dissolve lipids. Sonicate for 2 minutes (without probe). Vortex.
3. Dip 2 pieces of filter support in PBS, and place inside each of two O-rings on extruder.
4. Place 0.4 μm filter film atop one O-ring, and close extruder capsule.

5. Place 1 mL PBS in “in” syringe, and pump through 4 times to saturate supports and film.
6. Discard PBS. Pipette transfer lipid solution to a 15 mL centrifuge tube and then fill extruder syringe with lipid solution.
7. Extrude 11 times, or more, insuring to end at an odd number of extrusion so the lipid solution is finished in the “out” syringe.
8. Discard filter supports and membrane, and replace with fresh filter supports and 0.08 μm membrane.
9. The previous “out” syringe containing the 0.04 um vesicles becomes the new “in” syringe. Repeat step 7.
10. Transfer lipid solution to clean screw-cap vial and use as soon as possible, within 8 hours.
11. To clean extruder, rinse thoroughly with degassed, filtered deionized H_2O, and leave to dry in air. Rinse syringes 5 times with water, then 2 times with ethanol. Leave disassembled to air dry.

References

[1] Burton DR, Desrosiers, R.C., Doms, R.W., Koff, W.C., Kwong, P.D., Moore, J.P., Nabel, G.J., Sodroski, J., Wilson, I.A., Wyatt, R.T. HIV vaccine design and the neutralizing antibody problem. Nature Immunology 2004; 5: 233-36.

[2] Haynes BF, Montefiori DC. Aiming to induce broadly reactive neutralizing antibody responses with HIV-1 vaccine candidates. Expert Rev Vaccines 2006; 5: 347-63.

[3] Stiegler G, Kunert R, Purtscher M, Wolbank S, Voglauer R, Steindl F, Katinger H. A potent cross-clade neutralizing human monoclonal antibody against a novel epitope on gp41 of human immunodeficiency virus type 1. AIDS Res Hum Retroviruses 2001; 17: 1757-65.

[4] Haynes BF, Moody MA, Verkoczy L, Kelsoe G, Alam SM. Antibody polyspecificity and neutralization of HIV-1: a hypothesis. Hum Antibodies 2005; 14: 59-67.

[5] Ofek G, Guenaga FJ, Schief WR, Skinner J, Baker D, Wyatt R, Kwong PD. Elicitation of structure-specific antibodies by epitope scaffolds. Proc Natl Acad Sci U S A 2010; 107: 17880-7.

[6] Guenaga J, Dosenovic P, Ofek G, Baker D, Schief WR, Kwong PD, Karlsson Hedestam GB, Wyatt RT. Heterologous epitope-scaffold prime:boosting immuno-focuses B cell responses to the HIV-1 gp41 2F5 neutralization determinant. PLoS One 2011; 6: e16074.

[7] Dennison SM, Sutherland LL, Jaeger FH, Anasti KM, Parks R, Stewart S, Bowman C, Xia SM, Zhang R, Shen X, Scearce RM, Ofek G, Yang Y, Kwong PD, Santra S, Liao HX, Tomaras G, Letvin NL, Chen B, Alam SM, Haynes BF. Induction of Antibodies in Rhesus Macaques That Recognize a Fusion-Intermediate Conformation of HIV-1 gp41. PLoS One 2011; 6: e27824.

[8] Verkoczy L, Diaz M, Holl TM, Ouyang YB, Bouton-Verville H, Alam SM, Liao HX, Kelsoe G, Haynes BF. Autoreactivity in an HIV-1 broadly reactive neutralizing antibody variable region heavy chain induces immunologic tolerance. Proc Natl Acad Sci U S A 2010; 107: 181-6.

[9] Verkoczy L, Chen Y, Bouton-Verville H, Zhang J, Diaz M, Hutchinson J, Ouyang YB, Alam SM, Holl TM, Hwang KK, Kelsoe G, Haynes BF. Rescue of HIV-1

broad neutralizing antibody-expressing B cells in 2F5 VH x VL knockin mice reveals multiple tolerance controls. J Immunol 2011; 187: 3785-97.

[10] McLellan JS, Pancera M, Carrico C, Gorman J, Julien JP, Khayat R, Louder R, Pejchal R, Sastry M, Dai K, O'Dell S, Patel N, Shahzad-ul-Hussan S, Yang Y, Zhang B, Zhou T, Zhu J, Boyington JC, Chuang GY, Diwanji D, Georgiev I, Kwon YD, Lee D, Louder MK, Moquin S, Schmidt SD, Yang ZY, Bonsignori M, Crump JA, Kapiga SH, Sam NE, Haynes BF, Burton DR, Koff WC, Walker LM, Phogat S, Wyatt R, Orwenyo J, Wang LX, Arthos J, Bewley CA, Mascola JR, Nabel GJ, Schief WR, Ward AB, Wilson IA, Kwong PD. Structure of HIV-1 gp120 V1/V2 domain with broadly neutralizing antibody PG9. Nature 2011; 480: 336-43.

[11] Bonsignori M, Hwang KK, Chen X, Tsao CY, Morris L, Gray E, Marshall DJ, Crump JA, Kapiga SH, Sam NE, Sinangil F, Pancera M, Yongping Y, Zhang B, Zhu J, Kwong PD, O'Dell S, Mascola JR, Wu L, Nabel GJ, Phogat S, Seaman MS, Whitesides JF, Moody MA, Kelsoe G, Yang X, Sodroski J, Shaw GM, Montefiori DC, Kepler TB, Tomaras GD, Alam SM, Liao HX, Haynes BF. Analysis of a clonal lineage of HIV-1 envelope V2/V3 conformational epitope-specific broadly neutralizing antibodies and their inferred unmutated common ancestors. J Virol 2011; 85: 9998-10009.

[12] Mouquet H, Scheid JF, Zoller MJ, Krogsgaard M, Ott RG, Shukair S, Artyomov MN, Pietzsch J, Connors M, Pereyra F, Walker BD, Ho DD, Wilson PC, Seaman MS, Eisen HN, Chakraborty AK, Hope TJ, Ravetch JV, Wardemann H, Nussenzweig MC. Polyreactivity increases the apparent affinity of anti-HIV antibodies by heteroligation. Nature 2010; 467: 591-U117.

[13] Mouquet H, Nussenzweig MC. Polyreactive antibodies in adaptive immune responses to viruses. Cell Mol Life Sci 2011.

[14] Mouquet H, Klein F, Scheid JF, Warncke M, Pietzsch J, Oliveira TY, Velinzon K, Seaman MS, Nussenzweig MC. Memory B cell antibodies to HIV-1 gp140 cloned from individuals infected with clade A and B viruses. PLoS One 2011; 6: e24078.

[15] Dennison SM, Anasti K, Scearce RM, Sutherland L, Parks R, Xia SM, Liao HX, Gorny MK, Zolla-Pazner S, Haynes BF, Alam SM. Nonneutralizing HIV-1 gp41 envelope cluster II human monoclonal antibodies show polyreactivity for binding to phospholipids and protein autoantigens. J Virol 2011; 85: 1340-7.

[16] Matyas GR, Wieczorek L, Beck Z, Ochsenbauer-Jambor C, Kappes JC, Michael NL, Polonis VR, Alving CR. Neutralizing antibodies induced by liposomal HIV-1

glycoprotein 41 peptide simultaneously bind to both the 2F5 or 4E10 epitope and lipid epitopes. AIDS 2009; 23: 2069-77.

[17] Alam SM, McAdams M, Boren D, Rak M, Scearce RM, Gao F, Camacho ZT, Gewirth D, Kelsoe G, Chen PJ, Haynes BF. The role of antibody polyspecificity and lipid reactivity in binding of broadly neutralizing anti-HIV-1 envelope human monoclonal antibodies 2F5 and 4E10 to glycoprotein 41 membrane proximal envelope epitopes. J Immunol 2007; 178: 4424-35.

[18] Sun ZY, Oh KJ, Kim M, Yu J, Brusic V, Song L, Qiao Z, Wang JH, Wagner G, Reinherz EL. HIV-1 broadly neutralizing antibody extracts its epitope from a kinked gp41 ectodomain region on the viral membrane. Immunity 2008; 28: 52-63.

[19] Alam SM, Morelli M, Dennison SM, Liao HX, Zhang R, Xia SM, Rits-Volloch S, Sun L, Harrison SC, Haynes BF, Chen B. Role of HIV membrane in neutralization by two broadly neutralizing antibodies. Proc Natl Acad Sci U S A 2009; 106: 20234-9.

[20] Ofek G, Tang M, Sambor A, Katinger H, Mascola JR, Wyatt R, Kwong PD. Structure and mechanistic analysis of the anti-human immunodeficiency virus type 1 antibody 2F5 in complex with its gp41 epitope. J Virol 2004; 78: 10724-37.

[21] Cardoso RMF, Zwick MB, Stanfield RL, Kunert R, Binley JM, Katinger H, Burton DR, Wilson IA. Broadly neutralizing anti-HIV antibody 4E10 recognizes a helical conformation of a highly conserved fusion-associated motif in gp41. Immunity 2005; 22: 163-73.

[22] Burton DR, Stanfield RL, Wilson IA. Antibody vs. HIV in a clash of evolutionary titans. Proc Natl Acad Sci U S A 2005; 102: 14943-8.

[23] Meffre E, Wardemann H. B-cell tolerance checkpoints in health and autoimmunity. Curr Opin Immunol 2008; 20: 632-8.

[24] Verkoczy L, Kelsoe G, Moody MA, Haynes BF. Role of immune mechanisms in induction of HIV-1 broadly neutralizing antibodies. Curr Opin Immunol 2011; 23: 383-90.

[25] Diskin R, Marcovecchio PM, Bjorkman PJ. Structure of a clade C HIV-1 gp120 bound to CD4 and CD4-induced antibody reveals anti-CD4 polyreactivity. Nat Struct Mol Biol 2010; 17: 608-13.

[26] Haynes BF, Fleming J, St Clair EW, Katinger H, Stiegler G, Kunert R, Robinson J, Scearce RM, Plonk K, Staats HF, Ortel TL, Liao HX, Alam SM. Cardiolipin polyspecific autoreactivity in two broadly neutralizing HIV-1 antibodies. Science 2005; 308: 1906-08.

[27] Walker LM, Simek MD, Priddy F, Gach JS, Wagner D, Zwick MB, Phogat SK, Poignard P, Burton DR. A limited number of antibody specificities mediate broad and potent serum neutralization in selected HIV-1 infected individuals. Plos Pathogens 2010; 6: e1001028.

[28] Tsuiji M, Yurasov S, Velinzon K, Thomas S, Nussenzweig MC, Wardemann H. A checkpoint for autoreactivity in human IgM+ memory B cell development. J Exp Med 2006; 203: 393-400.

[29] Wardemann H, Yurasov S, Schaefer A, Young JW, Meffre E, Nussenzweig MC. Predominant autoantibody production by early human B cell precursors. Science 2003; 301: 1374-7.

[30] Tiller T, Kofer J, Kreschel C, Busse CE, Riebel S, Wickert S, Oden F, Mertes MM, Ehlers M, Wardemann H. Development of self-reactive germinal center B cells and plasma cells in autoimmune Fc gammaRIIB-deficient mice. J Exp Med 2010; 207: 2767-78.

[31] Alam SM, Liao HX, Dennison SM, Jaeger F, Parks R, Anasti K, Foulger A, Donathan M, Lucas J, Verkoczy L, Nicely N, Tomaras GD, Kelsoe G, Chen B, Kepler TB, Haynes BF. Differential reactivity of germ line allelic variants of a broadly neutralizing HIV-1 antibody to a gp41 fusion intermediate conformation. J Virol 2011; 85: 11725-31.

[32] Alving CR. Natural antibodies against phospholipids and liposomes in humans. Biochem Soc Trans 1984; 12: 342-4.

[33] Cabiedes J, Cabral AR, Alarcon-Segovia D. Hidden anti-phospholipid antibodies in normal human sera circulate as immune complexes whose antigen can be removed by heat, acid, hypermolar buffers or phospholipase treatments. Eur J Immunol 1998; 28: 2108-14.

[34] Alving CR, Swartz GM, Jr., Wassef NM. Naturally occurring autoantibodies to cholesterol in humans. Biochem Soc Trans 1989; 17: 637-9.

[35] Avila JL, Rojas M, Avila A. Cholesterol sulphate-reactive autoantibodies are specifically increased in chronic chagasic human patients. Clin Exp Immunol 1996; 103: 40-6.

[36] Matyas GR, Rao M, Pittman PR, Burge R, Robbins IE, Wassef NM, Thivierge B, Alving CR. Detection of antibodies to squalene: III. Naturally occurring antibodies to squalene in humans and mice. J Immunol Methods 2004; 286: 47-67.

[37] Armbruster C, Stiegler GM, Vcelar BA, Jager W, Michael NL, Vetter N, Katinger HW. A phase I trial with two human monoclonal antibodies (hMAb 2F5, 2G12) against HIV-1. AIDS 2002; 16: 227-33.

[38] Armbruster C, Stiegler GM, Vcelar BA, Jager W, Koller U, Jilch R, Ammann CG, Pruenster M, Stoiber H, Katinger HW. Passive immunization with the anti-HIV-1 human monoclonal antibody (hMAb) 4E10 and the hMAb combination 4E10/2F5/2G12. J Antimicrob Chemother 2004; 54: 915-20.

[39] Trkola A, Kuster H, Rusert P, Joos B, Fischer M, Leemann C, Manrique A, Huber M, Rehr M, Oxenius A, Weber R, Stiegler G, Vcelar B, Katinger H, Aceto L, Gunthard HF. Delay of HIV-1 rebound after cessation of antiretroviral therapy through passive transfer of human neutralizing antibodies. Nat Med 2005; 11: 615-22.

[40] Brugger B, Glass B, Haberkant P, Leibrecht I, Wieland FT, Krausslich HG. The HIV lipidome: a raft with an unusual composition. Proc Natl Acad Sci U S A 2006; 103: 2641-6.

[41] Aloia RC, Tian HR, Jensen FC. Lipid-Composition and Fluidity of the Human-Immunodeficiency-Virus Envelope and Host-Cell Plasma-Membranes. Proc Natl Acad Sci U S A 1993; 90: 5181-85.

[42] Dan N. Domain formation in mixed cholesterol/lipid bilayers. Abstracts of Papers of the American Chemical Society 2005; 230: U1185-U85.

[43] Bakht O, Pathak P, London E. Effect of the structure of lipids favoring disordered domain formation on the stability of cholesterol-containing ordered domains (lipid rafts): Identification of multiple raft-stabilization mechanisms. Biophys J 2007; 93: 4307-18.

[44] Yao XL, Hong M. Effects of anionic lipid and ion concentrations on the topology and segmental mobility of colicin Ia channel domain from solid-state NMR. Biochemistry 2006; 45: 289-95.

[45] Frazier ML, Wright JR, Pokorny A, Almeida PFF. Investigation of domain formation in sphingomyelin/cholesterol/POPC mixtures by fluorescence resonance energy transfer and Monte Carlo simulations. Biophys J 2007; 92: 2422-33.

[46] Gandhavadi M, Allende D, Vidal A, Simon SA, McIntosh TJ. Structure, composition, and peptide binding properties of detergent soluble bilayers and detergent resistant rafts. Biophy J 2002; 82: 1469-82.

[47] Lawrence JC, Saslowsky DE, Edwardson JM, Henderson RM. Real-time analysis of the effects of cholesterol on lipid raft behavior using atomic force microscopy. Biophys J 2003; 84: 1827-32.

[48] Simons K, Benting J, Lafont F, Ikonen E, Keller P, Scheiffele P. Involvement of sphingolipid-cholesterol rafts in apical transport. Faseb J 1997; 11: A1299-A99.

[49] Mcintosh TJ, Simon SA, Needham D, Huang CH. Structure and Cohesive Properties of Sphingomyelin Cholesterol Bilayers. Biochemistry 1992; 31: 2012-20.

[50] Kahya N, Scherfeld D, Bacia K, Poolman B, Schwille P. Probing lipid mobility of raft-exhibiting model membranes by fluorescence correlation spectroscopy. J Bio Chem 2003; 278: 28109-15.

[51] Filippov A, Oradd G, Lindblom G. Domain formation in model membranes studied by pulsed-field gradient-NMR: The role of lipid polyunsaturation. Biophys J 2007; 93: 3182-90.

[52] Almeida PFF, Vaz WLC, Thompson TE. Percolation and Diffusion in 3-Component Lipid Bilayers - Effect of Cholesterol on an Equimolar Mixture of 2 Phosphatidylcholines. Biophys J 1993; 64: 399-412.

[53] de Almeida RF, Fedorov A, Prieto M. Sphingomyelin/phosphatidylcholine/cholesterol phase diagram: boundaries and composition of lipid rafts. Biophys J 2003; 85: 2406-16.

[54] Sauerbrey G. Verwendung Von Schwingquarzen Zur Wagung Dunner Schichten Und Zur Mikrowagung. Zeitschrift Fur Physik 1959; 155: 206-22.

[55] Reviakine I, Brisson A. Formation of supported phospholipid bilayers from unilamellar vesicles investigated by atomic force microscopy. Langmuir 2000; 16: 1806-15.

[56] Zhdanov VP, Kasemo B. Van der Waals interaction during protein adsorption on a solid covered by a thin film. Langmuir 2001; 17: 5407-09.

[57] Reimhult E, Hook F, Kasemo B. Vesicle adsorption on SiO2 and TiO2: Dependence on vesicle size. J Chem Phys 2002; 117: 7401-04.

[58] Richter R, Mukhopadhyay A, Brisson A. Pathways of lipid vesicle deposition on solid surfaces: A combined QCM-D and AFM study. Biophys J 2003; 85: 3035-47.

[59] Keller CA, Kasemo B. Surface specific kinetics of lipid vesicle adsorption measured with a quartz crystal microbalance. Biophys J 1998; 75: 1397-402.

[60] Hardy GJ, Nayak R, Alam SM, Shapter JG, Heinrich F, Zauscher S. Biomimetic supported lipid bilayers with high cholesterol content formed by alpha-helical peptide-induced vesicle fusion. J Mater Chem 2012; 22: 19506-13.

[61] Sundh M, Svedhem S, Sutherland DS. Influence of phase separating lipids on supported lipid bilayer formation at SiO2 surfaces. Phys Chem Chem Phys 2010; 12: 453-60.

[62] Liedberg B, Nylander C, Lundstrom I. Biosensing with surface plasmon resonance--how it all started. Biosensors and Bioelectronics 1995; 10: i-ix.

[63] Hearty S, Conroy PJ, Ayyar BV, Byrne B, O'Kennedy R. Surface plasmon resonance for vaccine design and efficacy studies: recent applications and future trends. Expert Rev Vaccines 2010; 9: 645-64.

[64] Burns AR. Atomic force microscopy of lipid domains in supported model membranes. Methods Mol Biol 2007; 398: 263-82.

[65] Schonherr H, Johnson JM, Lenz P, Frank CW, Boxer SG. Vesicle adsorption and lipid bilayer formation on glass studied by atomic force microscopy. Langmuir 2004; 20: 11600-06.

[66] Fragneto-Cusani G. Neutron reflectivity at the solid/liquid interface: examples of applications in biophysics. J Phys-Condensed Matter 2001; 13: 4973-89.

[67] Keimer B. Neutron Scattering. October 31, 2012]; http://www2.fkf.mpg.de/keimer/lecture/Scattering_II/MS_01.pdf].

[68] Shen HH, Thomas RK, Chen CY, Darton RC, Baker SC, Penfold J. Aggregation of the Naturally Occurring Lipopeptide, Surfactin, at Interfaces and in Solution: An Unusual Type of Surfactant? Langmuir 2009; 25: 4211-18.

[69] Ivasenko O, Perepichka DF. Mastering fundamentals of supramolecular design with carboxylic acids. Common lessons from X-ray crystallography and scanning tunneling microscopy. Chem Soc Rev 2011; 40: 191-206.

[70] Wacklin HP. Neutron reflection from supported lipid membranes. Current Opinion in Colloid & Interface Science 2010; 15: 445-54.

[71] Heavens OS. Optical Properties of Thin Films. Reports on Progress in Physics 1960; 23: 2-65.

[72] Gutberlet T, Steitz R, Fragneto G, Klosgen B. Phospholipid bilayer formation at a bare Si surface: a time-resolved neutron reflectivity study. J Phys-Condensed Matter 2004; 16: S2469-S76.

[73] Hardy GJ, Lam Y, Stewart SM, Anasti K, Alam SM, Zauscher S. Screening the interactions between HIV-1 neutralizing antibodies and model lipid surfaces. J Immunol Methods 2012; 376: 13-19.

[74] Cooper MA. Advances in membrane receptor screening and analysis. J Molecular Recognition 2004; 17: 286-315.

[75] Wiltschi B, Knoll W, Sinner EK. Binding assays with artificial tethered membranes using surface plasmon resonance. Methods 2006; 39: 134-46.

[76] Im H, Wittenberg NJ, Lesuffleur A, Lindquist NC, Oh SH. Membrane protein biosensing with plasmonic nanopore arrays and pore-spanning lipid membranes. Chemical Science 2010; 1: 688-96.

[77] Giles I, Lambrianides N, Latchman D, Chen PJ, Chukwuocha R, Isenberg D, Rahman A. The critical role of arginine residues in the binding of human monoclonal antibodies to cardiolipin. Arthritis Res Ther 2005; 7: R47-R56.

[78] Zhu M, Olee T, Le DT, Roubey RAS, Hahn BH, Woods VL, Chen PP. Characterization of IgG monoclonal anti-cardiolipin/anti-beta(2)GP1 antibodies from two patients with antiphospholipid syndrome reveals three species of antibodies. Br J Haematol 1999; 105: 102-09.

[79] Zwick MB, Labrijn AF, Wang M, Spenlehauer C, Saphire EO, Binley JM, Moore JP, Stiegler G, Katinger H, Burton DR, Parren PW. Broadly neutralizing antibodies targeted to the membrane-proximal external region of human immunodeficiency virus type 1 glycoprotein gp41. J Virol 2001; 75: 10892-905.

[80] Conley AJ, Kessler JA, 2nd, Boots LJ, Tung JS, Arnold BA, Keller PM, Shaw AR, Emini EA. Neutralization of divergent human immunodeficiency virus type 1 variants and primary isolates by IAM-41-2F5, an anti-gp41 human monoclonal antibody. Proc Natl Acad Sci U S A 1994; 91: 3348-52.

[81] Giles IP, Lambrianides N, Latchman DS, Chen PP, Chukwuocha RC, Isenberg DA, Rahman A. The critical role of arginine residues in the binding of human monoclonal antibodies to cardiolipin. Arthritis Rheumatism 2003; 48: S164-S65.

[82] Dubois LH, Nuzzo RG. Synthesis, Structure, and Properties of Model Organic-Surfaces. Ann Rev Phys Chem 1992; 43: 437-63.

[83] Hauser H, Pascher I, Pearson RH, Sundell S. Preferred conformation and molecular packing of phosphatidylethanolamine and phosphatidylcholine. Biochimica et Biophysica Acta 1981; 650: 21-51.

[84] Scearce RM, Eisenbarth GS. Production of monoclonal antibodies reacting with the cytoplasm and surface of differentiated cells. Methods in Enzymology 1983; 103: 459-69.

[85] Zhu M, Olee T, Le DT, Roubey RA, Hahn BH, Woods VL, Jr., Chen PP. Characterization of IgG monoclonal anti-cardiolipin/anti-beta2GP1 antibodies from two patients with antiphospholipid syndrome reveals three species of antibodies. Br J Haematol 1999; 105: 102-9.

[86] Liao HX, Sutherland LL, Xia SM, Brock ME, Scearce RM, Vanleeuwen S, Alam SM, McAdams M, Weaver EA, Camacho ZT, Ma BJ, Li YY, Decker JM, Nabel GJ, Montefiori DC, Hahn BH, Korber BT, Gao F, Haynes BF. A group M consensus envelope glycoprotein induces antibodies that neutralize subsets of subtype B and CHIV-1 primary viruses. Virology 2006; 353: 268-82.

[87] Alam SM, McAdams M, Boren D, Rak M, Scearce RM, Gao F, Camacho ZT, Gewirth D, Kelsoe G, Chen P, Haynes BF. The role of antibody polyspecificity and lipid reactivity in binding of broadly neutralizing anti-HIV-1 envelope human monoclonal antibodies 2F5 and 4E10 to glycoprotein 41 membrane proximal envelope epitopes. J Immunol 2007; 178: 4424-35.

[88] MacDonald RC, MacDonald RI, Menco BP, Takeshita K, Subbarao NK, Hu LR. Small-volume extrusion apparatus for preparation of large, unilamellar vesicles. Biochimica et Biophysica Acta 1991; 1061: 297-303.

[89] Hardy GJ, Nayak R, Zauscher S. Model cell membranes: Techniques to form complex biomimetic supported lipid bilayers via vesicle fusion. Curr Opin Colloid Interface Sci 2013; 18: 448-58.

[90] Tamm LK, Mcconnell HM. Supported Phospholipid-Bilayers. Biophys J 1985; 47: 105-13.

[91] Mennicke U, Salditt T. Preparation of solid-supported lipid bilayers by spin-coating. Langmuir 2002; 18: 8172-77.

[92] Jung SY, Holden MA, Cremer PS, Collier CP. Two-component membrane lithography via lipid backfilling. Chem Phys Chem 2005; 6: 423-26.

[93] Hohner AO, David MPC, Radler JO. Controlled solvent-exchange deposition of phospholipid membranes onto solid surfaces. Biointerphases 2010; 5: 1-8.

[94] Tiberg F, Harwigsson I, Malmsten M. Formation of model lipid bilayers at the silica-water interface by co-adsorption with non-ionic dodecyl maltoside surfactant. Eu Biophys J Biophys Letters 2000; 29: 196-203.

[95] Brinker CJ, Lu YF, Sellinger A, Fan HY. Evaporation-induced self-assembly: Nanostructures made easy. Advanced Materials 1999; 11: 579-+.

[96] Mager MD, Melosh NA. Lipid bilayer deposition and patterning via air bubble collapse. Langmuir 2007; 23: 9369-77.

[97] Lenhert S, Mirkin CA, Fuchs H. In Situ Lipid Dip-Pen Nanolithography Under Water. Scanning 2010; 32: 15-23.

[98] Reimhult E, Hook F, Kasemo B. Intact vesicle adsorption and supported biomembrane formation from vesicles in solution: Influence of surface chemistry, vesicle size, temperature, and osmotic pressure. Langmuir 2003; 19: 1681-91.

[99] Eeman M, Deleu M. From biological membranes to biomimetic model membranes. Biotechnologie Agronomie Societe Et Environnement 2010; 14: 719-36.

[100] Czolkos I, Jesorka A, Orwar O. Molecular phospholipid films on solid supports. Soft Matter 2011; 7: 4562-76.

[101] Anderson TH, Min YJ, Weirich KL, Zeng HB, Fygenson D, Israelachvili JN. Formation of Supported Bilayers on Silica Substrates. Langmuir 2009; 25: 6997-7005.

[102] Dopico AM, Tigyi GJ. A glance at the structural and functional diversity of membrane lipids. Methods Mol Biol 2007; 400: 1-13.

[103] Owen DM, Magenau A, Williamson D, Gaus K. The lipid raft hypothesis revisited--new insights on raft composition and function from super-resolution fluorescence microscopy. Bioessays 2012; 34: 739-47.

[104] Block RC, Dorsey ER, Beck CA, Brenna JT, Shoulson I. Altered cholesterol and fatty acid metabolism in Huntington disease. J Clin Lipidol 2010; 4: 17-23.

[105] Di Paolo G, Kim TW. Linking lipids to Alzheimer's disease: cholesterol and beyond. Nat Rev Neurosci 2011; 12: 284-96.

[106] Liao Z, Graham DR, Hildreth JE. Lipid rafts and HIV pathogenesis: virion-associated cholesterol is required for fusion and infection of susceptible cells. AIDS Res Hum Retroviruses 2003; 19: 675-87.

[107] Honda A, Matsuzaki Y. Cholesterol and chronic hepatitis C virus infection. Hepatol Res 2011; 41: 697-710.

[108] Maguy A, Hebert TE, Nattel S. Involvement of lipid rafts and caveolae in cardiac ion channel function. Cardiovasc Res 2006; 69: 798-807.

[109] Sotgia F, Williams TM, Schubert W, Medina F, Minetti C, Pestell RG, Lisanti MP. Caveolin-1 deficiency (-/-) conveys premalignant alterations in mammary epithelia, with abnormal lumen formation, growth factor independence, and cell invasiveness. Am J Pathol 2006; 168: 292-309.

[110] Seifert U, Berndl K, Lipowsky R. Shape Transformations of Vesicles - Phase-Diagram for Spontaneous-Curvature and Bilayer-Coupling Models. Phys Rev A 1991; 44: 1182-202.

[111] Richter RP, Berat R, Brisson AR. Formation of solid-supported lipid bilayers: an integrated view. Langmuir 2006; 22: 3497-505.

[112] Anderson TH, Min Y, Weirich KL, Zeng H, Fygenson D, Israelachvili JN. Formation of supported bilayers on silica substrates. Langmuir 2009; 25: 6997-7005.

[113] Speight RE, Cooper MA. A Survey of the 2010 Quartz Crystal Microbalance Literature. J Molecular Recognition 2012; 25: 451-73.

[114] Reimhult E, Hook F, Kasemo B. Temperature dependence of formation of a supported phospholipid bilayer from vesicles on SiO2. Phys Rev E Stat Nonlin Soft Matter Phys 2002; 66: 051905.

[115] Cho NJ, Jackman JA, Liu M, Frank CW. pH-Driven Assembly of Various Supported Lipid Platforms: A Comparative Study on Silicon Oxide and Titanium Oxide. Langmuir 2011; 27: 3739-48.

[116] Cho NJ, Frank CW, Kasemo B, Hook F. Quartz crystal microbalance with dissipation monitoring of supported lipid bilayers on various substrates. Nature Protocols 2010; 5: 1096-106.

[117] Seantier B, Kasemo B. Influence of Mono- And Divalent Ions on the Formation of Supported Phospholipid Bilayers via Vesicle Adsorption. Langmuir 2009; 25: 5767-72.

[118] Simons K, Sampaio JL. Membrane Organization and Lipid Rafts. Cold Spring Harbor Perspectives in Biology 2011; 3.

[119] Redondo-Morata L, Giannotti MI, Sanz F. Influence of cholesterol on the phase transition of lipid bilayers: a temperature-controlled force spectroscopy study. Langmuir 2012; 28: 12851-60.

[120] Lawrence JC, Saslowsky DE, Edwardson JM, Henderson RM. Real-time analysis of the effects of cholesterol on lipid raft behavior using atomic force microscopy. Biophys J 2003; 84: 1827-32.

[121] Cevc G. Membrane Electrostatics. Biochim Biophys Acta 1990; 1031: 311-82.

[122] Marsh D. CRC handbook of lipid bilayers. Boca Raton: CRC press.1990.

[123] Cremer PS, Boxer SG. Formation and spreading of lipid bilayers on planar glass supports. J Phys Chem B 1999; 103: 2554-59.

[124] Kosmulski M. The pH-dependent surface charging and points of zero charge: V. Update. J Colloid Interface Sci 2011; 353: 1-15.

[125] Egawa H, Furusawa K. Liposome adhesion on mica surface studied by atomic force microscopy. Langmuir 1999; 15: 1660-66.

[126] Makino K, Yamada T, Kimura M, Oka T, Ohshima H, Kondo T. Temperature-Induced and Ionic Strength-Induced Conformational-Changes in the Lipid Head Group Region of Liposomes as Suggested by Zeta-Potential Data. Biophys Chem 1991; 41: 175-83.

[127] Garcia-Manyes S, Oncins G, Sanz F. Effect of ion-binding and chemical phospholipid structure on the nanomechanics of lipid bilayers studied by force spectroscopy. Biophys J 2005; 89: 1812-26.

[128] Rossetti FF, Textor M, Reviakine I. Asymmetric distribution of phosphatidyl serine in supported phospholipid bilayers on titanium dioxide. Langmuir 2006; 22: 3467-73.

[129] Richter RP, Brisson AR. Following the formation of supported lipid bilayers on mica: A study combining AFM, QCM-D, and ellipsometry. Biophys J 2005; 88: 3422-33.

[130] Ramirez DM, Ogilvie WW, Johnston LJ. NBD-cholesterol probes to track cholesterol distribution in model membranes. Biochim Biophys Acta 2010; 1798: 558-68.

[131] Schonherr H, Johnson JM, Lenz P, Frank CW, Boxer SG. Vesicle adsorption and lipid bilayer formation on glass studied by atomic force microscopy. Langmuir 2004; 20: 11600-6.

[132] Reich C, Horton MR, Krause B, Gast AP, Radler JO, Nickel B. Asymmetric structural features in single supported lipid bilayers containing cholesterol and GM1 resolved with synchrotron X-Ray reflectivity. Biophys J 2008; 95: 657-68.

[133] Brass V, Bieck E, Montserret R, Wolk B, Hellings JA, Blum HE, Penin F, Moradpour D. An amino-terminal amphipathic alpha-helix mediates membrane association of the hepatitis C virus nonstructural protein 5A. J Biol Chem 2002; 277: 8130-9.

[134] Cho NJ, Cho SJ, Cheong KH, Glenn JS, Frank CW. Employing an amphipathic viral peptide to create a lipid bilayer on Au and TiO2. J Am Chem Soc 2007; 129: 10050-1.

[135] Cho NJ, Cheong KH, Lee C, Frank CW, Glenn JS. Binding dynamics of hepatitis C virus' NS5A amphipathic peptide to cell and model membranes. J Virol 2007; 81: 6682-9.

[136] Penin F, Brass V, Appel N, Ramboarina S, Montserret R, Ficheux D, Blum HE, Bartenschlager R, Moradpour D. Structure and function of the membrane anchor domain of hepatitis C virus nonstructural protein 5A. J Bio Chem 2004; 279: 40835-43.

[137] Cho NJ, Wang GL, Edvardsson M, Glenn JS, Hook F, Frank CW. Alpha-Helical Peptide-Induced Vesicle Rupture Revealing New Insight into the Vesicle Fusion Process As Monitored in Situ by Quartz Crystal Microbalance-Dissipation and Reflectometry. Analytical Chem 2009; 81: 4752-61.

[138] Cho NJ, Wang G, Edvardsson M, Glenn JS, Hook F, Frank CW. Alpha-helical peptide-induced vesicle rupture revealing new insight into the vesicle fusion process as monitored in situ by quartz crystal microbalance-dissipation and reflectometry. Analytical Chem 2009; 81: 4752-61.

[139] Gidalevitz D, Ishitsuka Y, Muresan AS, Konovalov O, Waring AJ, Lehrer RI, Lee KY. Interaction of antimicrobial peptide protegrin with biomembranes. Proc Natl Acad Sci U S A 2003; 100: 6302-7.

[140] Tabaei SR, Rabe M, Zhdanov VP, Cho NJ, Hook F. Single vesicle analysis reveals nanoscale membrane curvature selective pore formation in lipid membranes by an antiviral alpha-helical peptide. Nano Lett 2012; 12: 5719-25.

[141] Cho NJ, Dvory-Sobol H, Xiong A, Cho SJ, Frank CW, Glenn JS. Mechanism of an amphipathic alpha-helical peptide's antiviral activity involves size-dependent virus particle lysis. ACS Chem Biol 2009; 4: 1061-7.

[142] Jackman JA, Cho NJ. Model membrane platforms for biomedicine: case study on antiviral drug development. Biointerphases 2012; 7: 18.

[143] Zasloff M. Antimicrobial peptides of multicellular organisms. Nature 2002; 415: 389-95.

[144] He K, Ludtke SJ, Huang HW, Worcester DL. Antimicrobial peptide pores in membranes detected by neutron in-plane scattering. Biochemistry 1995; 34: 15614-8.

[145] Henzler Wildman KA, Lee DK, Ramamoorthy A. Mechanism of lipid bilayer disruption by the human antimicrobial peptide, LL-37. Biochemistry 2003; 42: 6545-58.

[146] Rapaport D, Peled R, Nir S, Shai Y. Reversible surface aggregation in pore formation by pardaxin. Biophys J 1996; 70: 2502-12.

[147] Bobardt MD, Cheng G, de Witte L, Selvarajah S, Chatterji U, Sanders-Beer BE, Geijtenbeek TB, Chisari FV, Gallay PA. Hepatitis C virus NS5A anchor peptide disrupts human immunodeficiency virus. Proc Natl Acad Sci U S A 2008; 105: 5525-30.

[148] Cheng G, Montero A, Gastaminza P, Whitten-Bauer C, Wieland SF, Isogawa M, Fredericksen B, Selvarajah S, Gallay PA, Ghadiri MR, Chisari FV. A virocidal amphipathic {alpha}-helical peptide that inhibits hepatitis C virus infection in vitro. Proc Natl Acad Sci U S A 2008; 105: 3088-93.

[149] Alving CR, Beck Z, Karasavva N, Matyas GR, Rao M. HIV-1, lipid rafts, and antibodies to liposomes: implications for anti-viral-neutralizing antibodies (Review). Molecular Membrane Biology 2006; 23: 453-U1.

[150] Zhu P, Liu J, Bess J, Chertova E, Lifson JD, Grise H, Ofek GA, Taylor KA, Roux KH. Distribution and three-dimensional structure of AIDS virus envelope spikes. Nature 2006; 441: 847-52.

[151] Engelman DM. Membranes are more mosaic than fluid. Nature 2005; 438: 578-80.

[152] Groves JT, Ulman N, Cremer PS, Boxer SG. Substrate-membrane interactions: Mechanisms for imposing patterns on a fluid bilayer membrane. Langmuir 1998; 14: 3347-50.

[153] Kumar K, Tang CS, Rossetti FF, Textor M, Keller B, Voros J, Reimhult E. Formation of supported lipid bilayers on indium tin oxide for dynamically-patterned membrane-functionalized microelectrode arrays. Lab Chip 2009; 9: 718-25.

[154] Rossetti FF, Bally M, Reviakine I, Falconnet D, Michel R, Textor M. Formation of supported phospholipid bilayers on titanium oxide surfaces. Biophys J 2005; 88: 7A-7A.

[155] Mager MD, Almquist B, Melosh NA. Formation and Characterization of Fluid Lipid Bilayers on Alumina. Langmuir 2008; 24: 12734-37.

[156] Steltenkamp S, Muller MM, Deserno M, Hennesthal C, Steinem C, Janshoff A. Mechanical properties of pore-spanning lipid bilayers probed by atomic force microscopy. Biophys J 2006; 91: 217-26.

[157] Cha T, Guo A, Zhu XY. Formation of supported phospholipid bilayers on molecular surfaces: Role of surface charge density and electrostatic interaction. Biophys J 2006; 90: 1270-74.

[158] Rossetti FF, Bally M, Michel R, Textor M, Reviakine I. Interactions between titanium dioxide and phosphatidyl serine-containing liposomes: Formation and patterning of supported phospholipid bilayers on the surface of a medically relevant material. Langmuir 2005; 21: 6443-50.

[159] Hussain NF, Siegel AP, Ge Y, Jordan R, Naumann CA. Bilayer asymmetry influences integrin sequestering in raft-mimicking lipid mixtures. Biophys J 2013; 104: 2212-21.

[160] Varma S, Teng M, Scottt HL. Nonintercalating Nanosubstrates Create Asymmetry between Bilayer Leaflets. Langmuir 2012; 28: 2842-48.

[161] Wacklin HP. Composition and Asymmetry in Supported Membranes Formed by Vesicle Fusion. Langmuir 2011; 27: 7698-707.

[162] Richter RP, Maury N, Brisson AR. On the effect of the solid support on the interleaflet distribution of lipids in supported lipid bilayers. Langmuir 2005; 21: 299-304.

[163] Reinl HM, Bayerl TM. Lipid Transfer between Small Unilamellar Vesicles and Single Bilayers on a Solid Support - Self-Assembly of Supported Bilayers with Asymmetric Lipid Distribution. Biochemistry 1994; 33: 14091-99.

[164] Wacklin HP, Thomas RK. Spontaneous formation of asymmetric lipid bilayers by adsorption of vesicles. Langmuir 2007; 23: 7644-51.

[165] Stottrup BL, Veatch SL, Keller SL. Nonequilibrium behavior in supported lipid membranes containing cholesterol. Biophys J 2004; 86: 2942-50.

[166] Cho NJ, Cheong KH, Lee C, Frank CW, Glenn JS. Binding dynamics of hepatitis C virus' NS5A amphipathic peptide to cell and model membranes. Journal of Virology 2007; 81: 6682-89.

[167] Elazar M, Cheong KH, Liu P, Greenberg HB, Rice CM, Glenn JS. Amphipathic helix-dependent localization of NS5A mediates hepatitis C virus RNA replication. J Virol 2003; 77: 6055-61.

[168] Franquelim HG, Chiantia S, Veiga AS, Santos NC, Schwille P, Castanho MARB. Anti-HIV-1 antibodies 2F5 and 4E10 interact differently with lipids to bind their epitopes. AIDS 2011; 25: 419-28.

[169] Cho NJ, Dvory-Sobol H, Xiong AM, Cho SJ, Frank CW, Glenn JS. Mechanism of an Amphipathic alpha-Helical Peptide's Antiviral Activity Involves Size-Dependent Virus Particle Lysis. Acs Chemical Biology 2009; 4: 1061-67.

[170] Keller CA, Kasemo B. Surface specific kinetics of lipid vesicle adsorption measured with a quartz crystal microbalance. Biophys J 1998; 75: 1397-402.

[171] Thomas RK. Neutron reflection from liquid interfaces. Ann Rev Phys Chem 2004; 55: 391-426.

[172] Cho NJ, Cho SJ, Cheong KH, Glenn JS, Frank CW. Employing an amphipathic viral peptide to create a lipid bilayer on Au and TiO2. J Am Chem Soc 2007; 129: 10050-+.

[173] Varma S, Teng M, Scott HL. Nonintercalating nanosubstrates create asymmetry between bilayer leaflets. Langmuir 2012; 28: 2842-8.

[174] Janshoff A, Steinem C. Scanning force microscopy of artificial membranes. Chembiochem 2001; 2: 799-808.

[175] Dimitrievski K, Zach M, Zhdanov VP, Kasemo B. Imaging and manipulation of adsorbed lipid vesicles by an AFM tip: Experiment and Monte Carlo simulations. Colloids and Surfaces B-Biointerfaces 2006; 47: 115-25.

[176] Macdonald RC, Macdonald RI, Menco BPM, Takeshita K, Subbarao NK, Hu LR. Small-Volume Extrusion Apparatus for Preparation of Large, Unilamellar Vesicles. Biochimica Et Biophysica Acta 1991; 1061: 297-303.

[177] Dura JA, Pierce DJ, Majkrzak CF, Maliszewskyj NC, McGillivray DJ, Losche M, O'Donovan KV, Mihailescu M, Perez-Salas U, Worcester DL, White SH. AND/R: Advanced neutron diffractometer/reflectometer for investigation of thin films and multilayers for the life sciences. Rev Scientific Instruments 2006; 77.

[178] Kirby BJ, Kienzle PA, Maranville BB, Berk NF, Krycka J, Heinrich F, Majkrzak CF. Phase-sensitive specular neutron reflectometry for imaging the nanometer scale composition depth profile of thin-film materials. Curr Opin Colloid Interface Sci 2012; 17: 44–53.

[179] Ankner JF, Majkrzak CF. Subsurface Profile Refinement for Neutron Specular Reflectivity. Neutron Optical Devices and Applications 1992; 1738: 260-69.

[180] Parratt LG. Surface Studies of Solids by Total Reflection of X-Rays. Phys Rev 1954; 95: 359-69.

[181] Heinrich F, Ng T, Vanderah DJ, Shekhar P, Mihailescu M, Nanda H, Losche M. A New Lipid Anchor for Sparsely Tethered Bilayer Lipid Membranes. Langmuir 2009; 25: 4219-29.

[182] Reardon PN, Sage H, Dennison SM, Martin JW, Donald BR, Alam SM, Haynes BF, Spicer LD. Structure of an HIV-1-neutralizing antibody target, the lipid-bound gp41 envelope membrane proximal region trimer. Proc Natl Acad Sci U S A 2014; 111: 1391-6.

[183] Morandat S, Azouzi S, Beauvais E, Mastouri A, El Kirat K. Atomic force microscopy of model lipid membranes. Analytical and Bioanalytical Chem 2013; 405: 1445-61.

[184] Simons K, Ikonen E. Functional rafts in cell membranes. Nature 1997; 387: 569-72.

[185] Ofek G, Tang, M., Sambor, A., Katinger, H., Mascola, J.R., Wyatt, R., Kwong, P.D. Structure and mechanistic analysis of the anti-human immunodeficiency virus type 1 antibody 2F5 in complex with its gp41 epitope. J Virol 2004; 78: 10724-37.

[186] Alam SM, Morelli M, Dennison SM, Liao HX, Zhang RJ, Xia SM, Rits-Volloch S, Sun L, Harrison SC, Haynes BF, Chen B. Role of HIV membrane in neutralization by two broadly neutralizing antibodies. Proc Natl Acad Sci U S A 2009; 106: 20234-39.

[187] Dennison SM, Sutherland LL, Jaeger FH, Anasti KM, Parks R, Stewart S, Bowman C, Xia SM, Zhang RJ, Shen XY, Scearce RM, Ofek G, Yang YP, Kwong

PD, Santra S, Liao HX, Tomaras G, Letvin NL, Chen B, Alam SM, Haynes BF. Induction of Antibodies in Rhesus Macaques That Recognize a Fusion-Intermediate Conformation of HIV-1 gp41. PloS One 2011; 6.

[188] Guenaga J, Dosenovic P, Ofek G, Baker D, Schief WR, Kwong PD, Hedestam GBK, Wyatt RT. Heterologous Epitope-Scaffold Prime:Boosting Immuno-Focuses B Cell Responses to the HIV-1 gp41 2F5 Neutralization Determinant. PloS One 2011; 6.

[189] Cser L, Gladkih IA, Franek F, Ostanevich YM. Investigation of Antibody Structures by Scattering Techniques. Colloid Polymer Sci 1981; 259: 625-40.

[190] Dennison SM, Stewart SM, Stempel KC, Liao HX, Haynes BF, Alam SM. Stable docking of neutralizing human immunodeficiency virus type 1 gp41 membrane-proximal external region monoclonal antibodies 2F5 and 4E10 is dependent on the membrane immersion depth of their epitope regions. J Virol 2009; 83: 10211-23.

[191] Sun ZYJ, Oh KJ, Kim MY, Yu J, Brusic V, Song LK, Qiao ZS, Wang JH, Wagner G, Reinherz EL. HIV-1 broadly neutralizing antibody extracts its epitope from a kinked gp41 ectodomain region on the viral membrane. Immunity 2008; 28: 52-63.

[192] Saez-Cirion A, Nir S, Lorizate M, Agirre A, Cruz A, Perez-Gil J, Nieva JL. Sphingomyelin and cholesterol promote HIV-1 gp41 pretransmembrane sequence surface aggregation and membrane restructuring. J Bio Chem 2002; 277: 21776-85.

[193] Brugger B, Glass B, Haberkant P, Leibrecht I, Wieland FT, Krausslich HG. The HIV lipidome: A raft with an unusual composition. Proc Natl Acad Sci U S A 2006; 103: 2641-46.

[194] Hardy GJ, Nayak R, Alam SM, Shapter JG, Heinrich F, Zauscher S. Biomimetic supported lipid bilayers with high cholesterol content formed by alpha-helical peptide-induced vesicle fusion. J Mater Chem 2012; 22: 19506-13.

[195] Mecke A, Lee DK, Ramamoorthy A, Orr BG, Holl MMB. Membrane thinning due to antimicrobial peptide binding: An atomic force microscopy study of MSI-78 in lipid bilayers. Biophys J 2005; 89: 4043-50.

[196] M'Baye G, Mely Y, Duportail G, Klymchenko AS. Liquid ordered and gel phases of lipid bilayers: Fluorescent probes reveal close fluidity but different hydration. Biophys J 2008; 95: 1217-25.

[197] An H, Nussio MR, Huson MG, Voelcker NH, Shapter JG. Material properties of lipid microdomains: force-volume imaging study of the effect of cholesterol on lipid microdomain rigidity. Biophy J 2010; 99: 834-44.

[198] Rinia HA, Snel MM, van der Eerden JP, de Kruijff B. Visualizing detergent resistant domains in model membranes with atomic force microscopy. FEBS Letters 2001; 501: 92-6.

[199] Hoopes MI, Faller R, Longo ML. Lipid Domain Depletion at Small Localized Bends Imposed by a Step Geometry. Langmuir 2011; 27: 2783-88.

[200] Pretzl M, Schweikart A, Hanske C, Chiche A, Zettl U, Horn A, Boker A, Fery A. A Lithography-Free Pathway for Chemical Microstructuring of Macromolecules from Aqueous Solution Based on Wrinkling. Langmuir 2008; 24: 12748-53.

[201] Hovis JS, Boxer SG. Patterning and composition arrays of supported lipid bilayers by microcontact printing. Langmuir 2001; 17: 3400-05.

[202] Doyle AW, Fick J, Himmelhaus M, Eck W, Graziani I, Prudovsky I, Grunze M, Maciag T, Neivandt DJ. Protein deformation of lipid hybrid bilayer membranes studied by sum frequency generation vibrational spectroscopy. Langmuir 2004; 20: 8961-65.

[203] Howell C, Schmidt R, Kurz V, Koelsch P. Sum-frequency-generation spectroscopy of DNA films in air and aqueous environments. Biointerphases 2008; 3: Fc47-Fc51.

[204] Chen J, Frey G, Peng H, Rits-Volloch S, Garrity J, Seaman MS, Chen B. Mechanism of HIV-1 Neutralization by Antibodies Targeting a Membrane-Proximal Region of gp41. J Virol 2014; 88: 1249-58.

[205] Doores KJ, Burton DR. Variable Loop Glycan Dependency of the Broad and Potent HIV-1-Neutralizing Antibodies PG9 and PG16. J Virol 2010; 84: 10510-21.

[206] Pejchal R, Walker LM, Stanfield RL, Phogat SK, Koff WC, Poignard P, Burton DR, Wilson IA. Structure and function of broadly reactive antibody PG16 reveal an H3 subdomain that mediates potent neutralization of HIV-1. Proc Natl Acad Sci U S A 2010; 107: 11483-88.

[207] Piner RD, Zhu J, Xu F, Hong SH, Mirkin CA. "Dip-pen" nanolithography. Science 1999; 283: 661-63.

[208] Huo FW, Zheng ZJ, Zheng GF, Giam LR, Zhang H, Mirkin CA. Polymer pen lithography. Science 2008; 321: 1658-60.

[209] Su M, Aslam M, Fu L, Wu NQ, Dravid VP. Dip-pen nanopatterning of photosensitive conducting polymer using a monomer ink. Applied Phys Letters 2004; 84: 4200-02.

[210] Lee WK, Whitman LJ, Lee J, King WP, Sheehan PE. The nanopatterning of a stimulus-responsive polymer by thermal dip-pen nanolithography. Soft Matter 2008; 4: 1844-47.

[211] Demers LM, Ginger DS, Park SJ, Li Z, Chung SW, Mirkin CA. Direct patterning of modified oligonucleotides on metals and insulators by dip-pen nanolithography. Science 2002; 296: 1836-38.

[212] Senesi AJ, Rozkiewicz DI, Reinhoudt DN, Mirkin CA. Agarose-Assisted Dip-Pen Nanolithography of Oligonucleotides and Proteins. Acs Nano 2009; 3: 2394-402.

[213] Valiokas R, Vaitekonis A, Klenkar G, Trinkunas G, Liedberg B. Selective recruitment of membrane protein complexes onto gold substrates patterned by dip-pen nanolithography. Langmuir 2006; 22: 3456-60.

[214] Sekula S, Fuchs J, Weg-Remers S, Nagel P, Schuppler S, Fragala J, Theilacker N, Franueb M, Wingren C, Ellmark P, Borrebaeck CAK, Mirkin CA, Fuchs H, Lenhert S. Multiplexed Lipid Dip-Pen Nanolithography on Subcellular Scales for the Templating of Functional Proteins and Cell Culture. Small 2008; 4: 1785-93.

[215] Borrebaeck CAK, Wingren C. Design of high-density antibody microarrays for disease proteomics: Key technological issues. J Proteomics 2009; 72: 928-35.

[216] Loh O, Lam R, Chen M, Moldovan N, Huang HJ, Ho D, Espinosa HD. Nanofountain-Probe-Based High-Resolution Patterning and Single-Cell Injection of Functionalized Nanodiamonds. Small 2009; 5: 1667-74.

[217] Nelson BA, King WP, Laracuente AR, Sheehan PE, Whitman LJ. Direct deposition of continuous metal nanostructures by thermal dip-pen nanolithography. Applied Phys Letters 2006; 88.

[218] Slater JH, Frey W. Nanopatterning of fibronectin and the influence of integrin clustering on endothelial cell spreading and proliferation. J Biomed Materials Research Part A 2008; 87A: 176-95.

[219] Suo ZY, Yang XH, Avci R, Deliorman M, Rugheimer P, Pascual DW, Idzerda Y. Antibody Selection for Immobilizing Living Bacteria. Analytical Chem 2009; 81: 7571-78.

[220] Ariga K, Nakanishi T, Michinobu T. Immobilization of biomaterials to nano-assembled films (self-assembled monolayers, Langmuir-Blodgett films, and layer-by-layer assemblies) and their related functions. J Nanoscience and Nanotechnology 2006; 6: 2278-301.

[221] Piner RD, Zhu J, Xu F, Hong S, Mirkin CA. "Dip-Pen" nanolithography. Science 1999; 283: 661-3.

[222] Lenhert S, Sun P, Wang YH, Fuchs H, Mirkin CA. Massively parallel dip-pen nanolithography of heterogeneous supported phospholipid multilayer patterns. Small 2007; 3: 71-75.

[223] Sekula-Neuner S, Maier J, Oppong E, Cato ACB, Hirtz M, Fuchs H. Allergen Arrays for Antibody Screening and Immune Cell Activation Profiling Generated by Parallel Lipid Dip-Pen Nanolithography. Small 2012; 8: 585-91.

[224] Mitsakakis K, Sekula-Neuner S, Lenhert S, Fuchs H, Gizeli E. Convergence of Dip-Pen Nanolithography and acoustic biosensors towards a rapid-analysis multi-sample microsystem. Analyst 2012; 137: 3076-82.

[225] Nafday OA, Lenhert S. High-throughput optical quality control of lipid multilayers fabricated by dip-pen nanolithography. Nanotechnology 2011; 22.

[226] Kusi-Appiah AE, Vafai N, Cranfill PJ, Davidson MW, Lenhert S. Lipid multilayer microarrays for in vitro liposomal drug delivery and screening. Biomaterials 2012; 33: 4187-94.

[227] Deng Y, Wang Y, Holtz B, Li JY, Traaseth N, Veglia G, Stottrup BJ, Elde R, Pei DQ, Guo A, Zhu XY. Fluidic and air-stable supported lipid bilayer and cell-mimicking microarrays. J Am Chem Soc 2008; 130: 6267-71.

[228] Tekin E, Smith PJ, Schubert US. Inkjet printing as a deposition and patterning tool for polymers and inorganic particles. Soft Matter 2008; 4: 703-13.

[229] Orth RN, Kameoka J, Zipfel WR, Ilic B, Webb WW, Clark TG, Craighead HG. Creating biological membranes on the micron scale: Forming patterned lipid bilayers using a polymer lift-off technique. Biophys J 2003; 85: 3066-73.

[230] Maheshwari G, Brown G, Lauffenburger DA, Wells A, Griffith LG. Cell adhesion and motility depend on nanoscale RGD clustering. J Cell Science 2000; 113: 1677-86.

[231] Massia SP, Hubbell JA. An Rgd Spacing of 440nm Is Sufficient for Integrin Alpha-V-Beta-3-Mediated Fibroblast Spreading and 140nm for Focal Contact and Stress Fiber Formation. J Cell Biol 1991; 114: 1089-100.

[232] Maheshwari G, Wells A, Griffith LG, Lauffenburger DA. Biophysical integration of effects of epidermal growth factor and fibronectin on fibroblast migration. Biophys J 1999; 76: 2814-23.

[233] Hirtz M, Corso R, Sekula-Neuner S, Fuchs H. Comparative Height Measurements of Dip-Pen Nanolithography-Produced Lipid Membrane Stacks with Atomic Force, Fluorescence, and Surface-Enhanced Ellipsometric Contrast Microscopy. Langmuir 2011; 27: 11605-08.

[234] Nissen J, Jacobs K, Radler JO. Interface dynamics of lipid membrane spreading on solid surfaces. Phys Rev Letters 2001; 86: 1904-07.

[235] Howland MC, Sapuri-Butti AR, Dixit SS, Dattelbaum AM, Shreve AP, Parikh AN. Phospholipid morphologies on photochemically patterned silane monolayers. J Am Chem Soc 2005; 127: 6752-65.

Biography

Gregory Hardy was born on October 24th, 1984 in Albany, New York to Thomas and Teresa Hardy. After graduating from Maple Hill High School in Castleton, NY, Greg moved to Rochester, NY to attend the University of Rochester. He received his B.S. in 2007 in biomedical engineering with minors in chemical engineering and biology. After graduation, Greg moved to Boston, MA to work at Massachusetts General Hospital where he studied cardiovascular rheumatology. In August of 2009, Greg began his doctoral studies at Duke University (Durham, NC) under Professor Stefan Zauscher. In addition to his primary department of Mechanical Engineering and Materials Science, Greg belongs to the Center of Bimolecular and Tissue Engineering. Greg's research has focused on understanding the interactions between model lipid systems and HIV-1 vaccine antigen and antibodies.